Soft X-ray Tomography

National Center for X-ray Tomography

Soft X-ray Microscope

Full-field transmission X-ray microscope

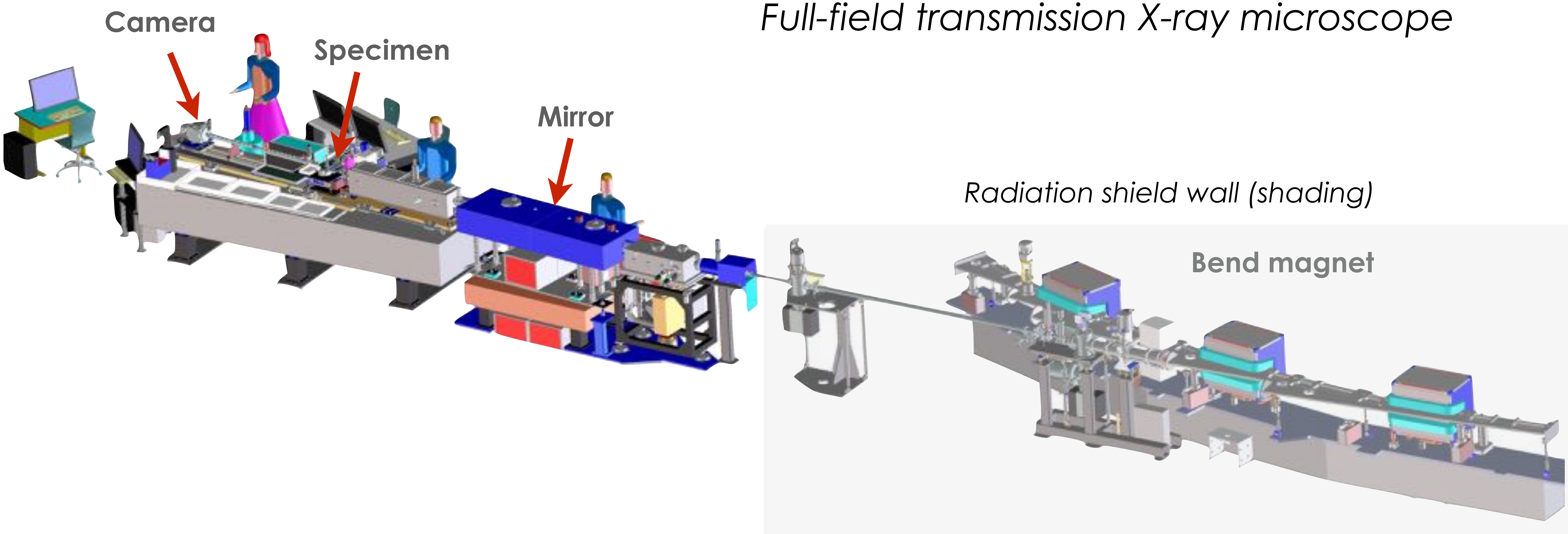

- Light source: synchrotron radiation - 2.4 nm λ, 517 eV
- Optics: zone plates (nano-fabricated nickel Fresnel lenses)
- Contrast mechanism: X-ray absorption by cellular components

National Center for X-ray Tomography (NCXT), supported by NIH-NIGMS and DOE-BER

Image Physics

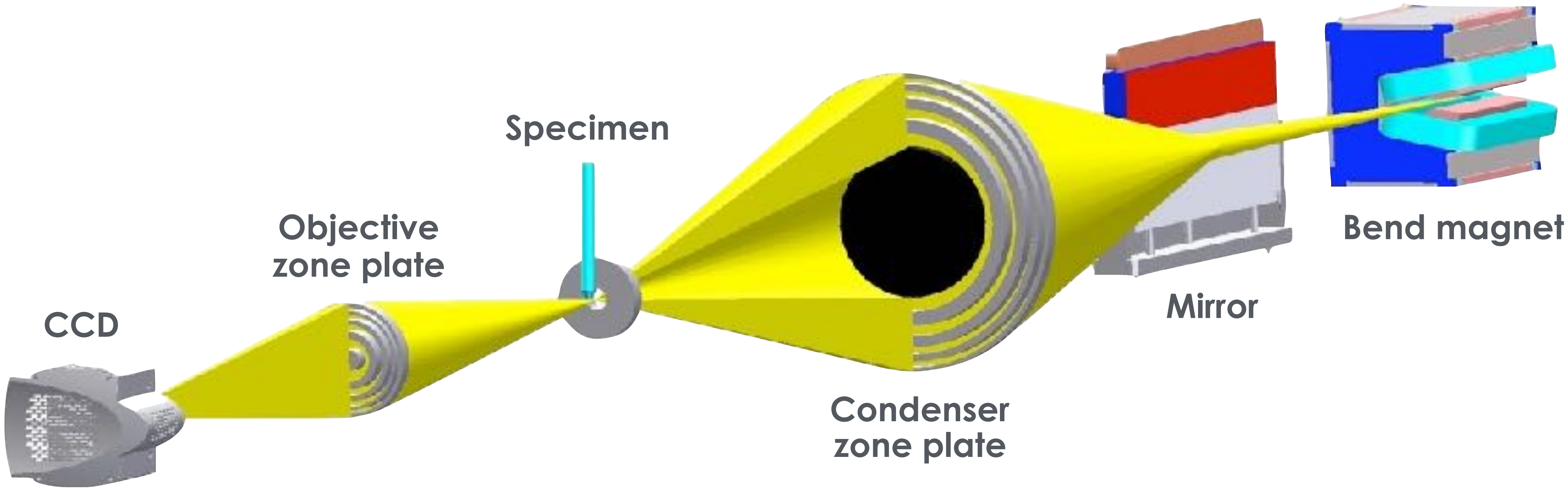

- Condenser zone plate focuses source onto specimen
- Objective zone plate magnifies object onto CCD camera

References:

- *Streible N. Three-dimensional imaging by a microscope. J. Opt. Soc. Am. (1985) 2, 121- 127.*
- *Schmahl et al. X-ray microscopy. Naturwissenschaften. (1996) 83, 61-70.*
- *Attwood DT. Soft X-rays and Extreme Ultraviolet Radiation: Principles & Applications. (Cambridge University Press). 1999.*

Zone Plate Lenses - Diffractive Optics

Condenser lens

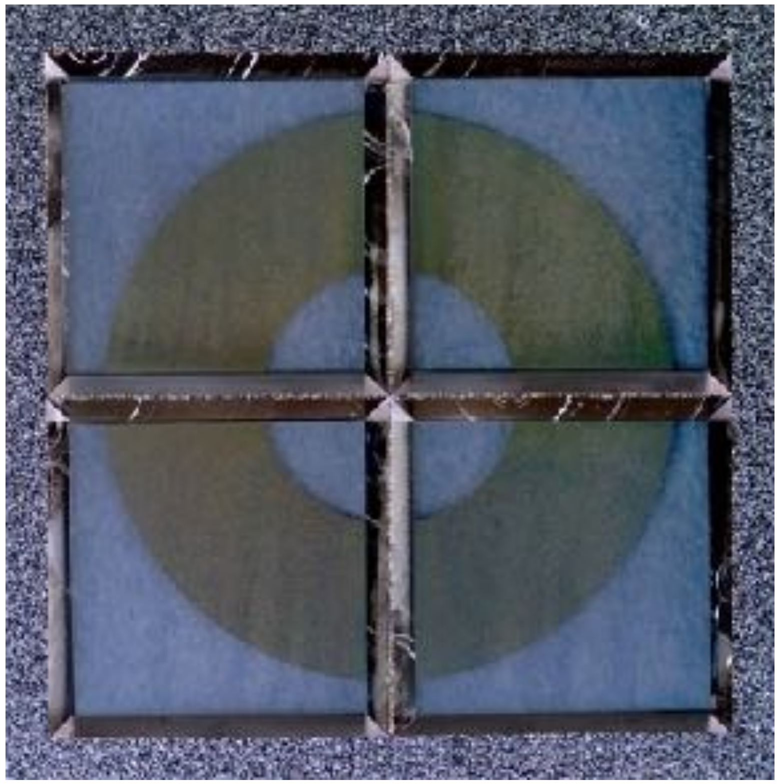

Specs of this specific lens:
Diameter = 1 cm
No. of zones = 41,700
Outer zone width = 50 nm
Central stop diameter = 5 mm

Objective lens

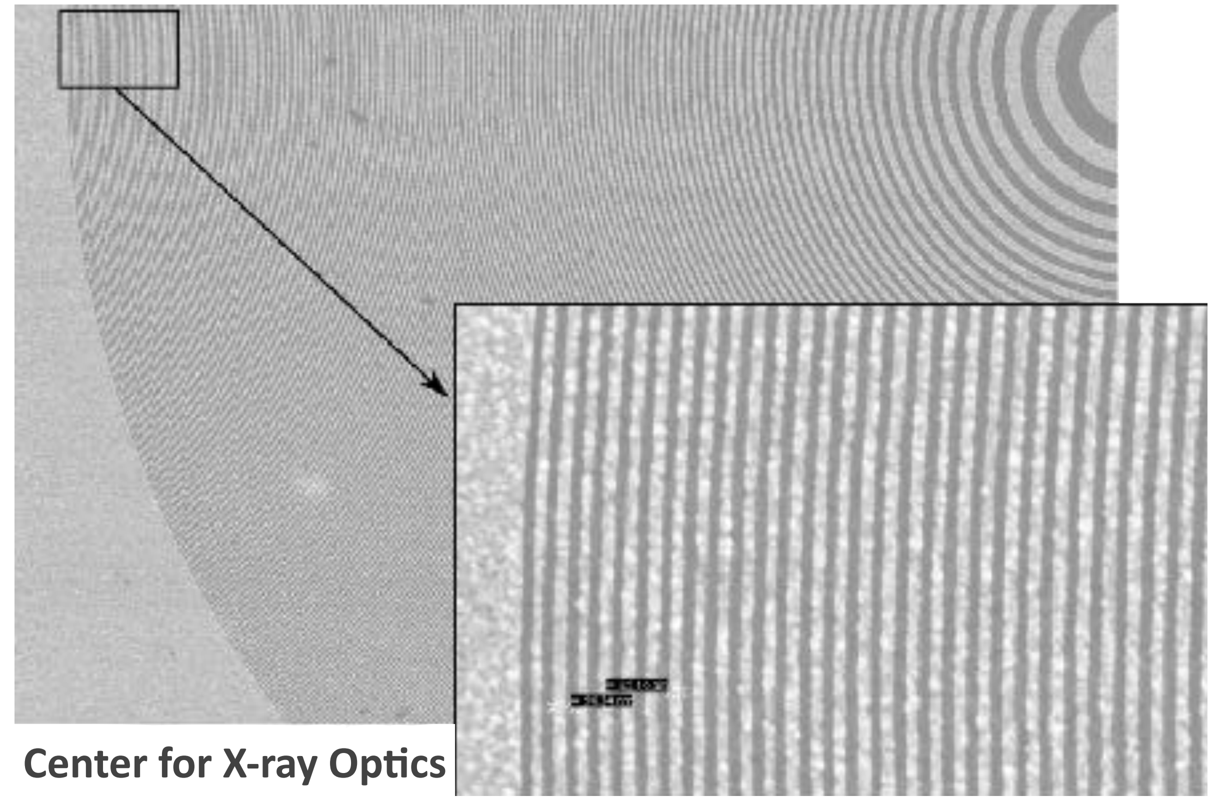

Specs of this specific lens:
Diameter = 63 µm
No. of zones = 628
Outer zone width = 25 nm
Nickel plating

- Resolution determined by width of outermost zone of the lens
- As resolution of zone plate increases, depth of focus decreases

Imaging in the Water Window - Absorption Contrast

Between K shell absorption edges of Carbon (284 eV, 4.4nm) and Oxygen (543 eV, 2.3nm)

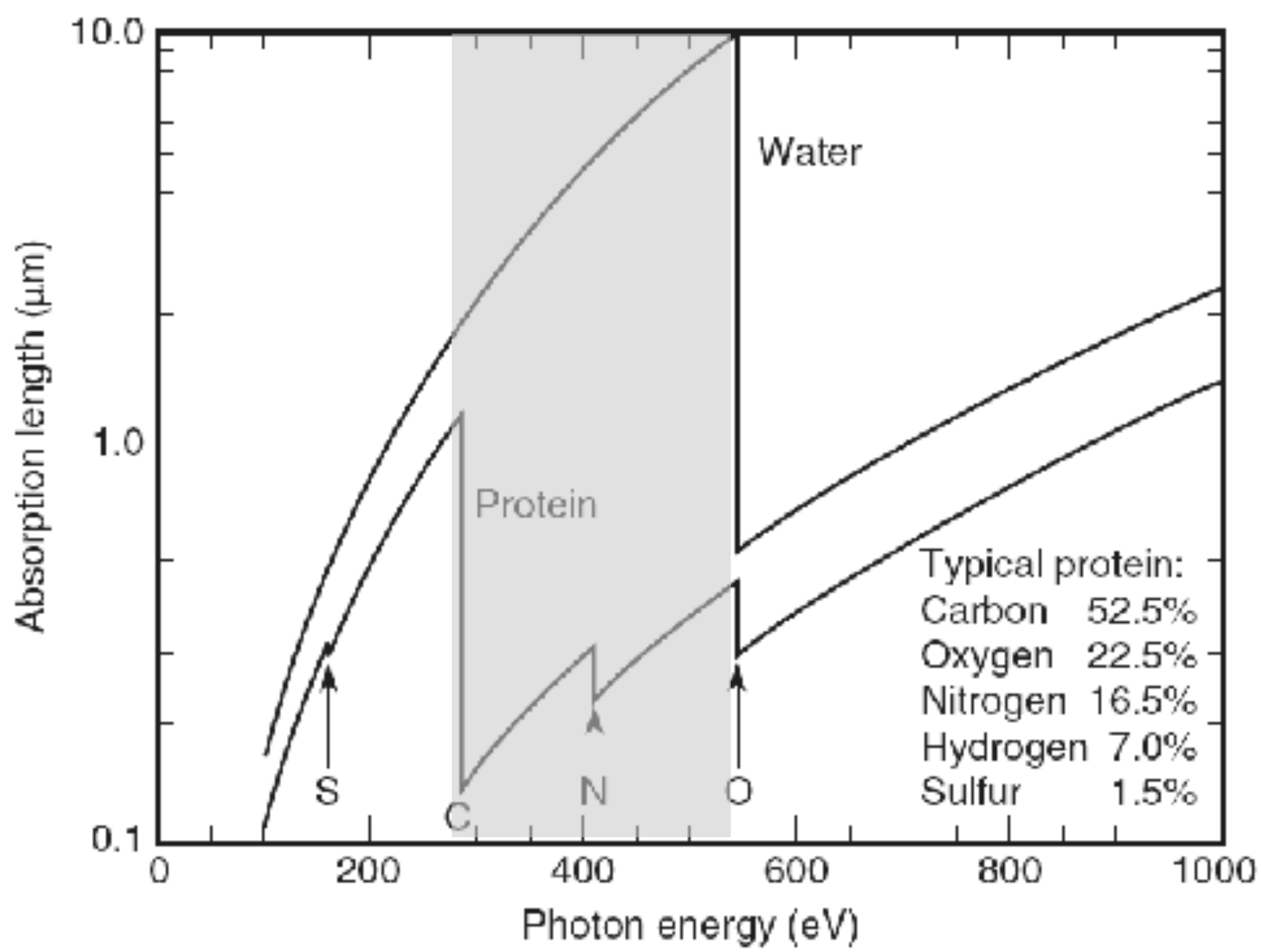

XM-2 operates at:

517 eV

2.4 nm λ

Contrast of cell structures is generated by the concentration of organic material (C- and N- containing biomolecules) in each voxel (3D pixel)

Imaging in the Water Window - Absorption Contrast

Structures with many carbon molecules per voxel, such as lipids, have high contrast

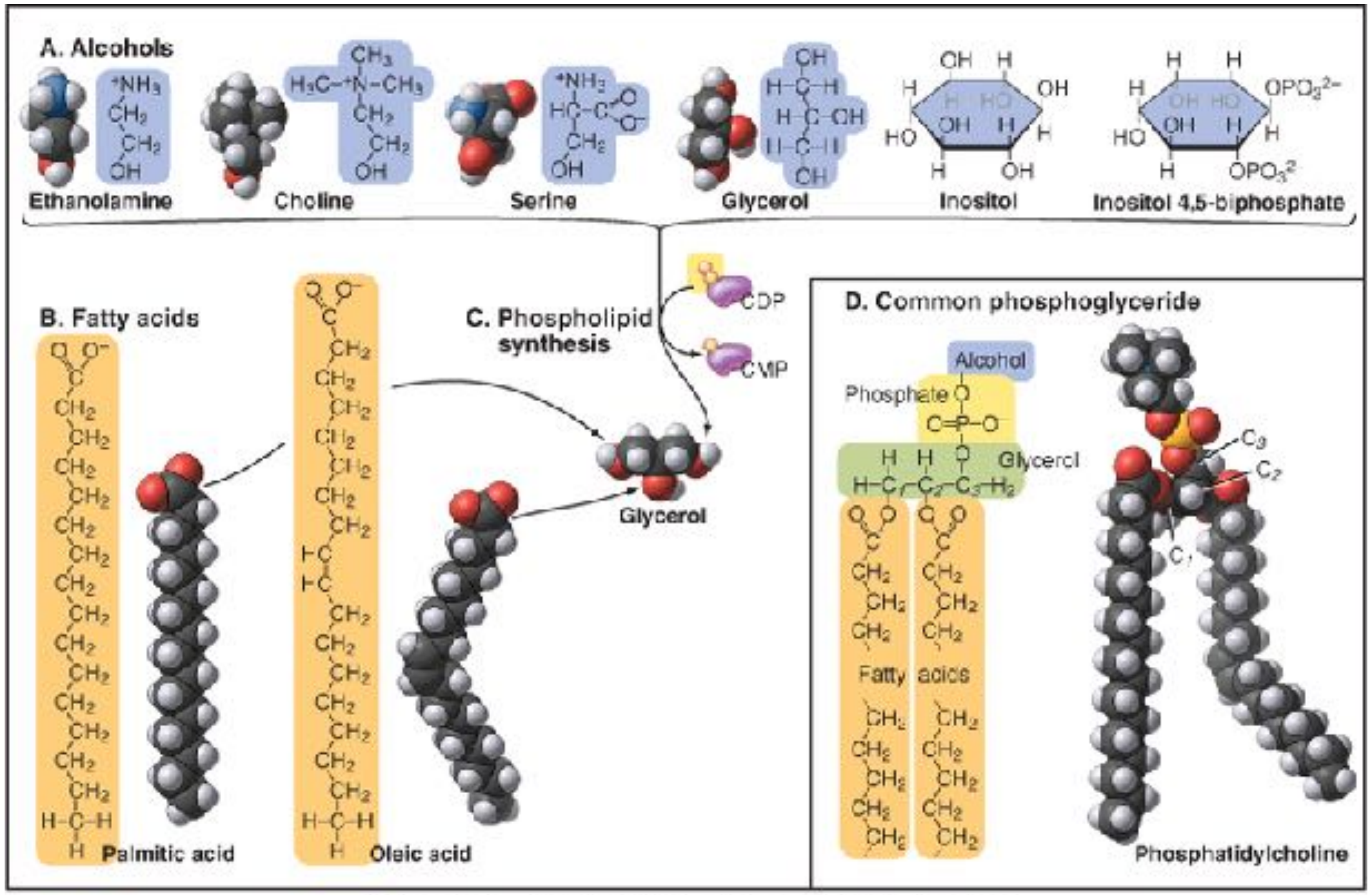

© Elsevier. Pollard et al: Cell Biology 2e - www.studentconsult.com

X-ray Tomography is Quantitative

Absorption adheres to Beer-Lambert's law; is linear with thickness, composition & concentration

Absorption coefficient measurements

BSA and hemoglobin

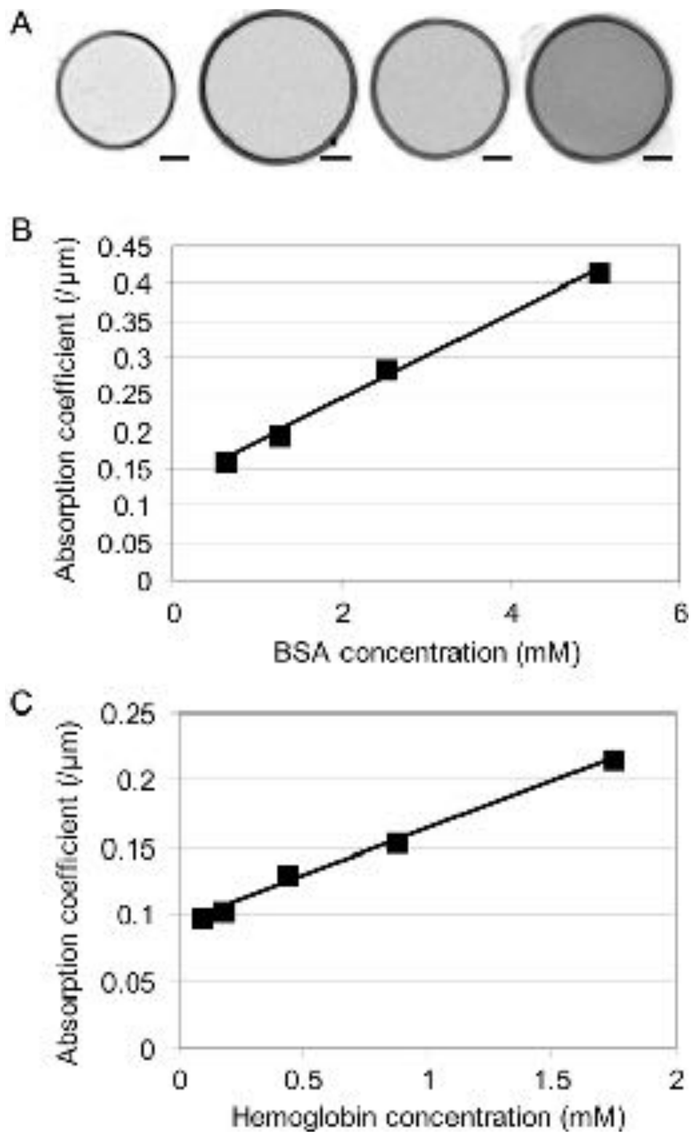

Hemoglobin concentration validated spectrophotometrically

Hanssen et al. J. Structural Biology. (2012) 177, 224-232

Alcohol oxidase crystal in yeast

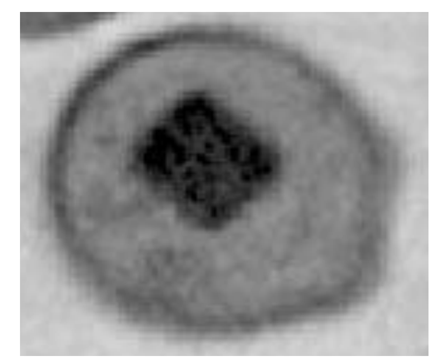

Calculated LAC - 0.625 μm^{-1}

Measured LAC - 0.626 ± 0.02 μm^{-1}

Le Gros et al. Cell Reports. (2016) 17(8), 2125-2136

Soft X-ray Tomography

- Whole, hydrated cells in near-native state (cryo-immobilized)
- Natural, quantitative contrast

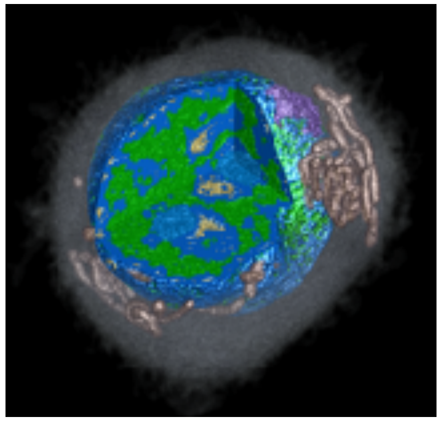

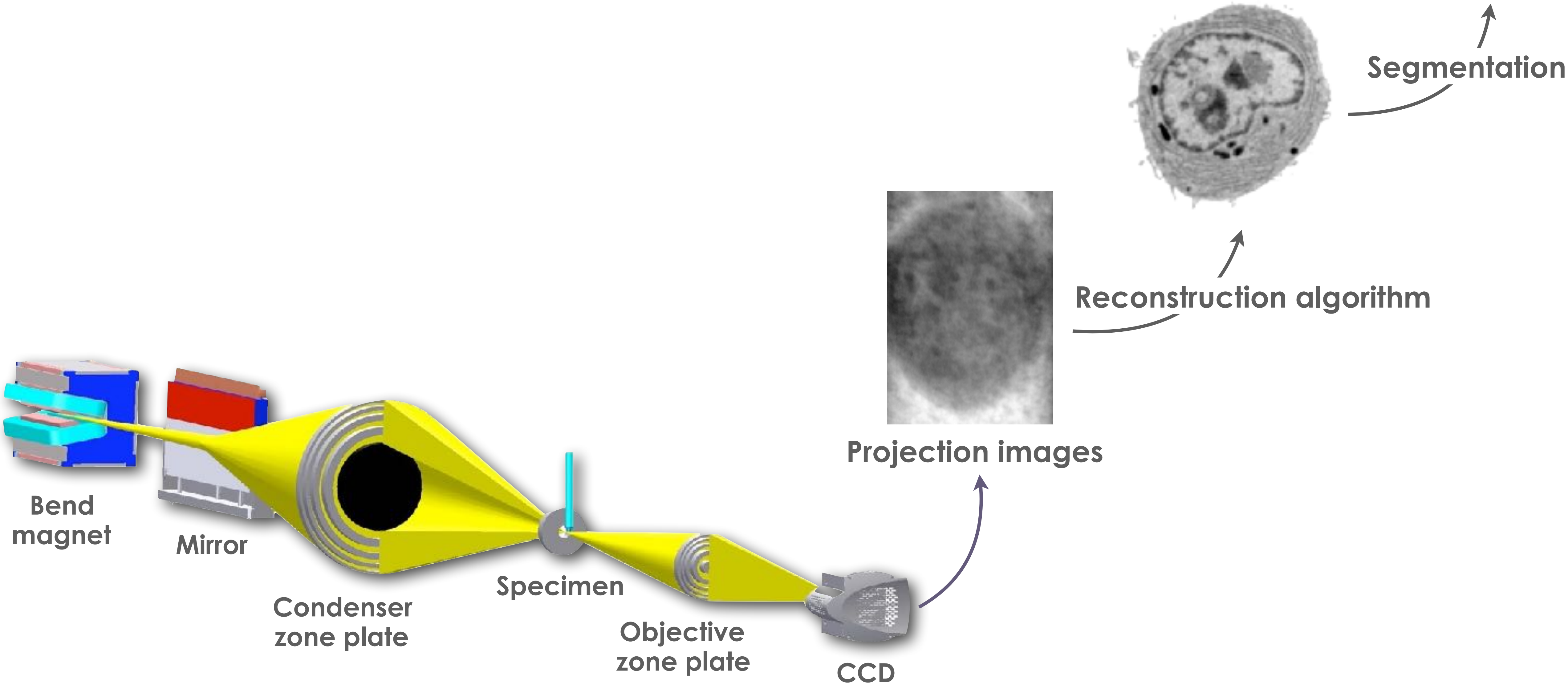

National Center for X-ray Tomography (NCXT), supported by NIH-NIGMS and DOE-BER

Tomographic Reconstruction Methods

Types of reconstruction methods:

Iterative reconstruction methods

Filtered back projection (FBP)	Conjugate Gradient Least Squares	Penalized-Likelihood	L1 regularized Conjugate Gradient Least Squares

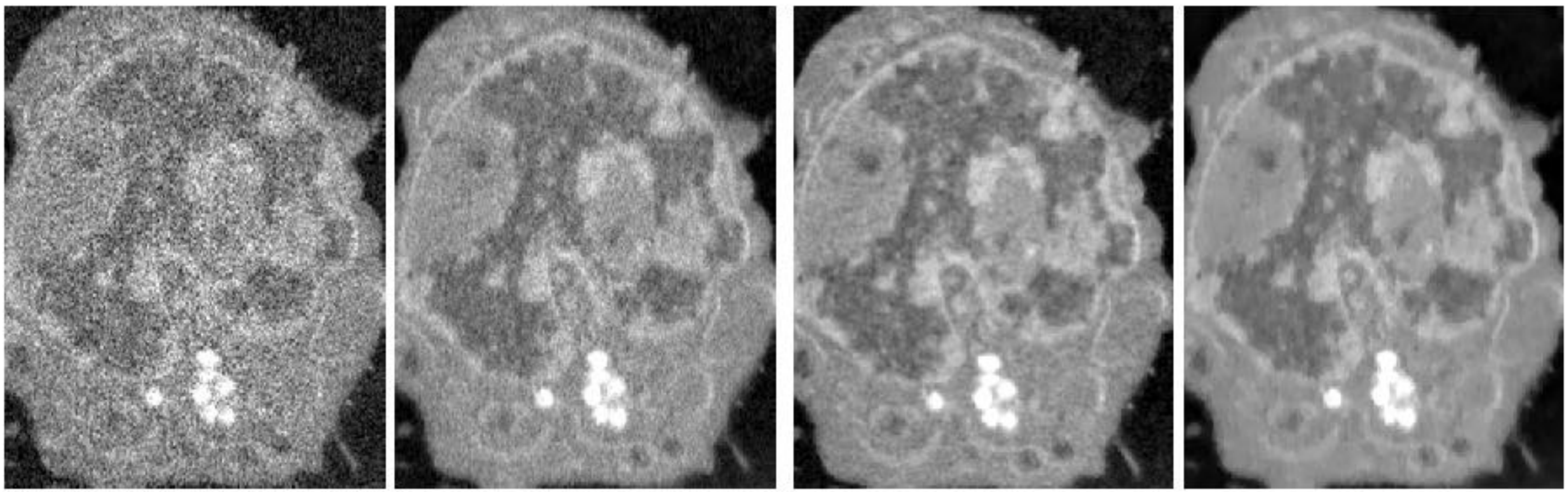

Noisy *Fast*	Good	Good	Over smoothed *Slow*

Computationally intense

Tomographic Reconstruction Methods

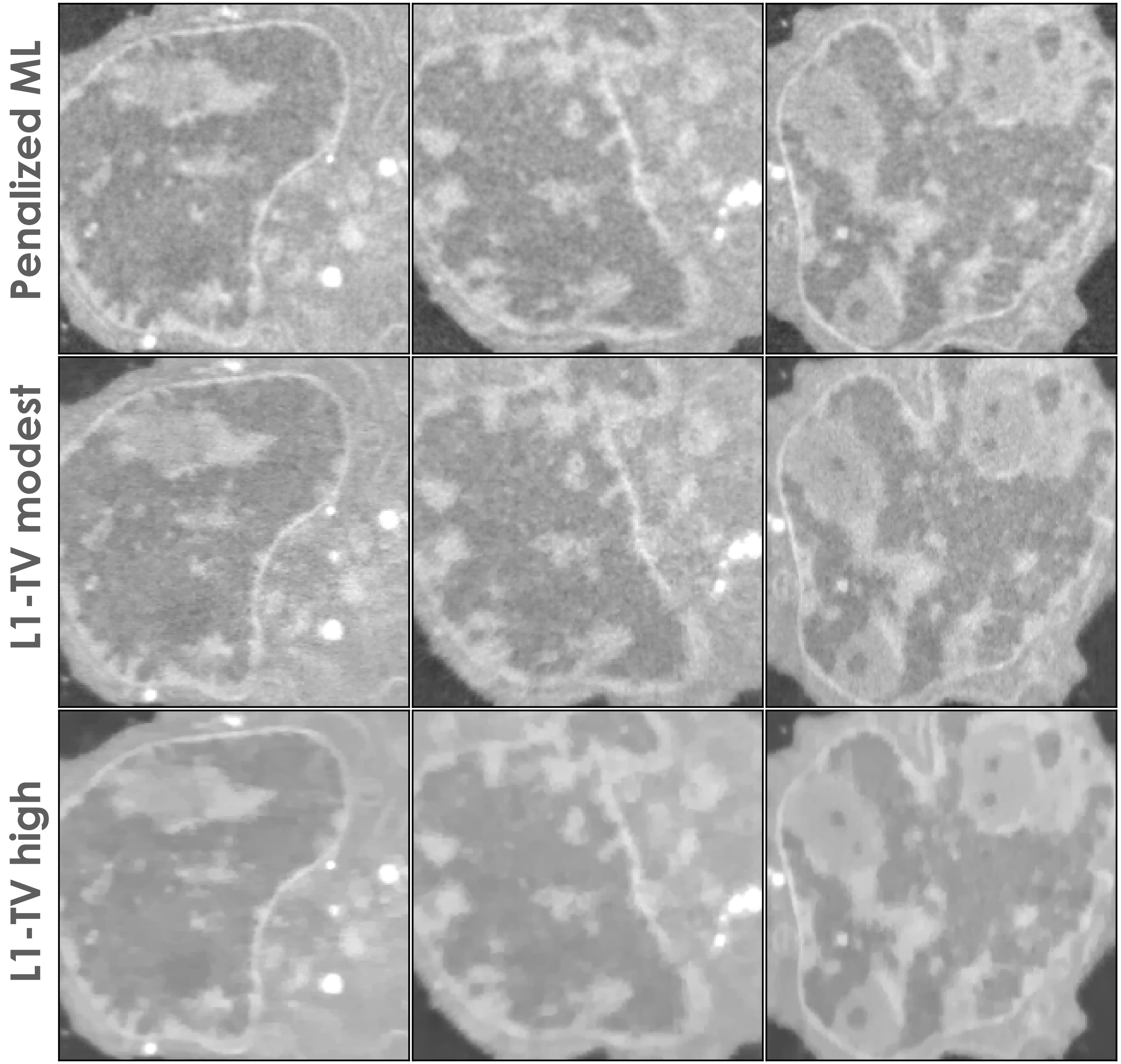

Measuring Radiation Damage in Full-rotation SXT

Radiation damage - visual inspection

SXT Reconstructions

No visible radiation damage after typical radiation dose

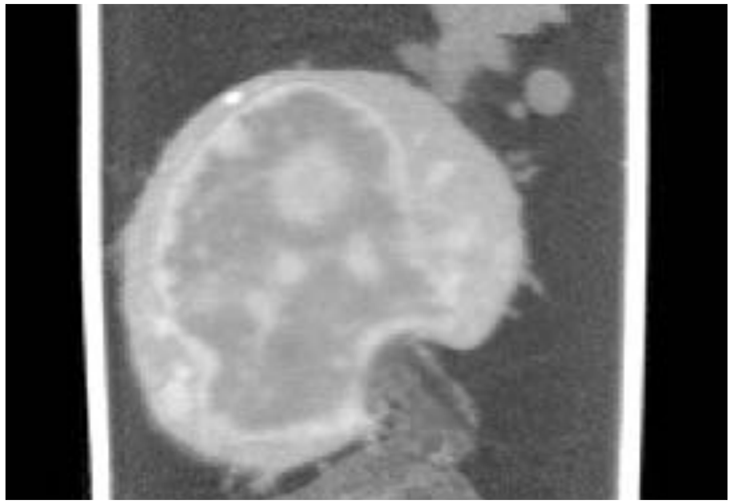

Visible radiation damage after 3x the typical dose

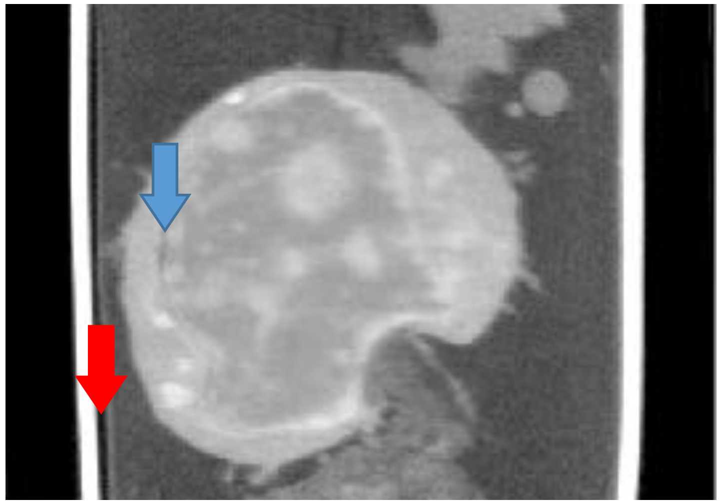

- Red arrowhead: region where the glass capillary has stretched.
- Blue arrowhead: indicates a crack in the specimen.

Radiation damage - quantification

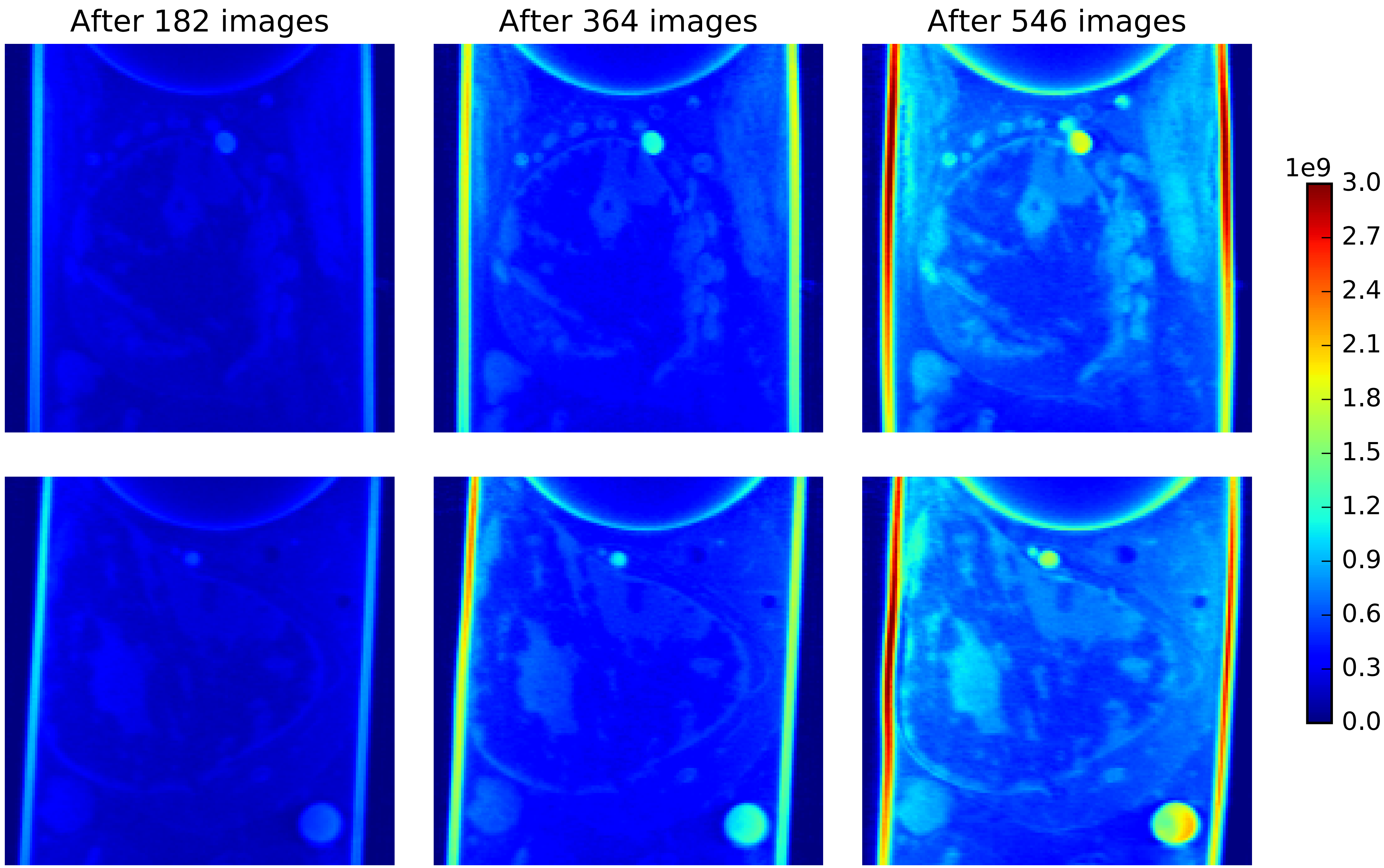

Orthoslices from two fields of view, color-coded according to absorbed radiation dose (see key). Capillary walls absorb highest dose.

Radiation damage - quantification

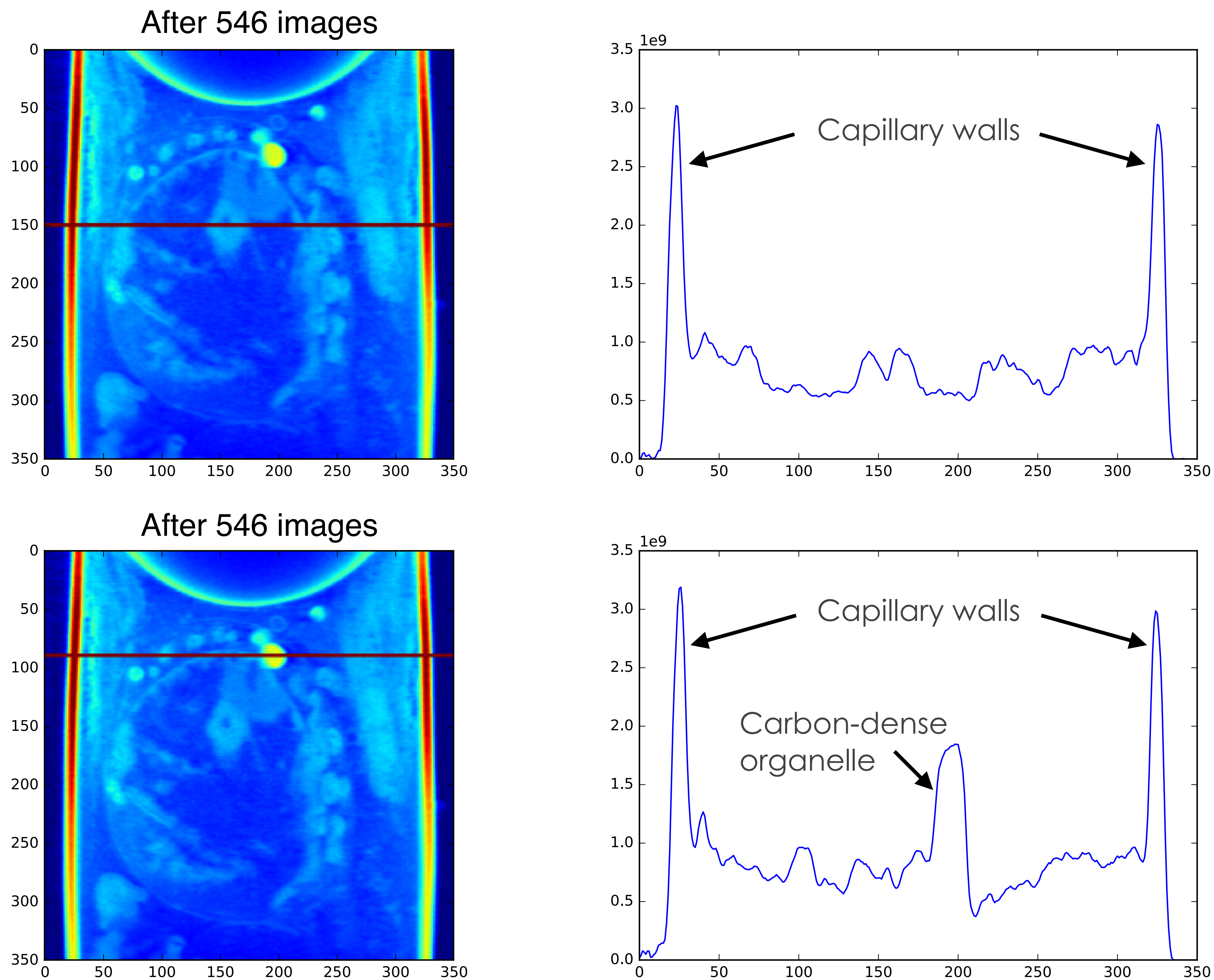

Orthoslices through a reconstruction of a cell

Graphs of calculated absorbed dose at points on a line (red) drawn through the orthoslices

Radiation damage - inspection with TEM

Vaccinia infected PtK2 cells

Cells on grids imaged with TEM:

Freeze subsitute, embedded in Lowicryl, thin section. **a, b)** Not previously imaged with soft x-ray tomography. **c, d)** Imaged with TEM after two x-ray tomograms.

No SXT **After SXT**

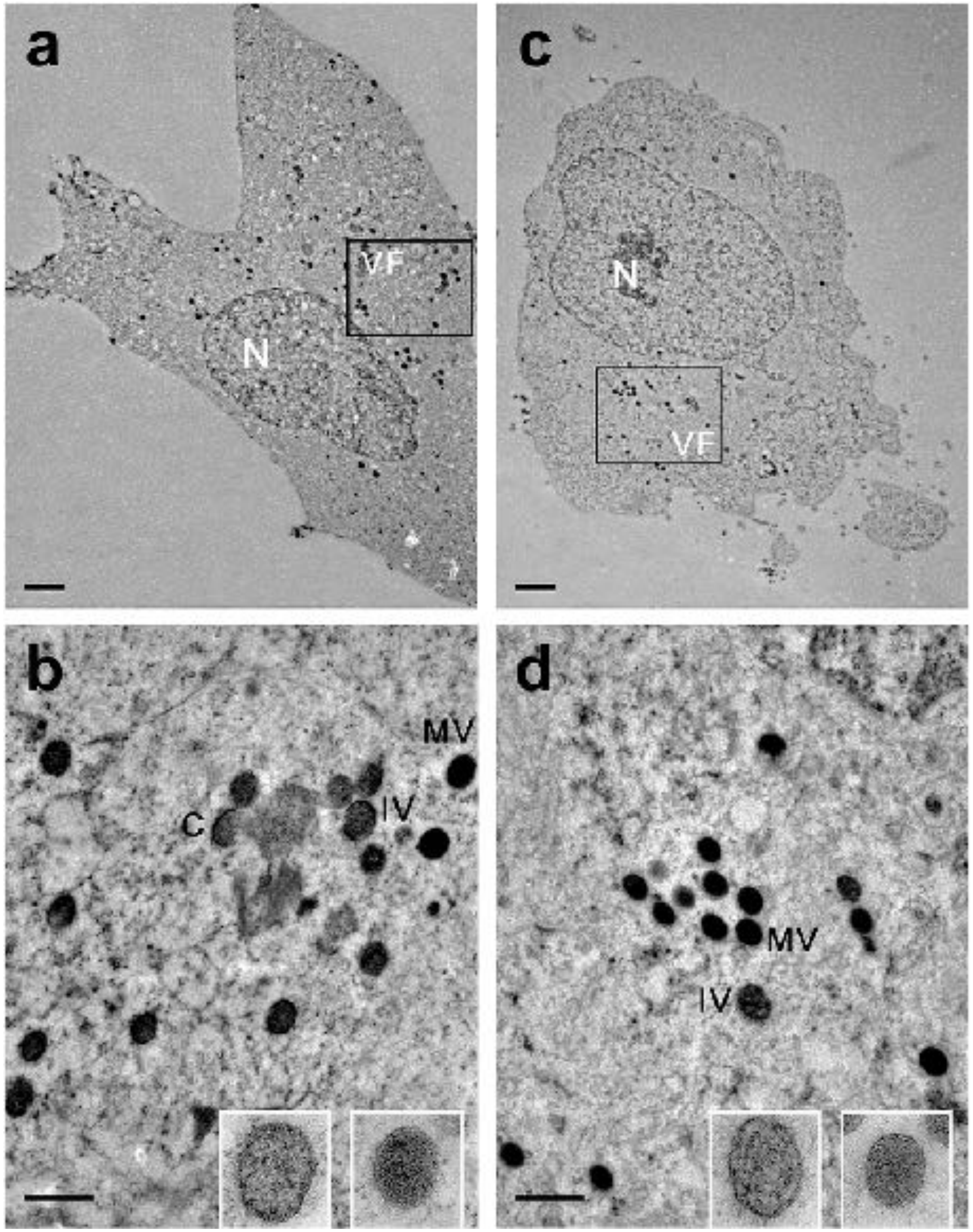

N, nucleus
VF, viral factory
C, viral crescent
IV, immature virus
MV, mature virus

Chichon et al., J. Structural Biology (2012) 177:202-211

Measuring Resolution

Full-rotation Tomography

Measuring resolution of soft x-ray microscope

SXM images of test objects

25 nm ZP | 15 nm ZP

19.5 nm half period

15.1 nm half period

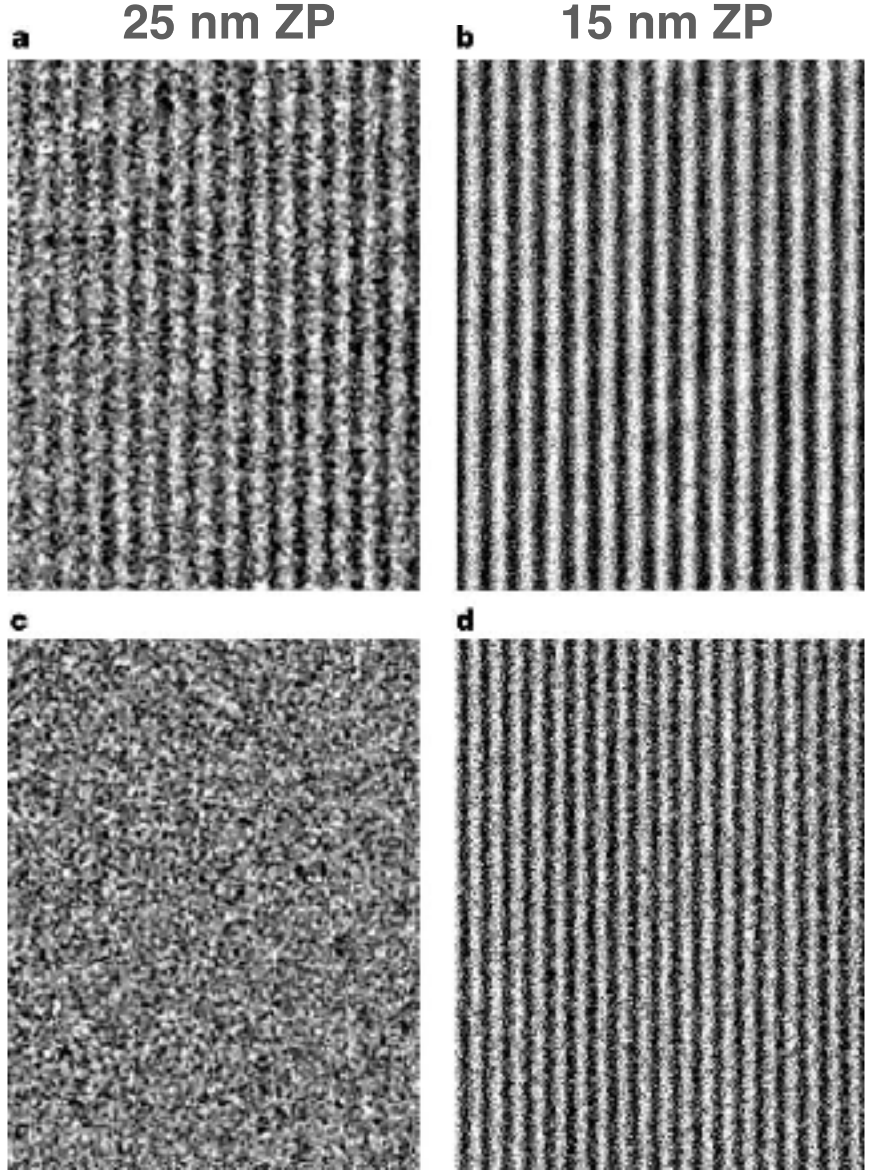

Modulation transfer functions

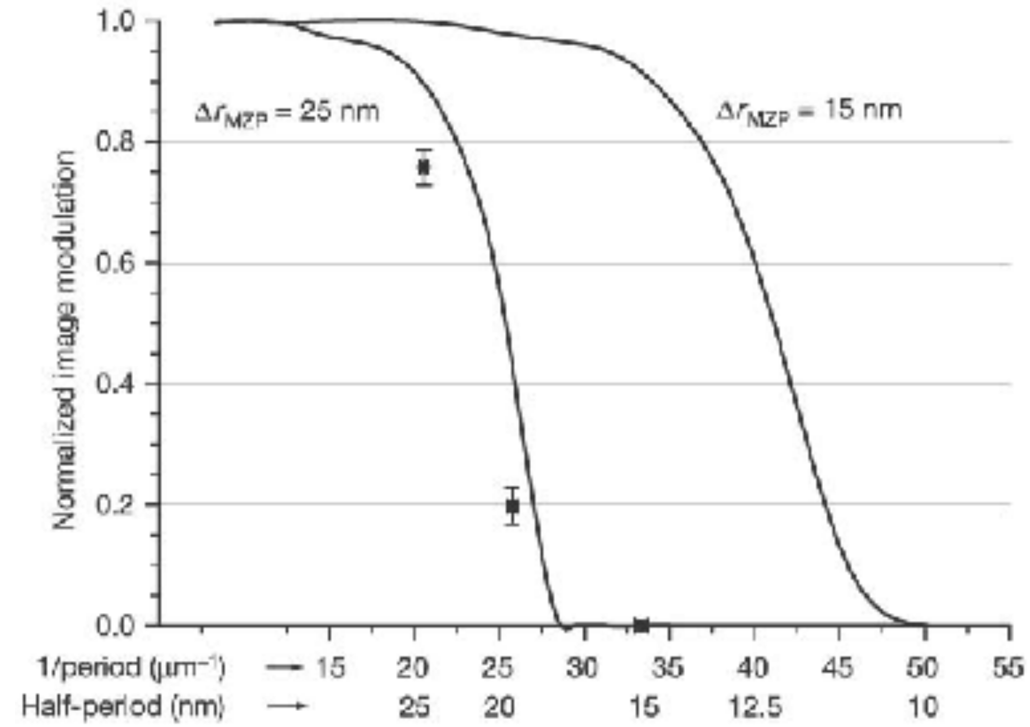

Chao et al. Nature. (2005) 435, 1210-1213.

Resolution Measurement of Yeast Cell

Full rotation tomography with 50 nm resolution zone plate on XM-2

S. cerevisiae

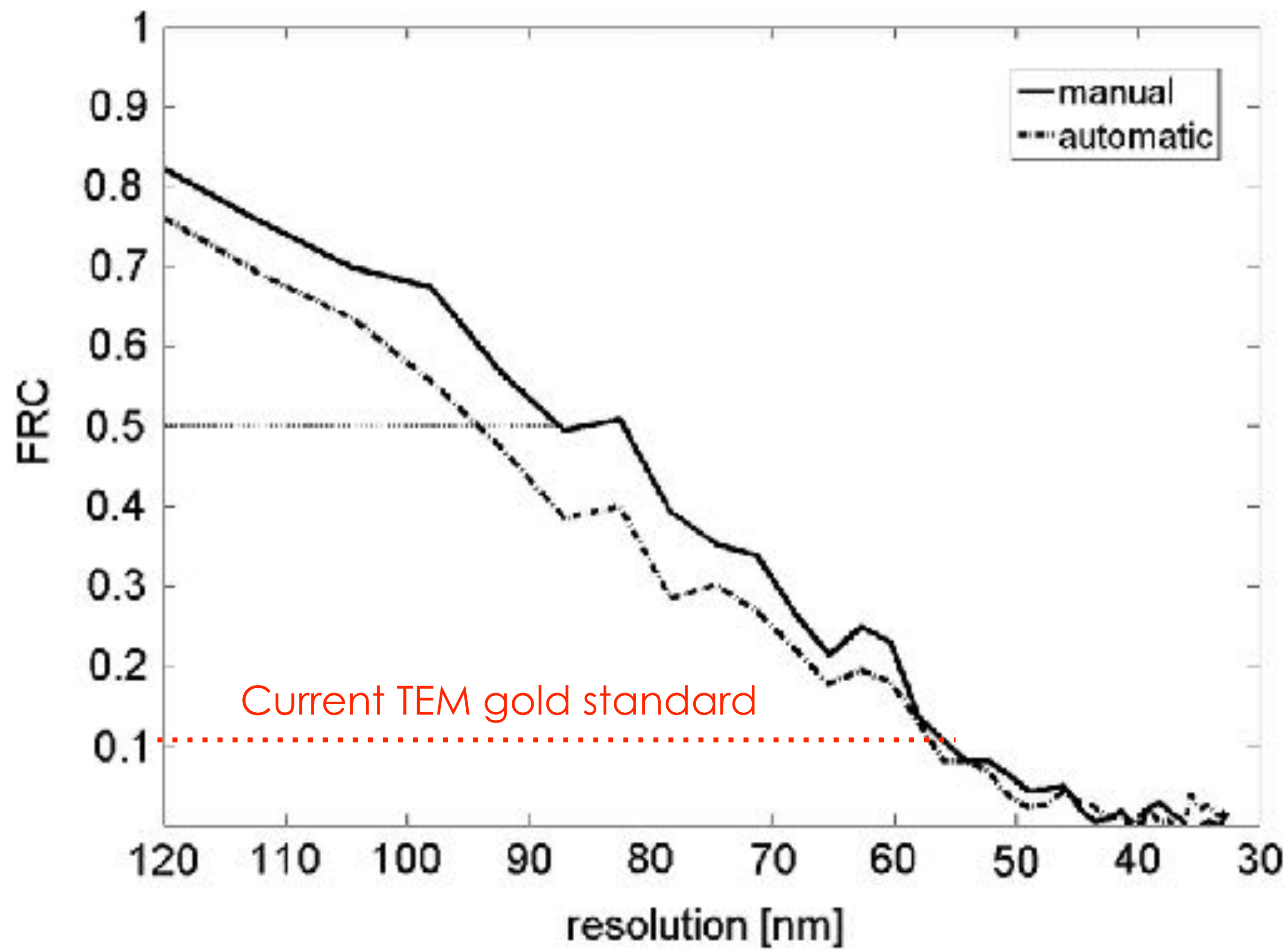

Comparison of Fourier Ring Correlation (FRC) curves calculated with the leave-one-out method.

Parkinson et al. J Structural Biology. (2012) 177, 259-266.

Resolution Measurement of Mammalian Cell

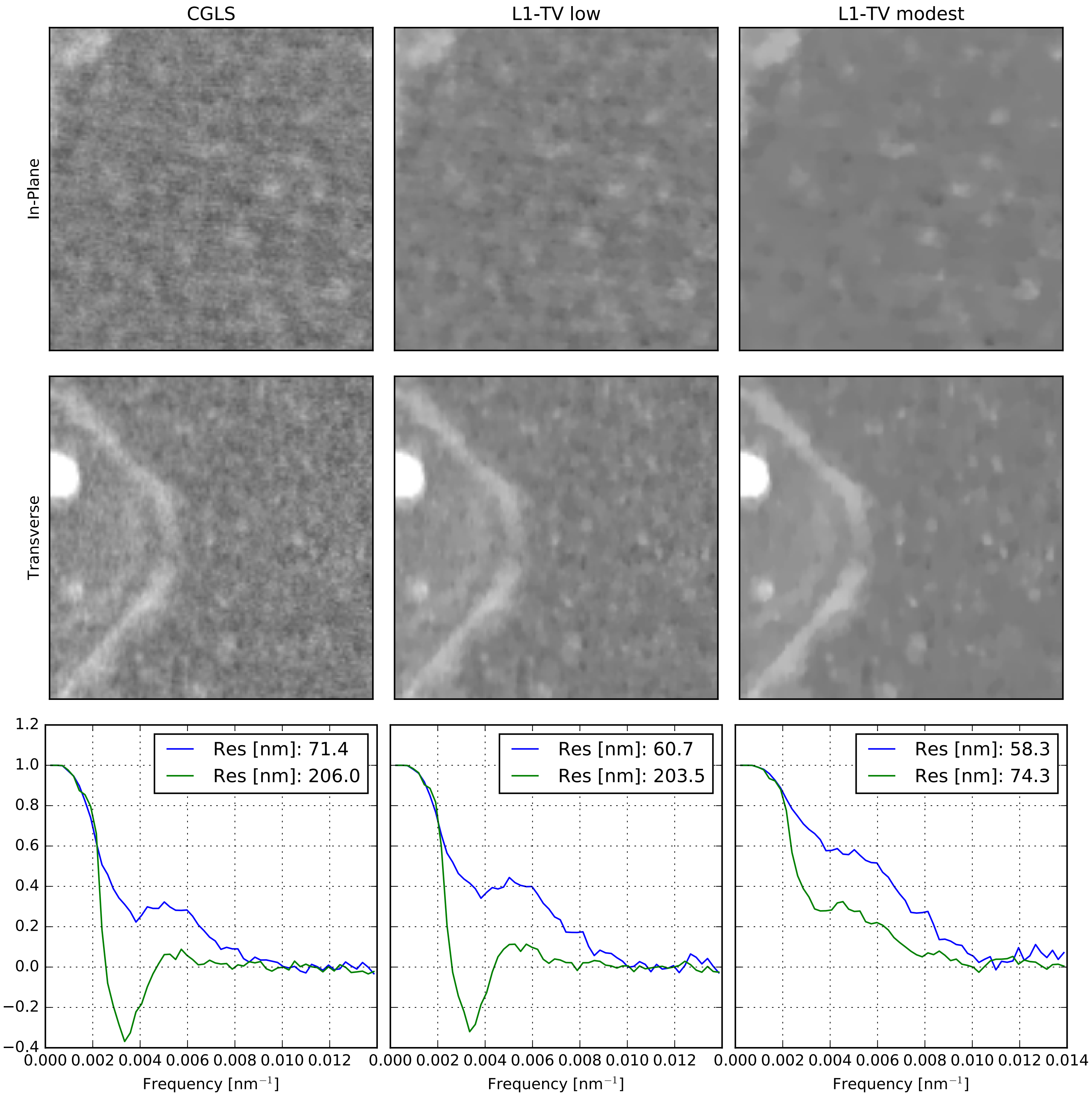

60 nm resolution zone plate

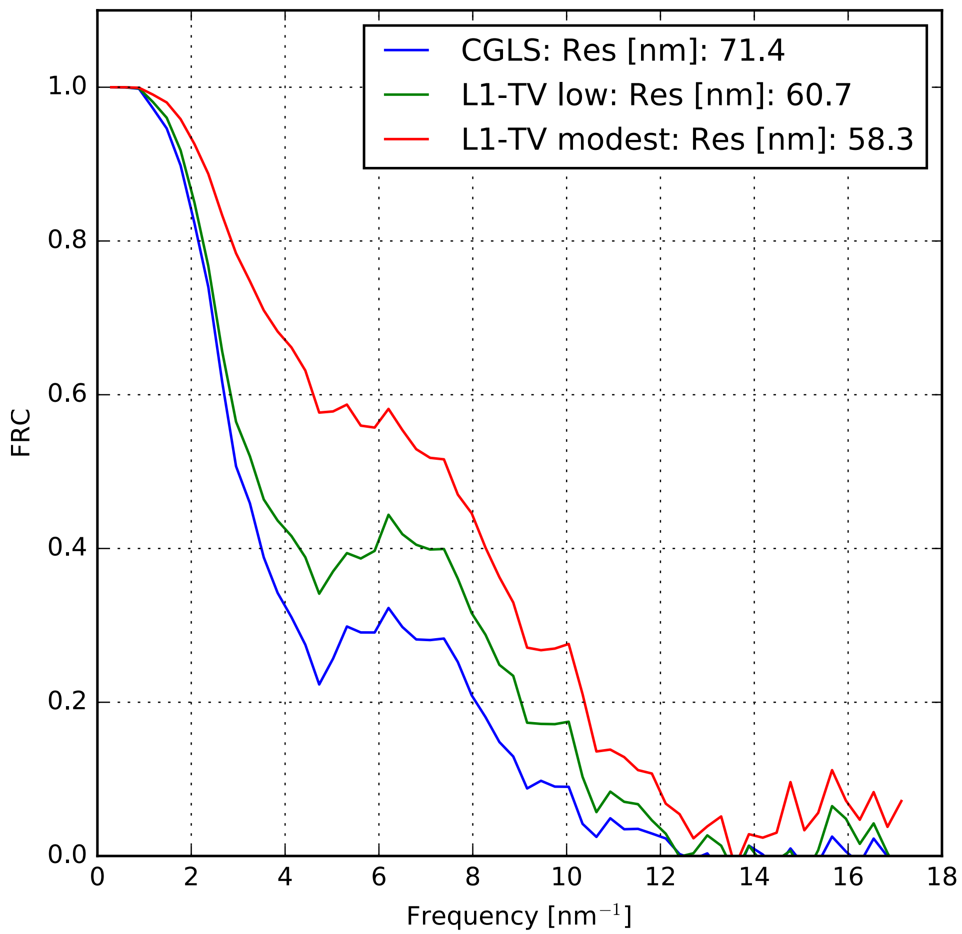

Resolution Measurement of Mouse Sperm

Full rotation tomography with 50 nm resolution zone plate on XM-2

Rayleigh resolution measured to be 61 nm (50 nm zone plate)

Mouse sperm

Measuring Resolution

Limited-tilt Tomography

Full Rotation vs. Limited-Tilt Tomography

± 90°

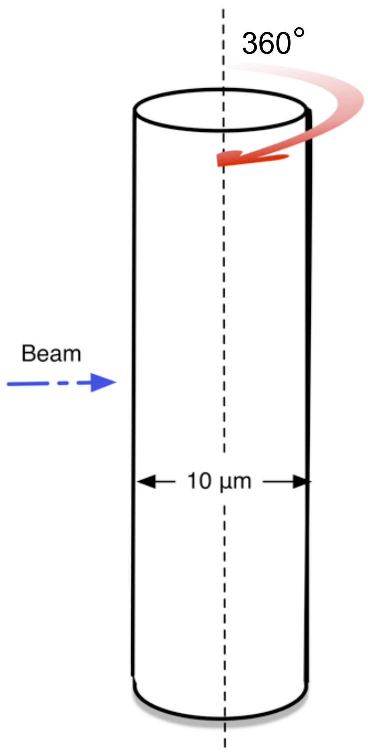

± 72°

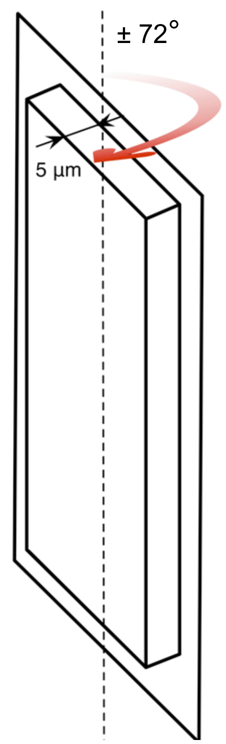

16 µm thick at ± 72°

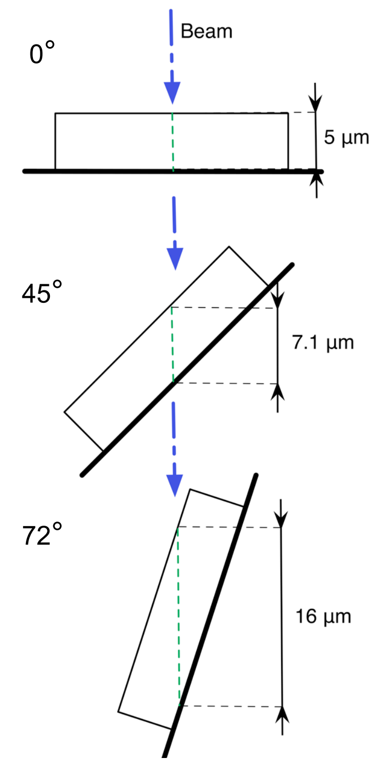

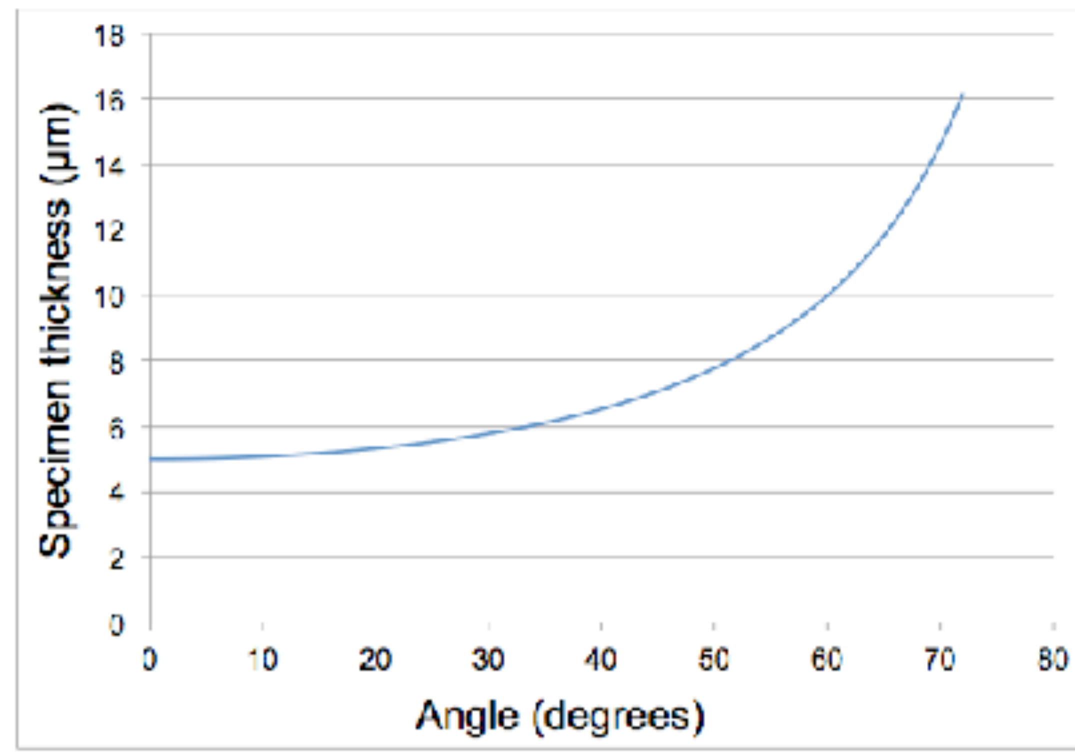

Cinquin et al. J Cellular Biochemistry. (2014) 115, 2009-216.

Full Rotation vs. Limited-tilt Tomography

Doesn't take into consideration out-of-focus information with increased thickness

180° rotation (± 90°) | **150° rotation (± 75°)** | **120° rotation (± 60°)** | **90° rotation (± 45°)**

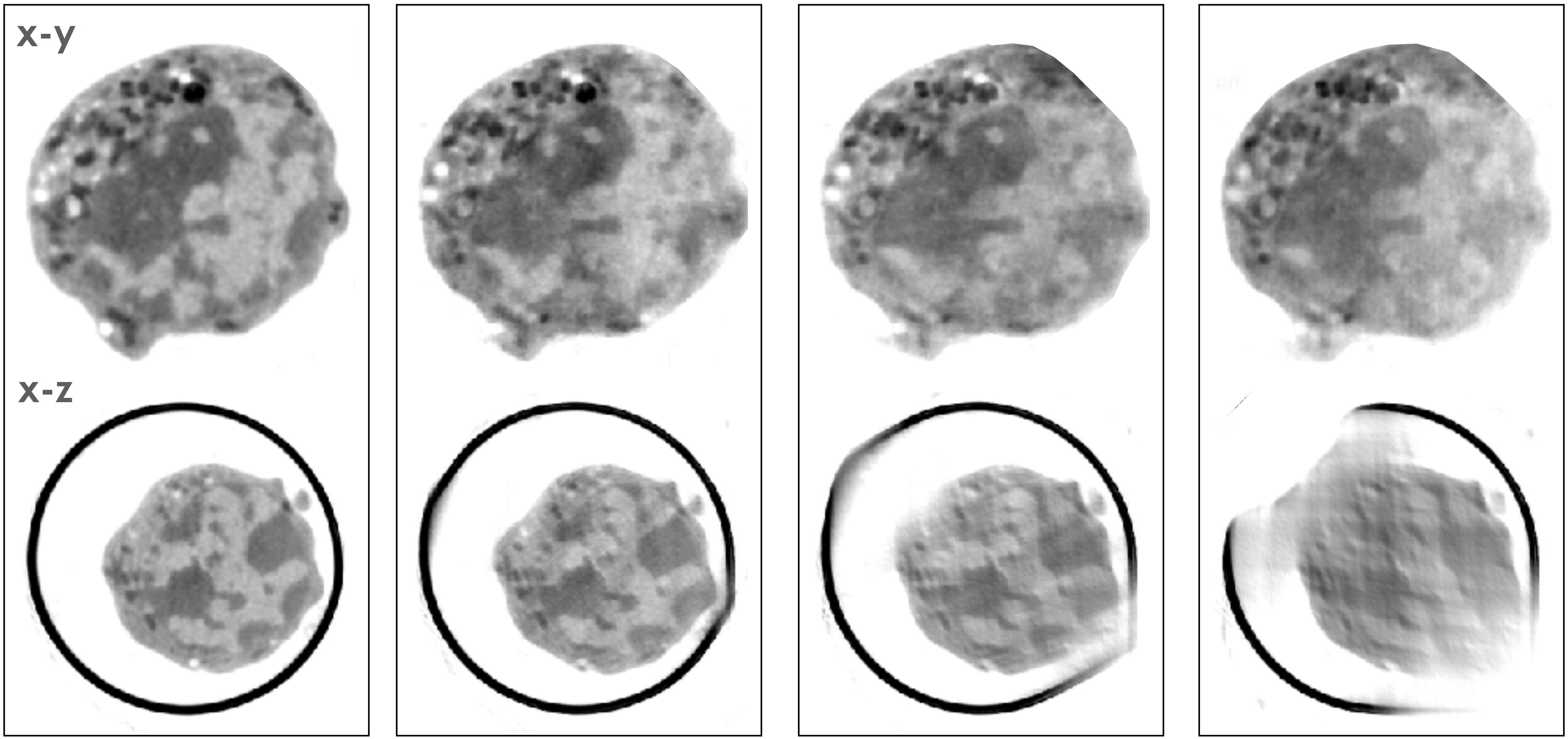

Measuring Resolution

Limited-tilt tomography using 25 nm resolution zone plate

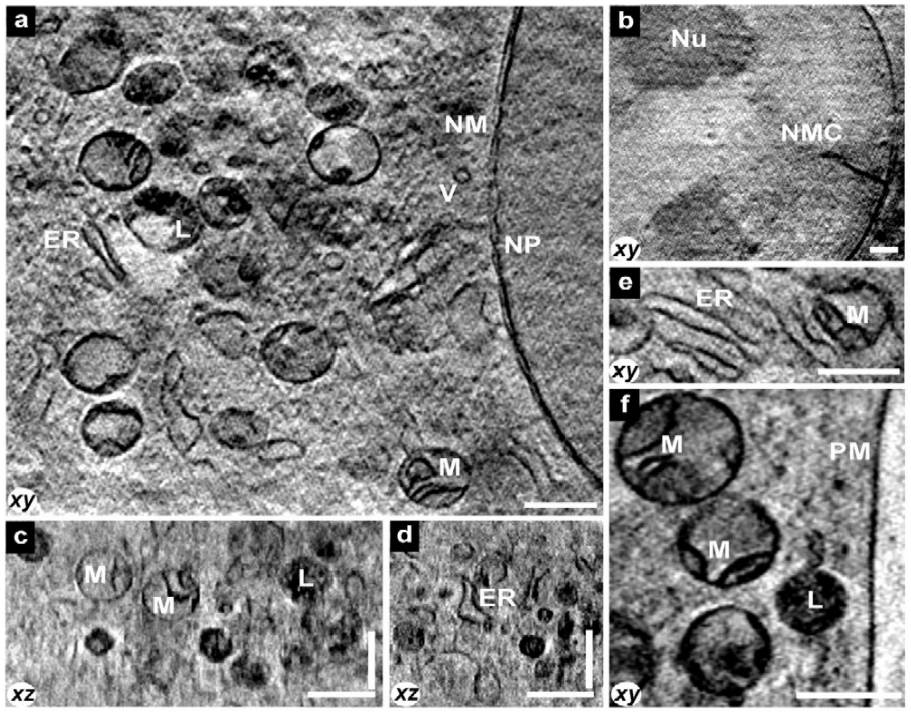

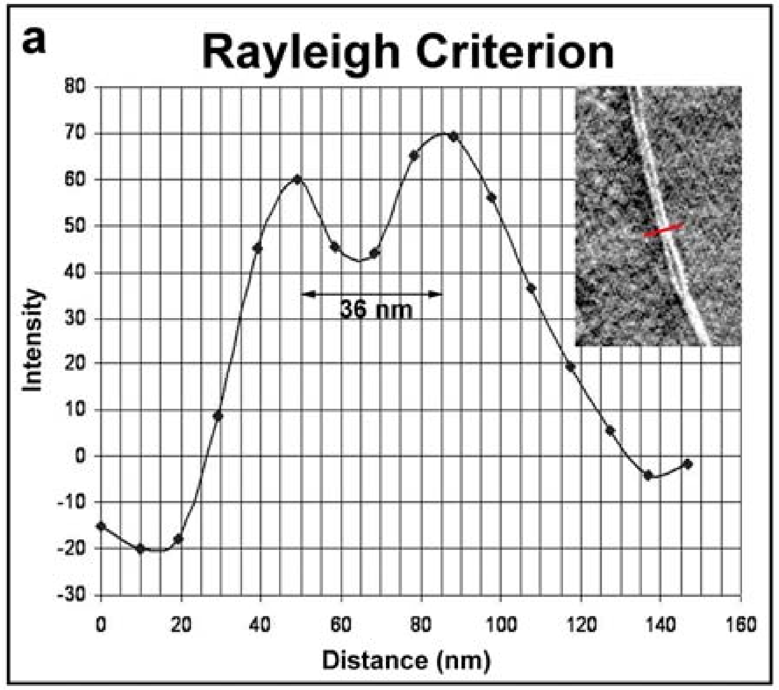

Calculated from high contrast features in the x,y slice

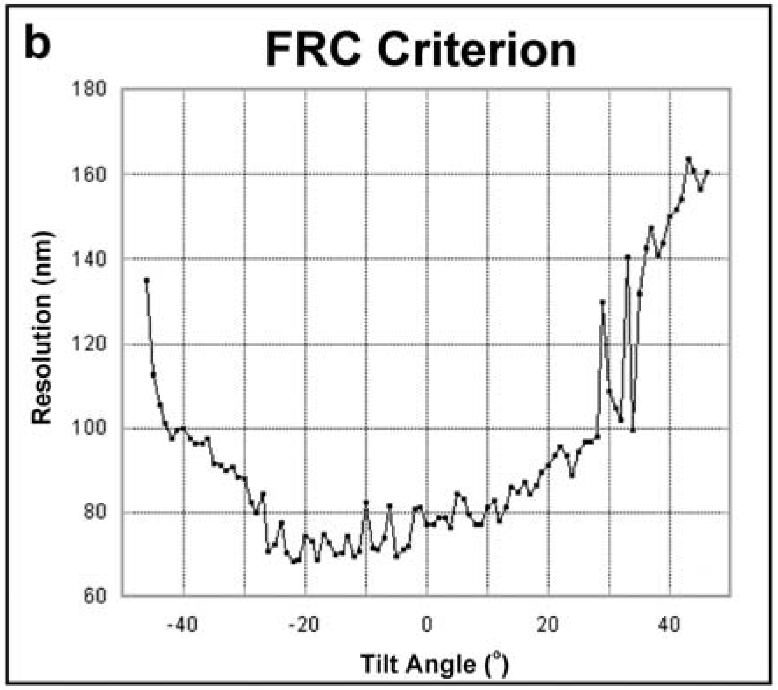

Calculated from the entire tomogram, for all contrast ranges

FRC Criterion: *Unlike the Rayleigh criterion which is calculated from high contrast features in an xy slice, the FRC criterion is calculated from the entire tomogram and for all contrast ranges. The resolution achieved at each tilt angle is shown (b). Because this method is sensitive to the thickness of the specimen, the highly tilted images have the worst resolution, while those with lower tilt angles show a best resolution of ~70 nm. While a good comparative measure of the quality of a tomogram, the FRC analysis reflects all the imperfections in the tomographic data, such as the restriction to a limited tilt range, the inclusion of adjacent areas in the tomographic reconstruction, variations in focus due to specimen thickness, and the ever-present noise.*

Schneider et al. Nature Methods. (2010) 7(12), 985-987.

Measuring Resolution

Limited-tilt tomography

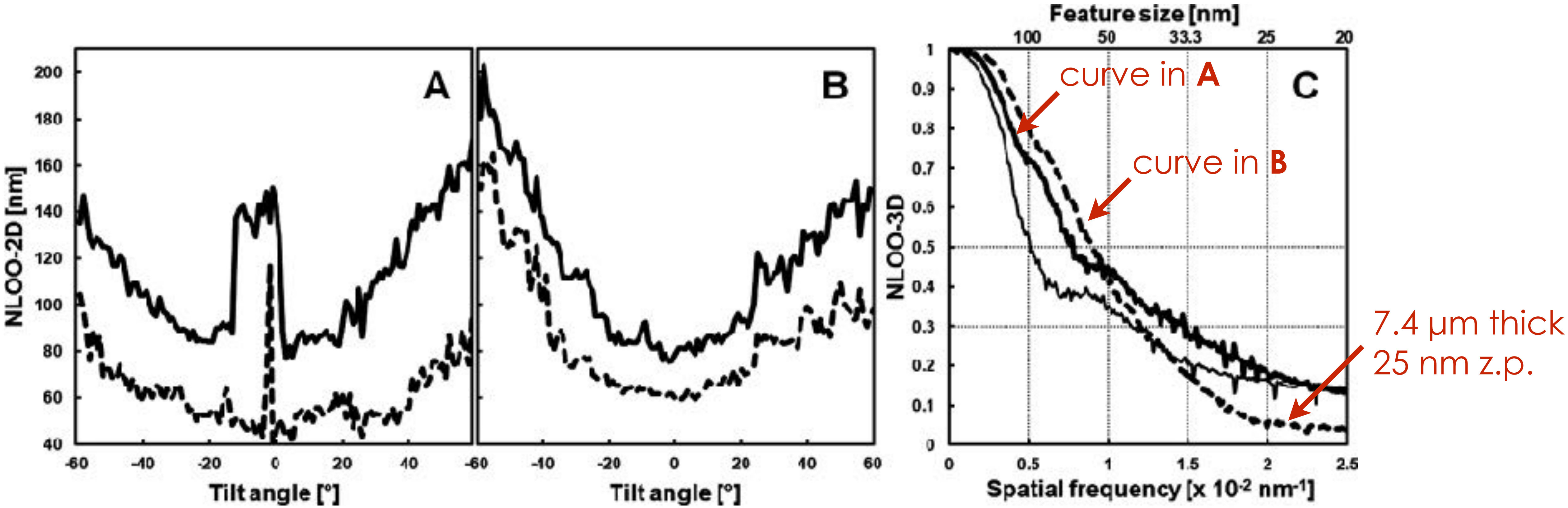

4.4 µm thick sample
25 nm zone plate

4.4 µm thick sample
40 nm zone plate

cutoff threshold 0.3

Hagen et al. J. Structural Biology. (2012) 177, 193-201.

Linear Absorption Coefficient

(LAC) Measurements

X-ray Tomography is Quantitative

Absorption adheres to Beer-Lambert's law; is linear with thickness, composition & concentration

Absorption coefficient measurements

BSA and hemoglobin

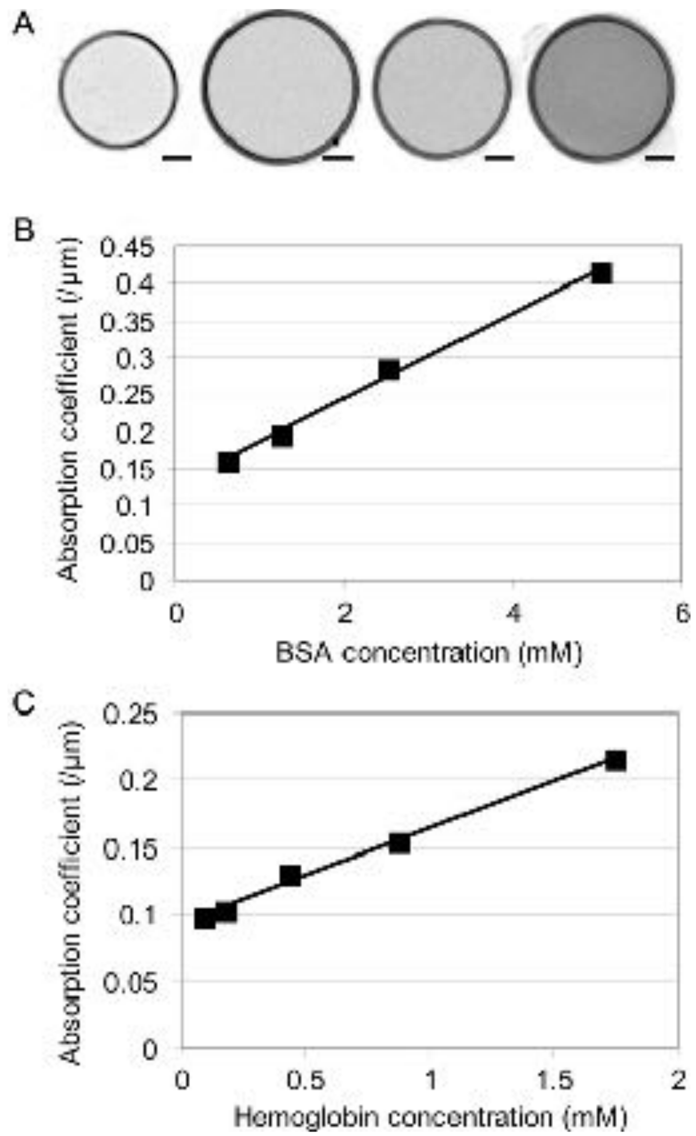

Hemoglobin concentration
validated spectrophotometrically

Alcohol oxidase crystal in yeast

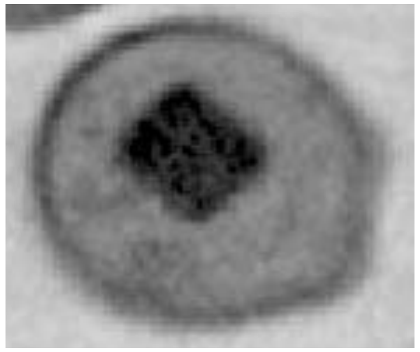

Calculated LAC - 0.625 μm^{-1}

Measured LAC - 0.626 μm^{-1}

Hanssen et al. J. Structural Biology. (2012) 177, 224-232

Candida albicans

	Average LAC (μm^{-1})
Lipid droplets	0.75 ± 0.09
Mitochondria	0.45 ± 0.03
Nuclei	0.28 ± 0.03
Nucleoli	0.37 ± 0.04
Vacuoles	0.20 ± 0.03

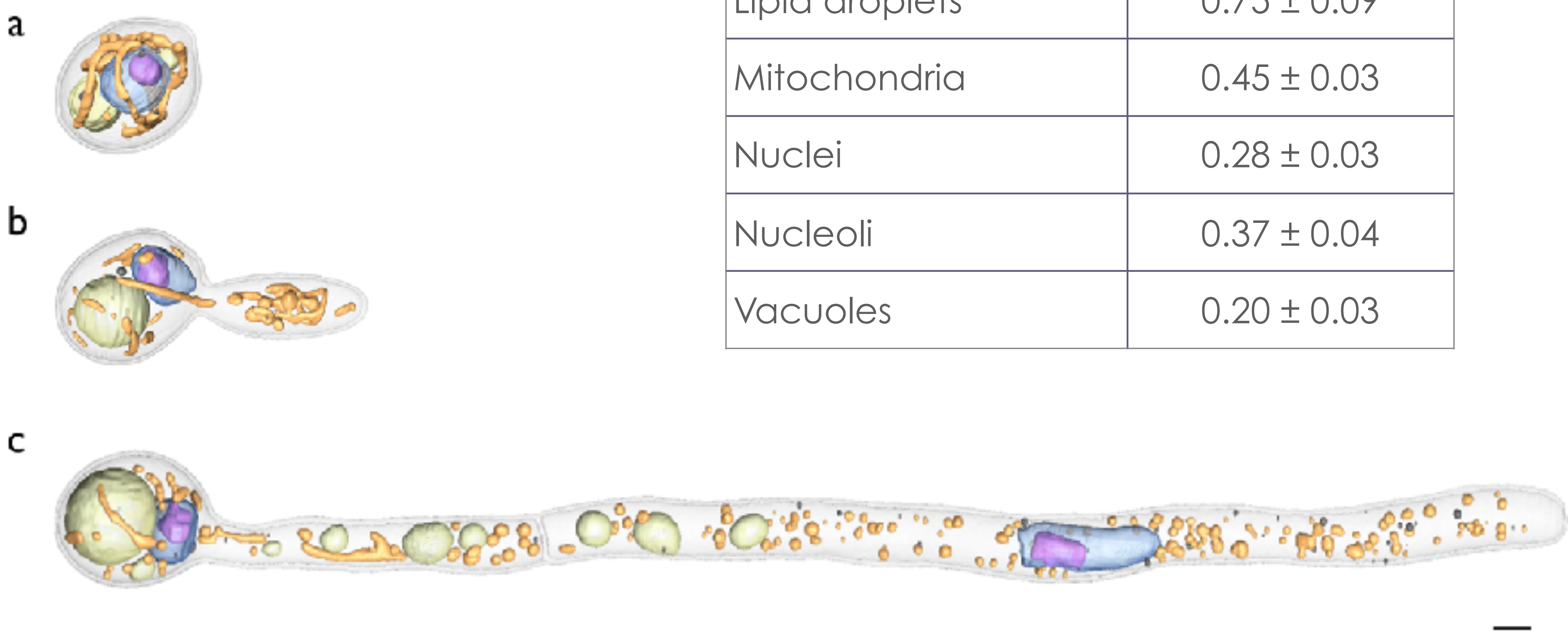

McDermott et al. Trends Cell Biol. (2009) 19(11), 587-595

Saccharomyces cerevisiae

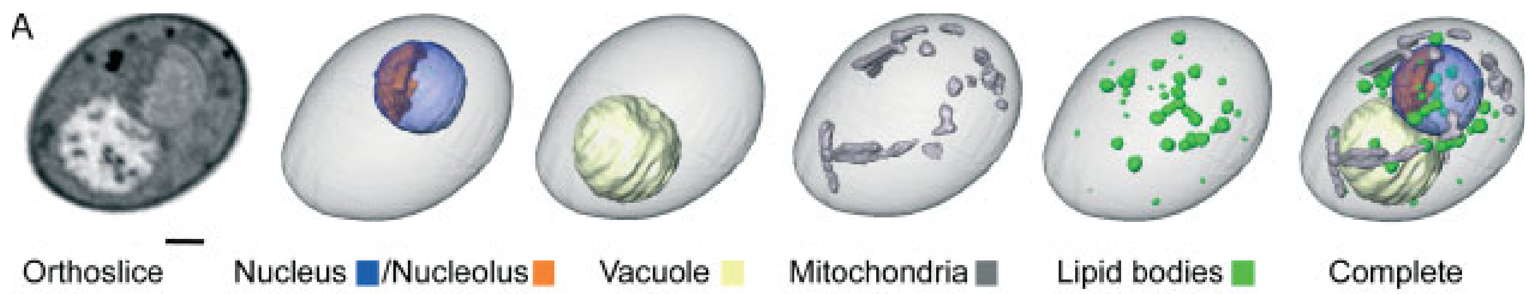

B

	LAC values (μm^{-1})
Nucleus	0.26 ± 0.01
Nucleolus	0.33 ± 0.01
Vacuole	0.22 ± 0.07
Mitochondria	0.36 ± 0.02
Lipid bodies	0.55 ± 0.05

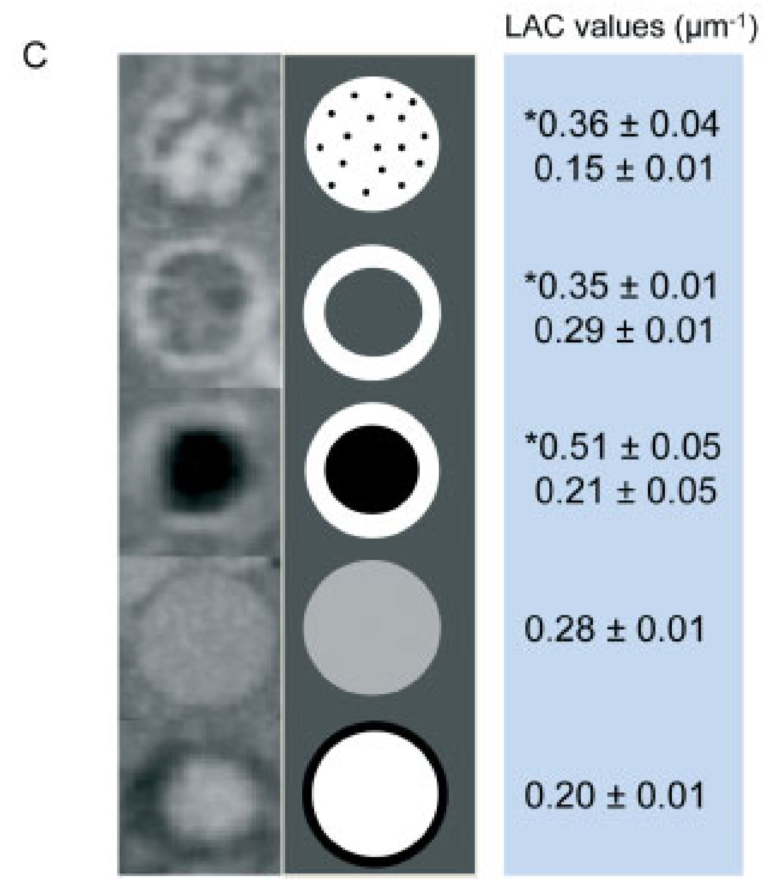

Uchida et al. Yeast. (2011) 28, 227-236.

Schizosaccharomyces pombe

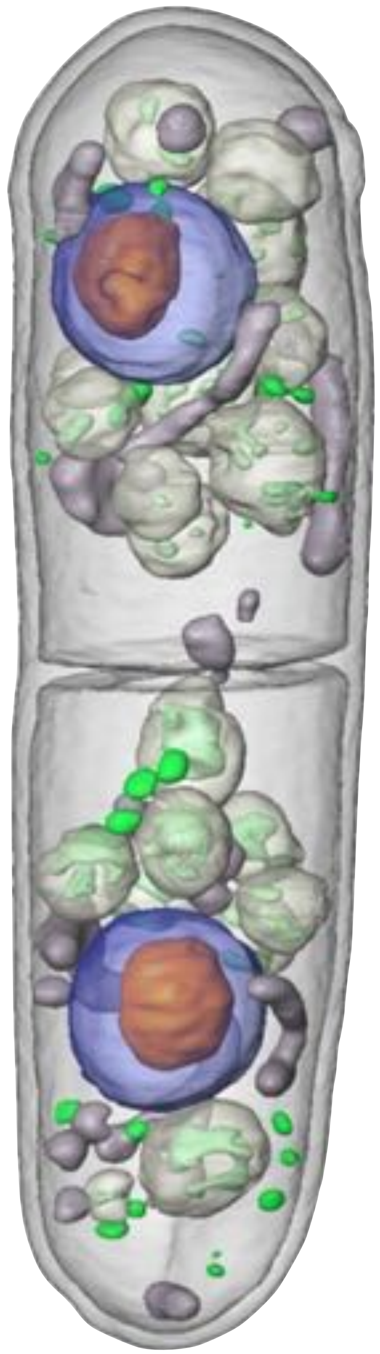

	Volume (μm^3)	Average LAC (μm^{-1})
Growth medium		0.11
Model protein ($C_{94}H_{139}N_{24}O_{31}$)		1.35
Glass capillary		1.0
Lipids	0.45	0.72
Mitochondria	2.97	0.42
Nuclei	4.59, 4.90	0.31
Nucleoli	0.74, 0.71	0.37
Endosomes	13.9	0.23
Endosome inclusions	1.15	0.42

McDermott et al. Trends Cell Biol. (2009) 19(11), 587-595
Uchida et al. Mol Biol. Cell. (2010) 21, 4299, 2654/B

Human Lymphoblastoid Cell

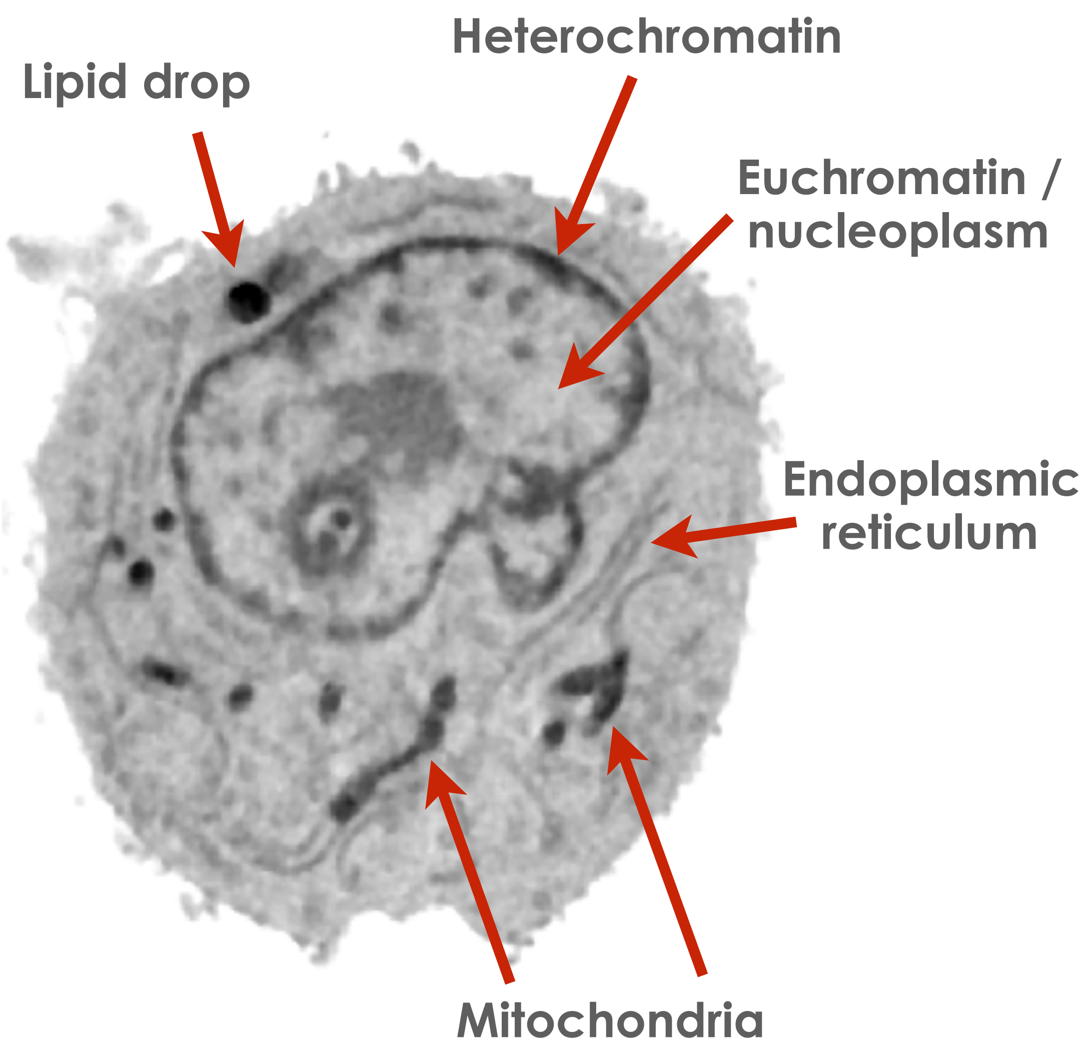

	Average LAC (μm^{-1})
Growth medium	0.11
Glass capillary	1.0
Lipid drops	0.73
Mitochondria	0.31 - 0.36
Endoplasmic reticulum	0.26 - 0.31
Golgi apparatus	0.25 - 0.29
Heterochromatin	> 0.25
Euchromatin	< 0.25

National Center for X-ray Tomography (NCXT), supported by NIH-NIGMS and DOE-BER

3D Volumes of Organelles

Manual Segmentation

Saccharomyces cerevisiae

Diploid

Haploid

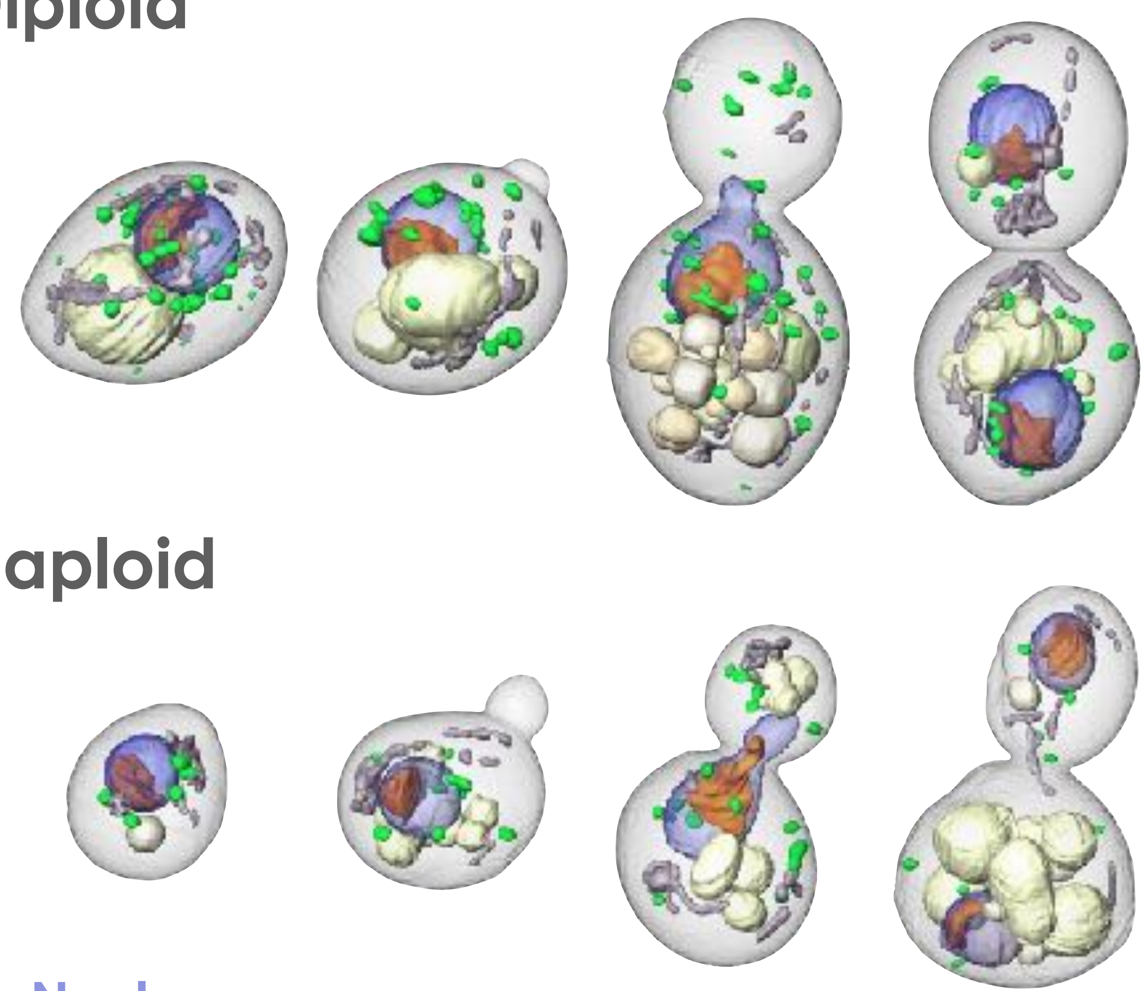

Nucleus
Nucleolus
Mitochondria
Vacuole
Lipid

Tutorials at ncxt.lbl.gov

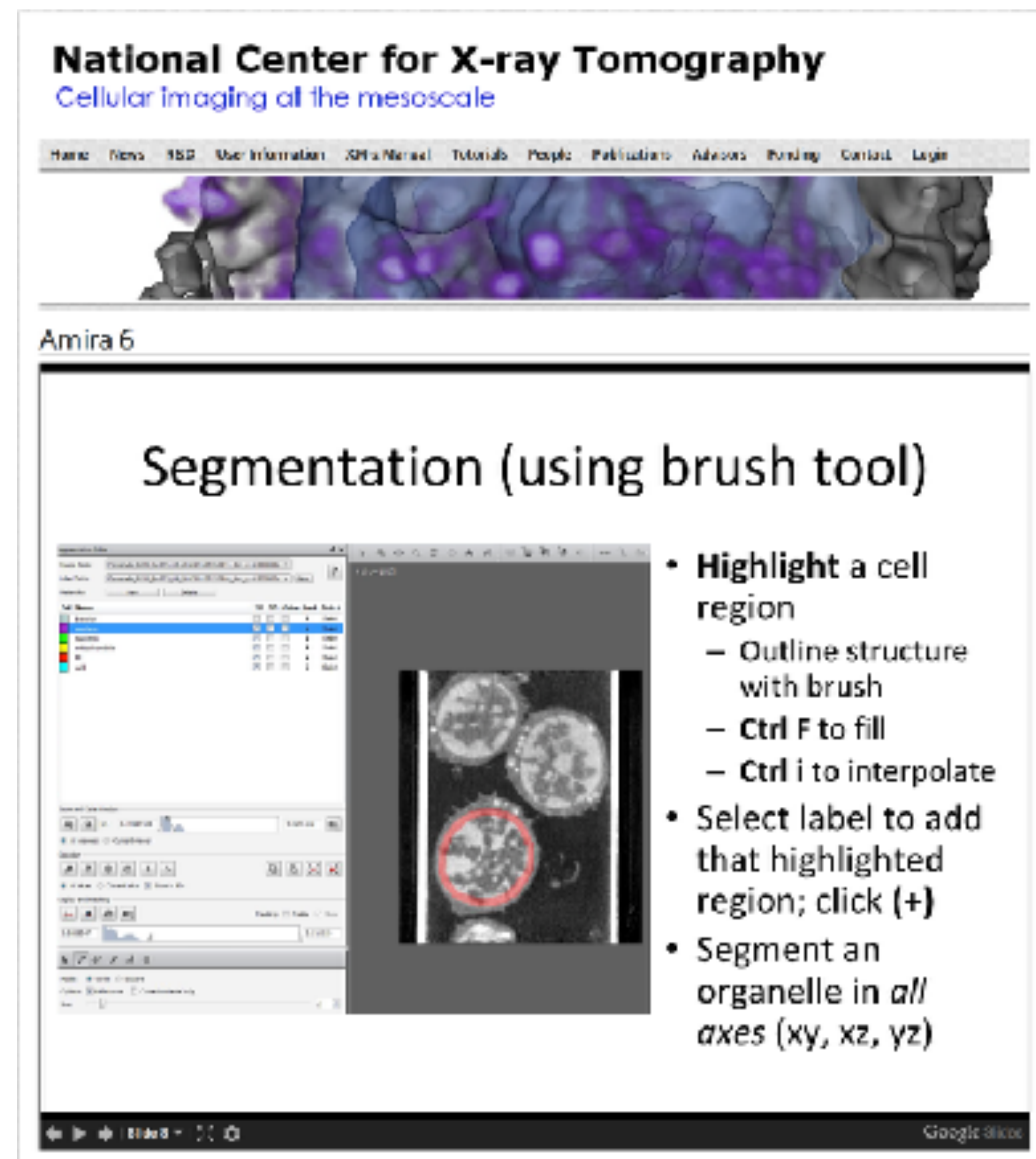

Slide from segmentation tutorial

3D Volumes of Organelles

Semi-Automatic Segmentation

Segment using Linear Absorption Coefficient

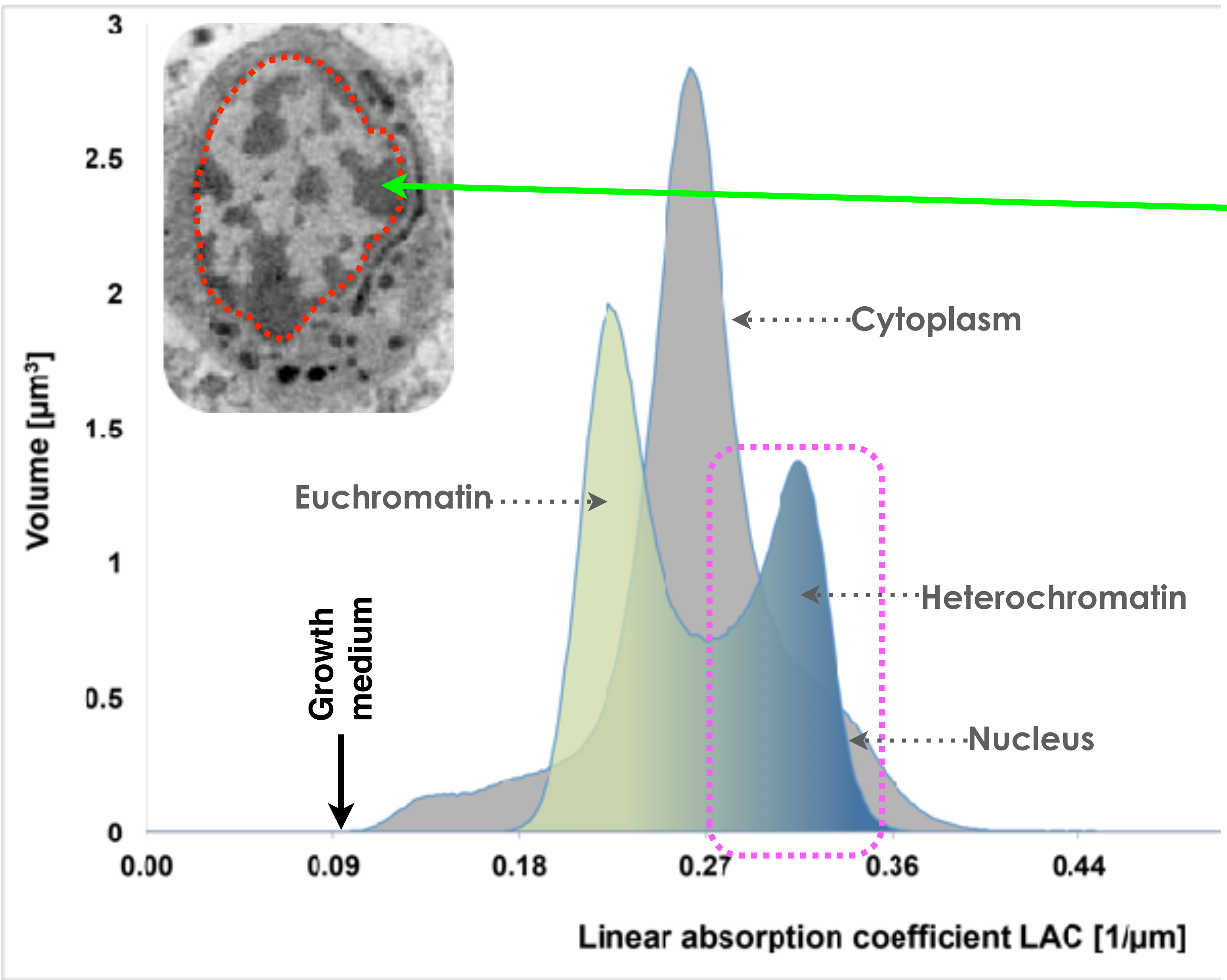

Nucleus seen in Amira

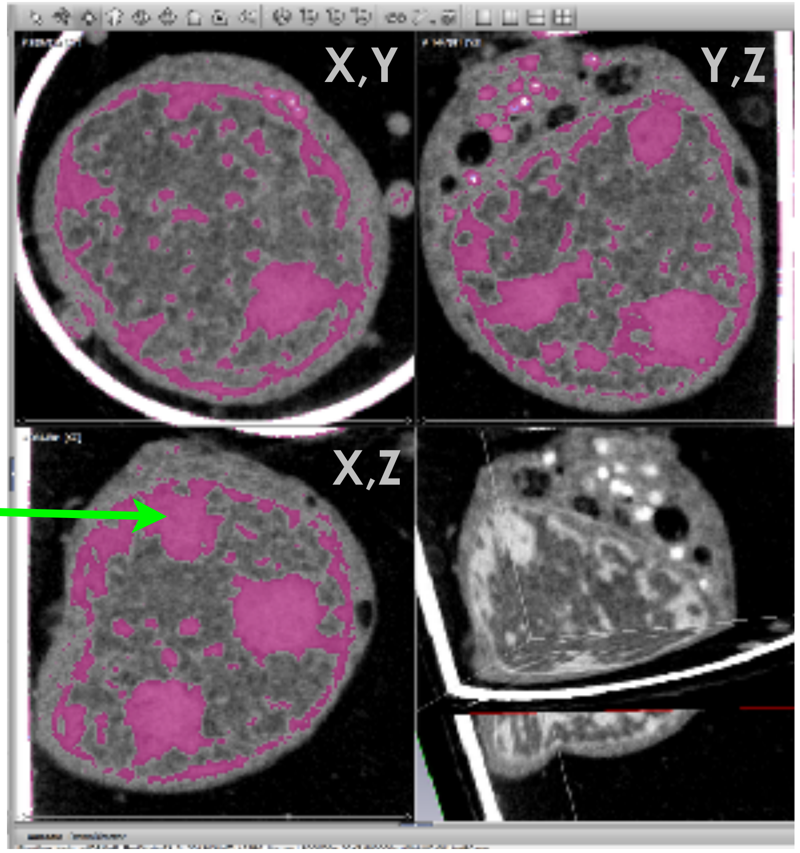

- Manually segment nucleus (red)
- Plot histogram
- High LAC peak corresponds to region of nucleus called heterochromatin (in program Amira)

Segment using Linear Absorption Coefficient

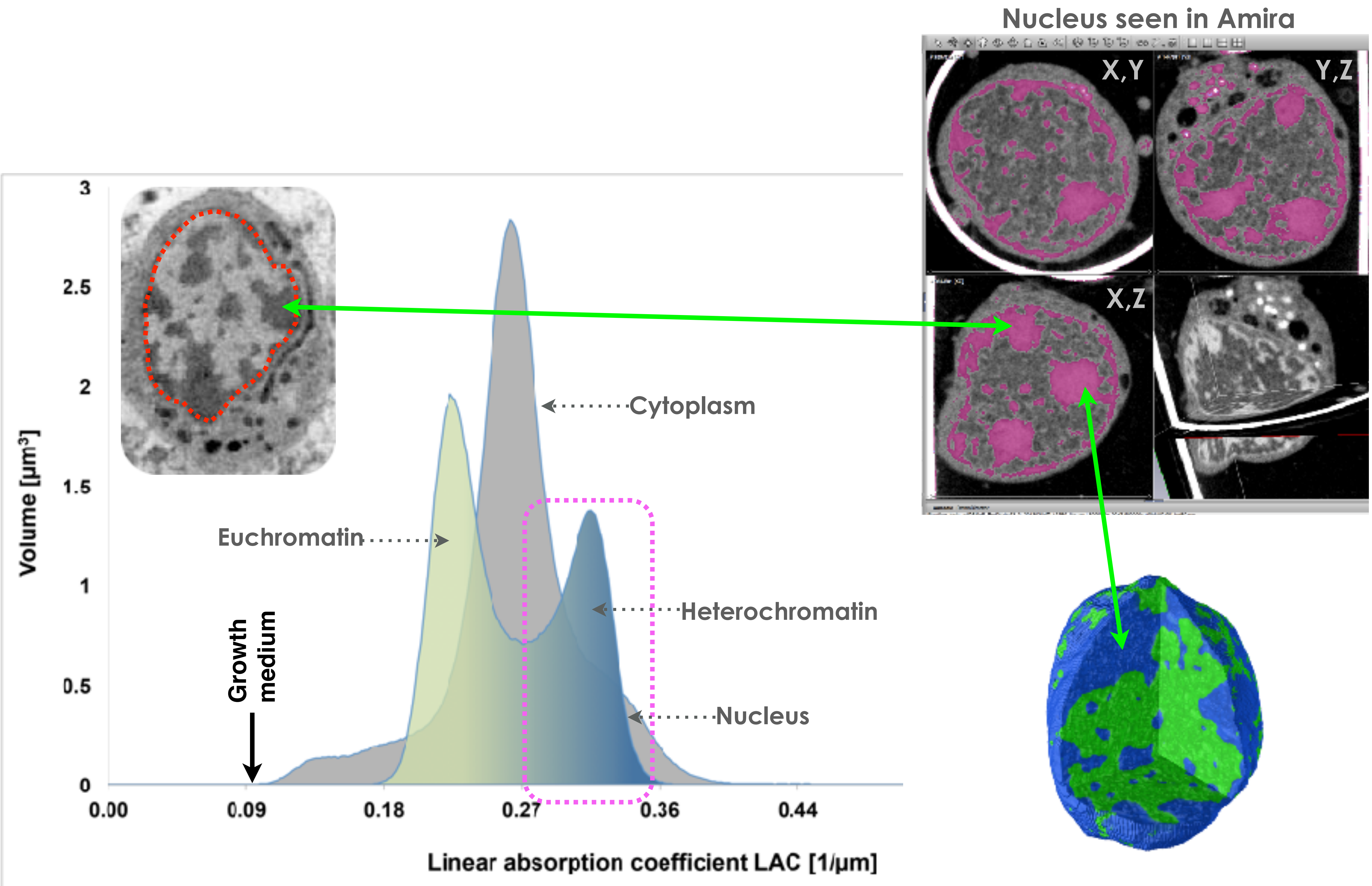

Segment using Linear Absorption Coefficient

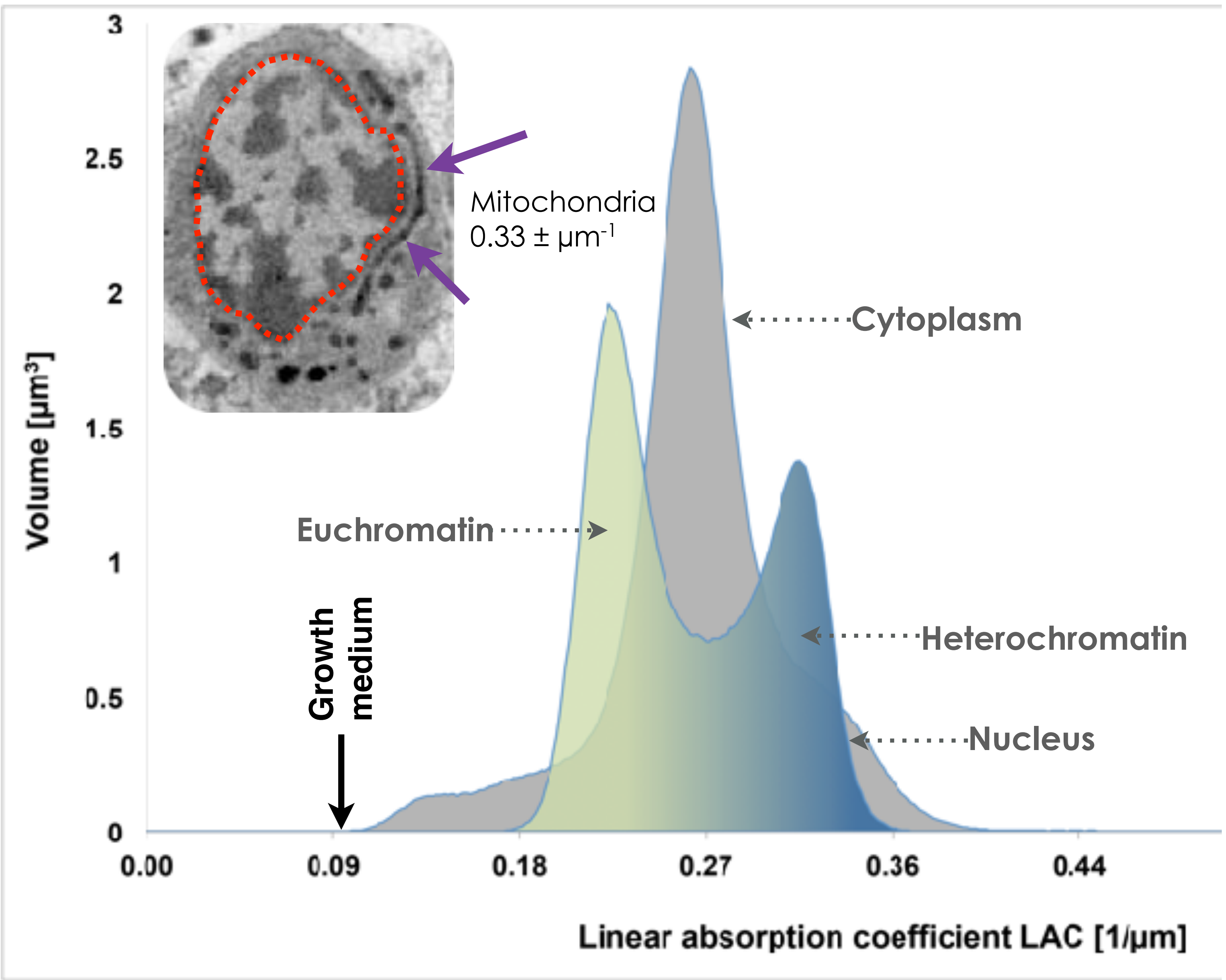

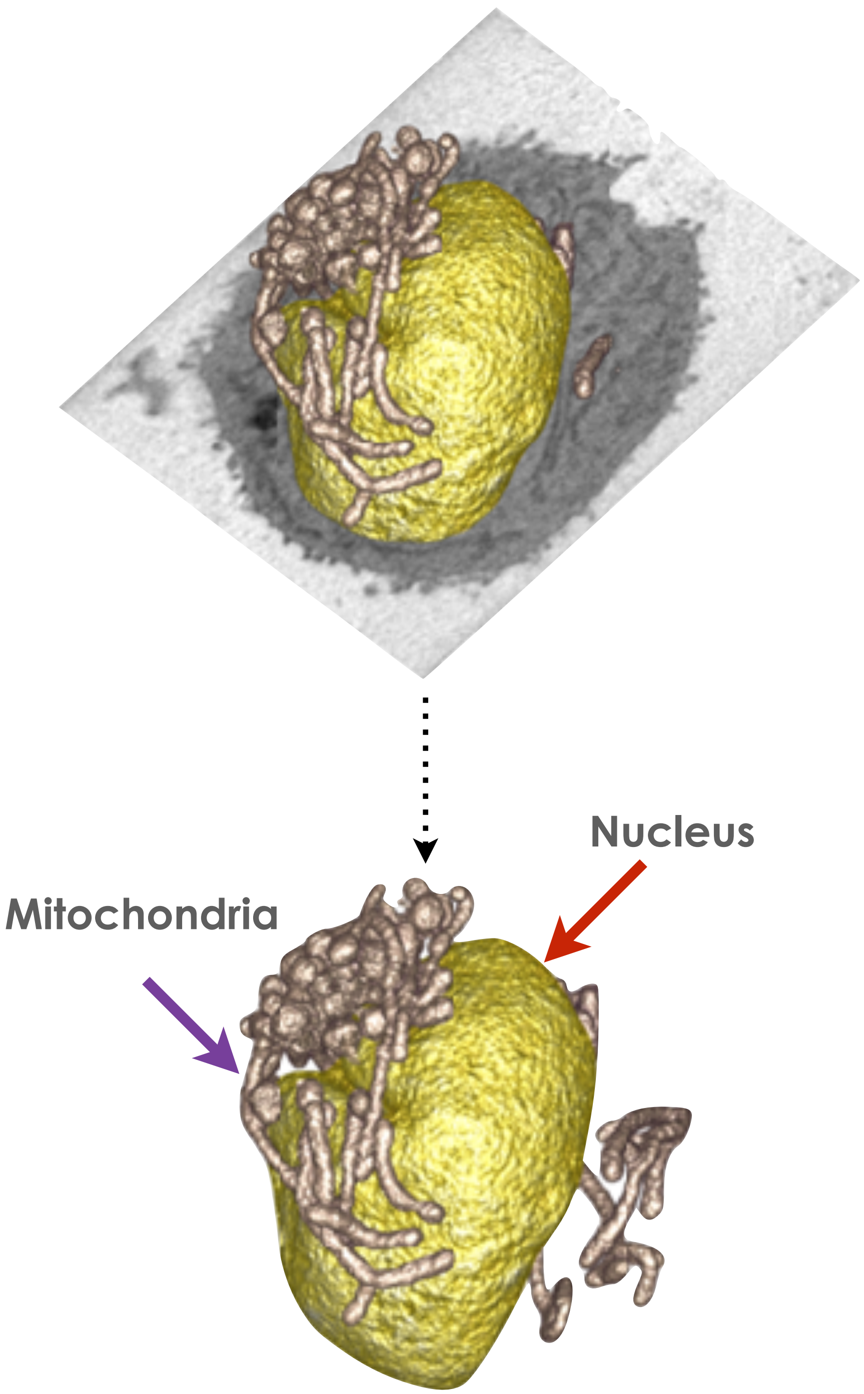

Segment using LAC and manual assist

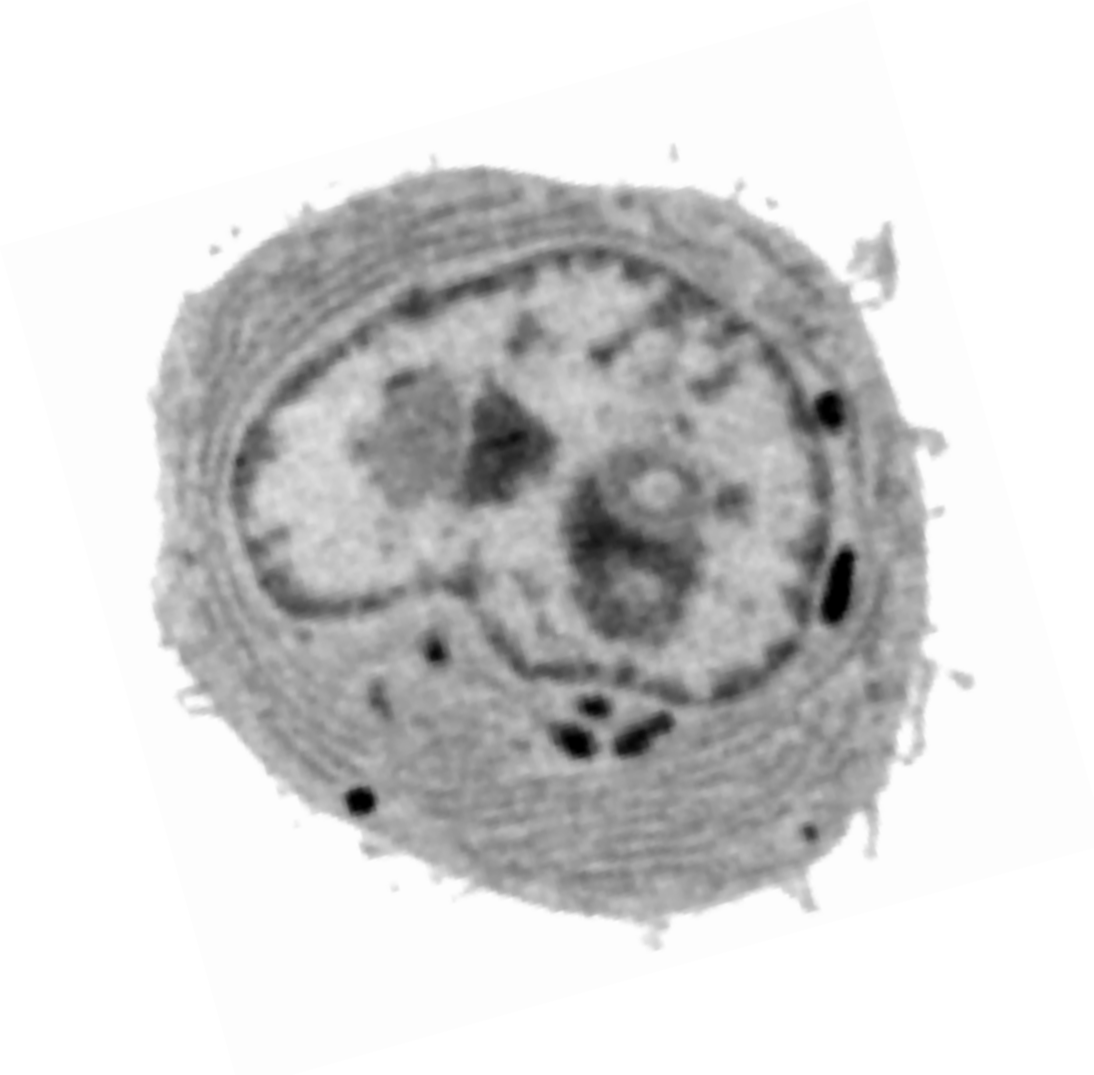

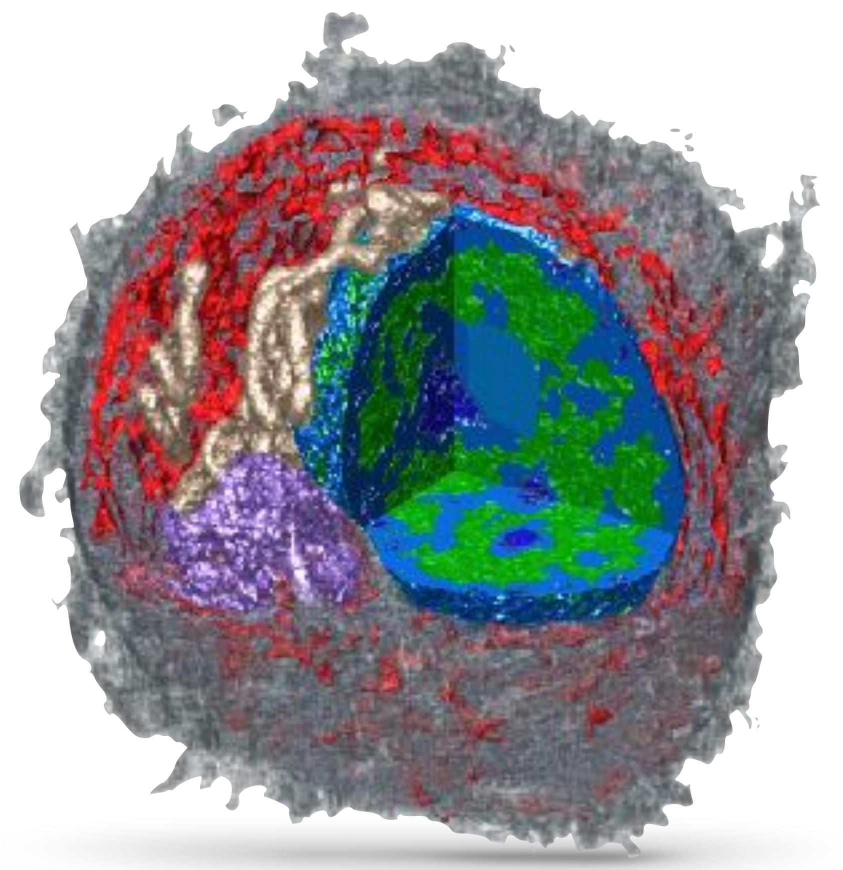

- Cytoplasm
- Heterochromatin
- Euchromatin / nucleoplasm
- Mitochondria
- Golgi apparatus
- Endoplasmic reticulum

Comparing Soft X-ray Tomography (SXT)

and

Transmission Electron Microscopy (TEM)

SXT and TEM Comparisons

Vaccinia-infected PtK2 cells

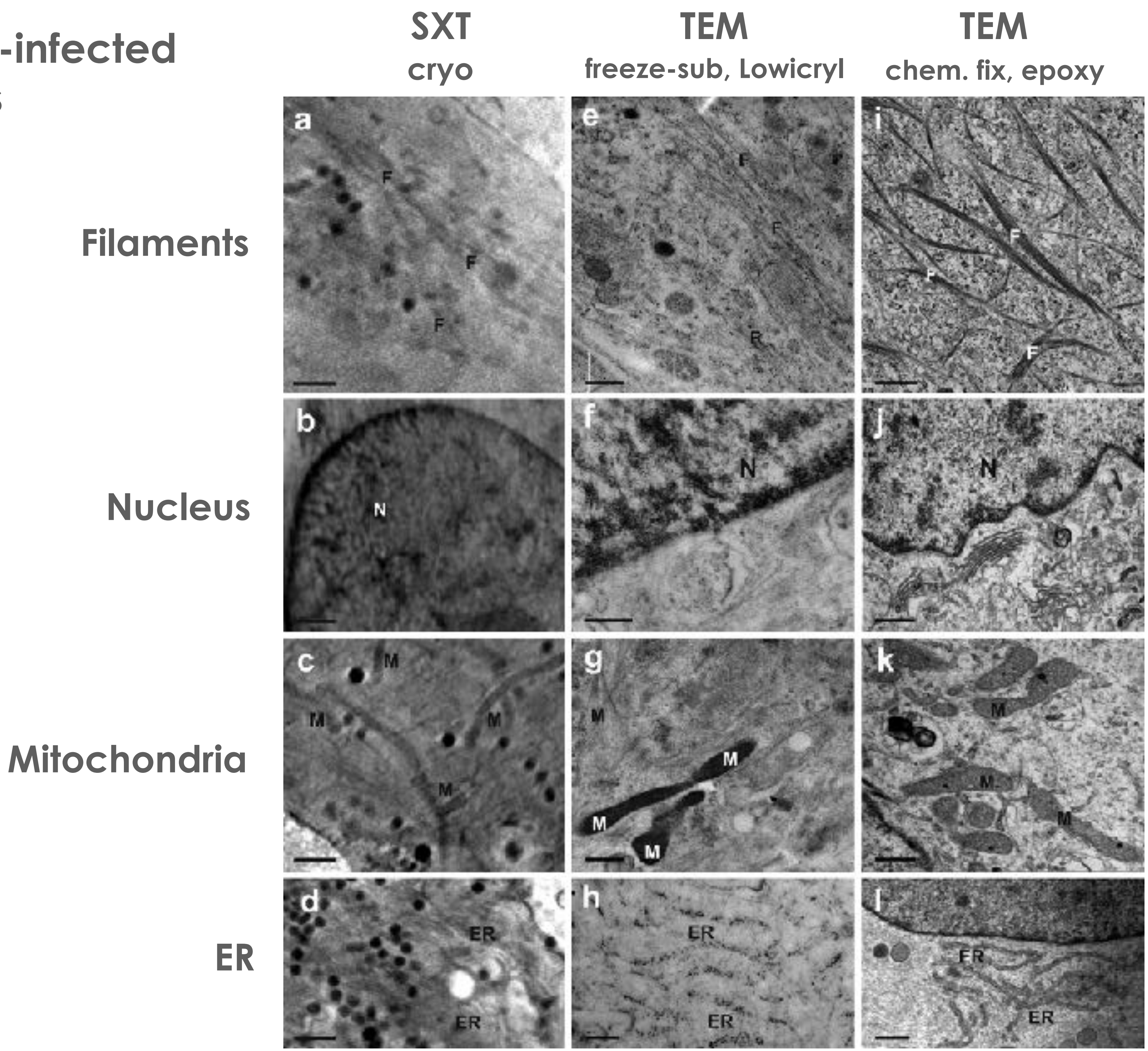

Chichon et al., J. Structural Biology (2012) 177:202-211

SXT and TEM Comparisons

Lysosomes

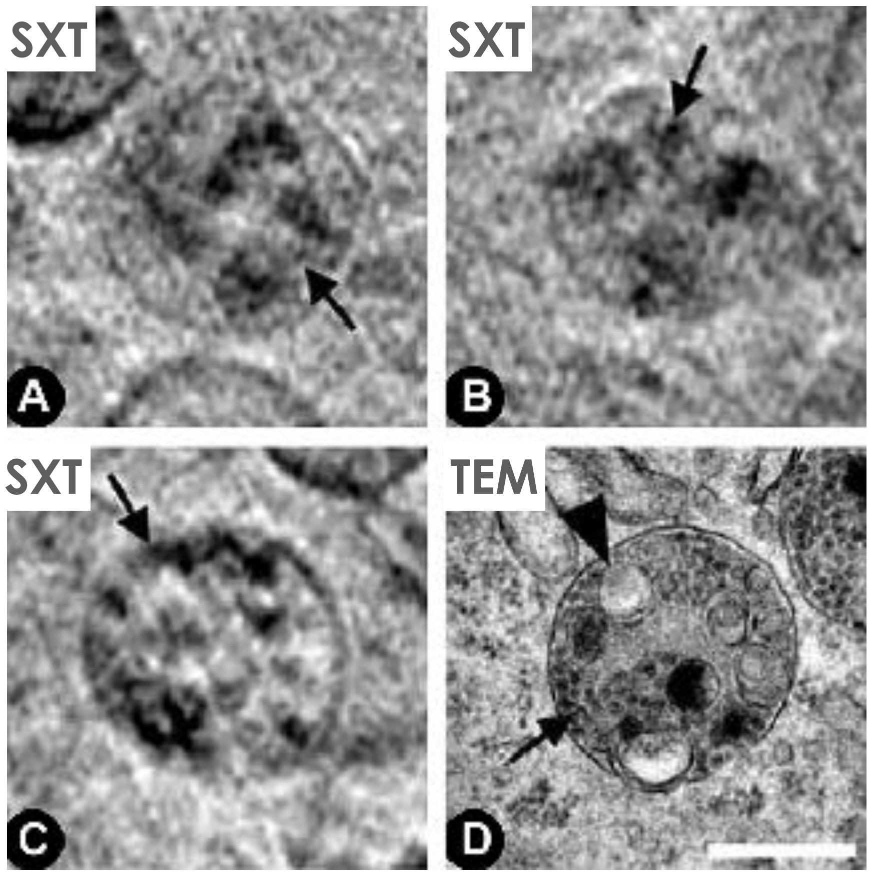

Golgi apparatus

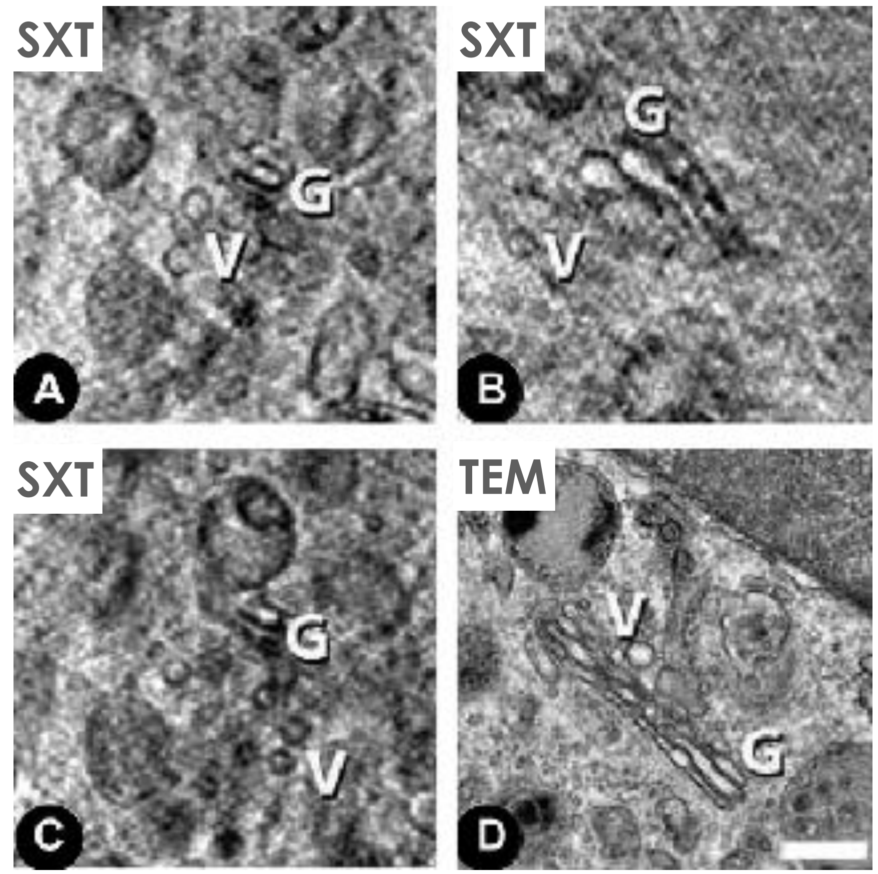

Endoplasmic reticulum

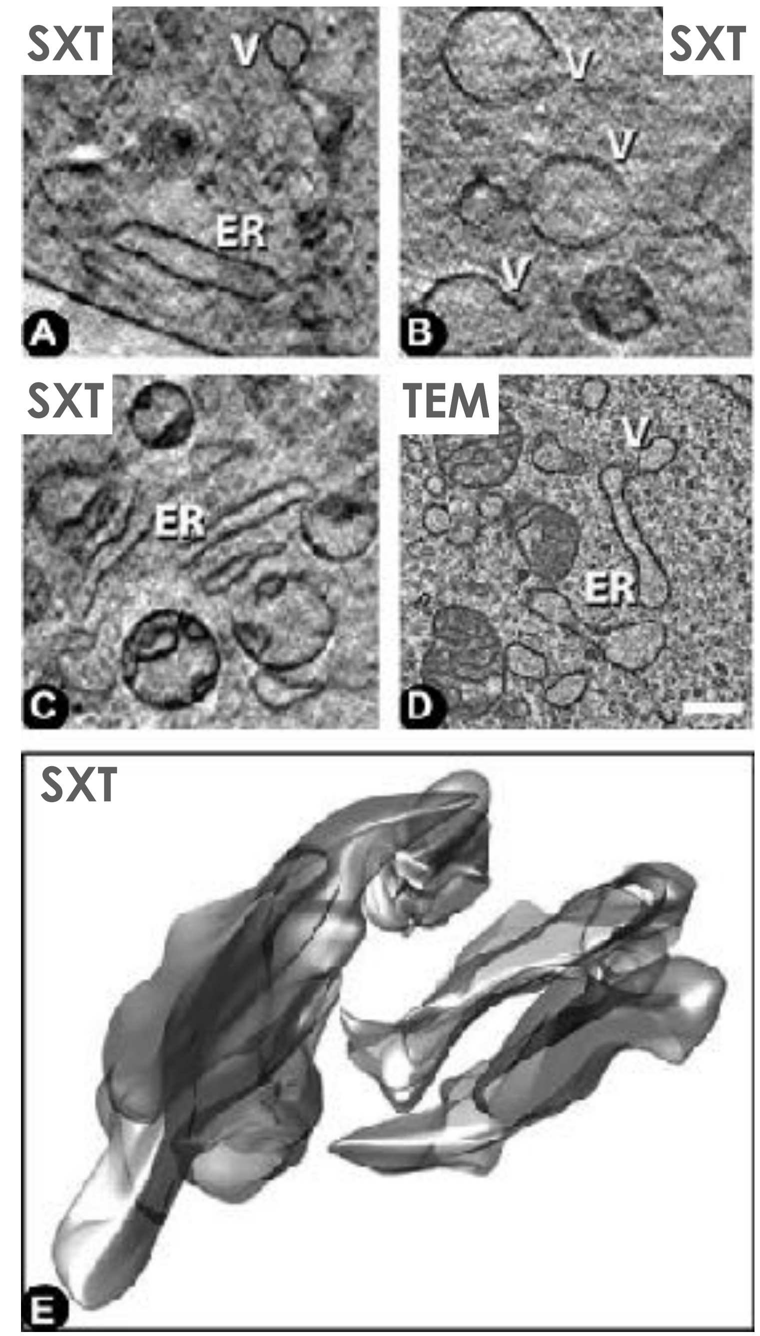

Müller et al. J. Structural Biology. (2012) 177, 179-192

SXT and TEM Comparisons

Filaments

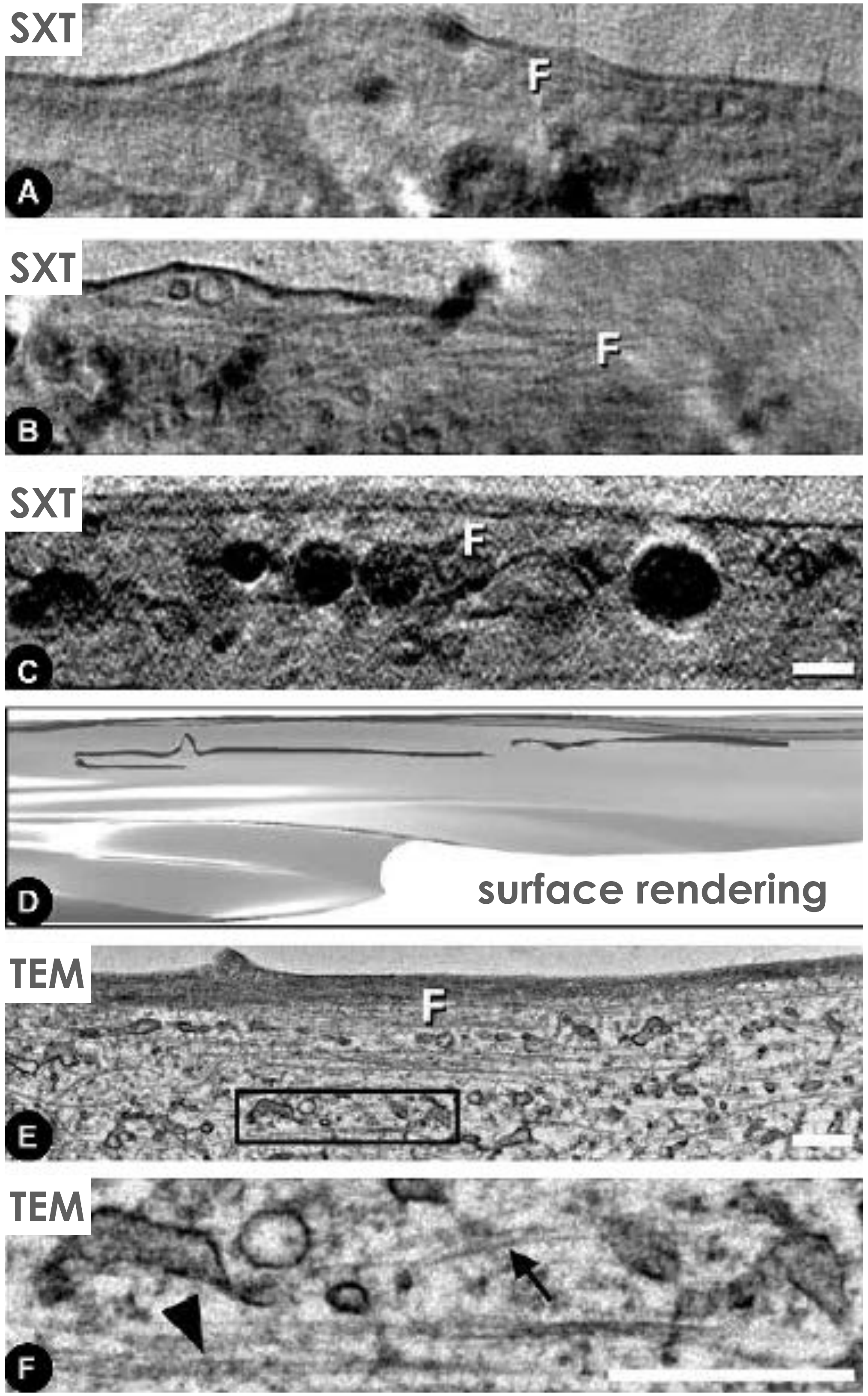

Müller et al. J. Structural Biology. (2012) 177, 179-192

SXT and TEM Comparisons

Microvilli
&
Plasma membrane

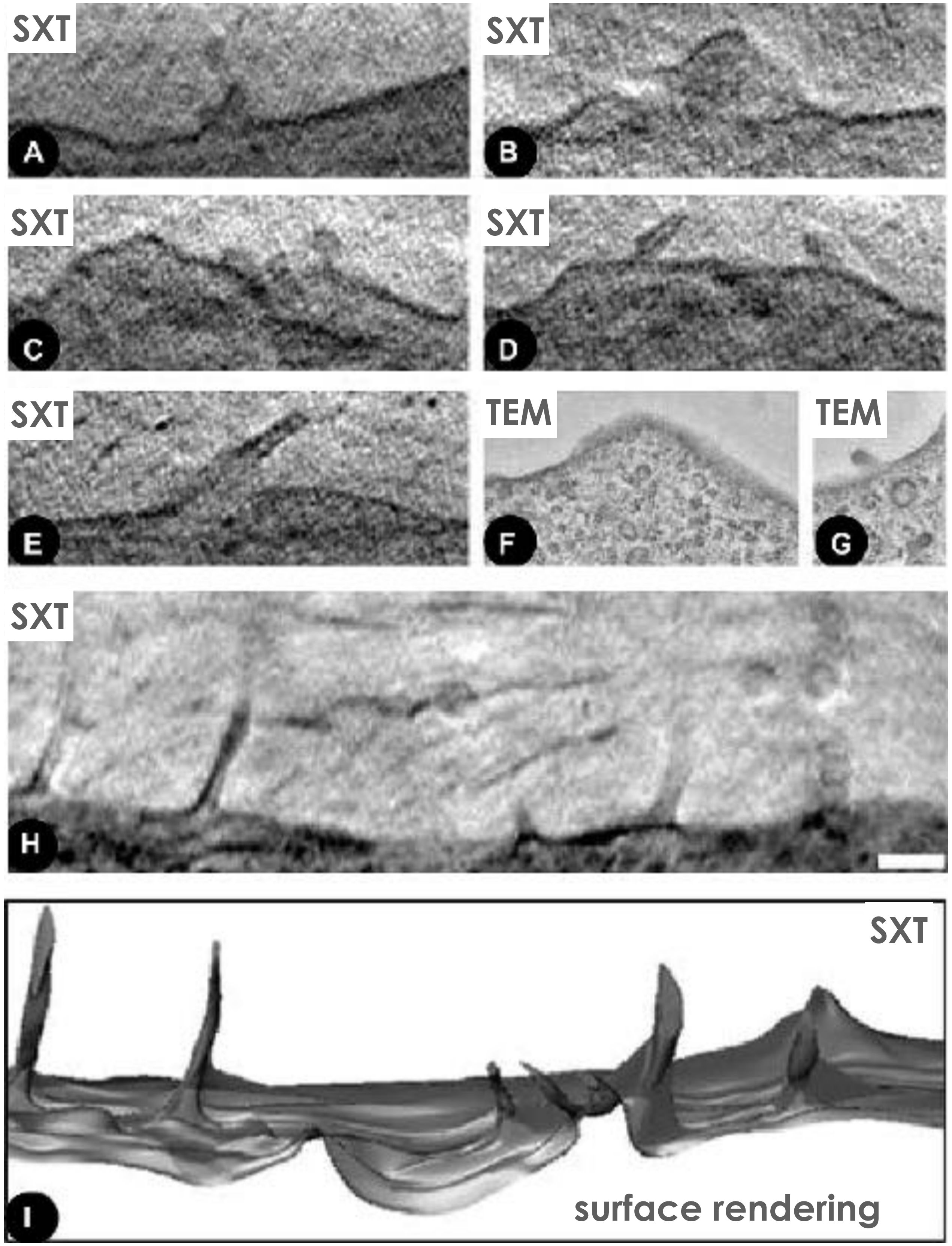

Müller et al. J. Structural Biology. (2012) 177, 179-192

SXT and TEM Comparisons

Nuclear Envelope

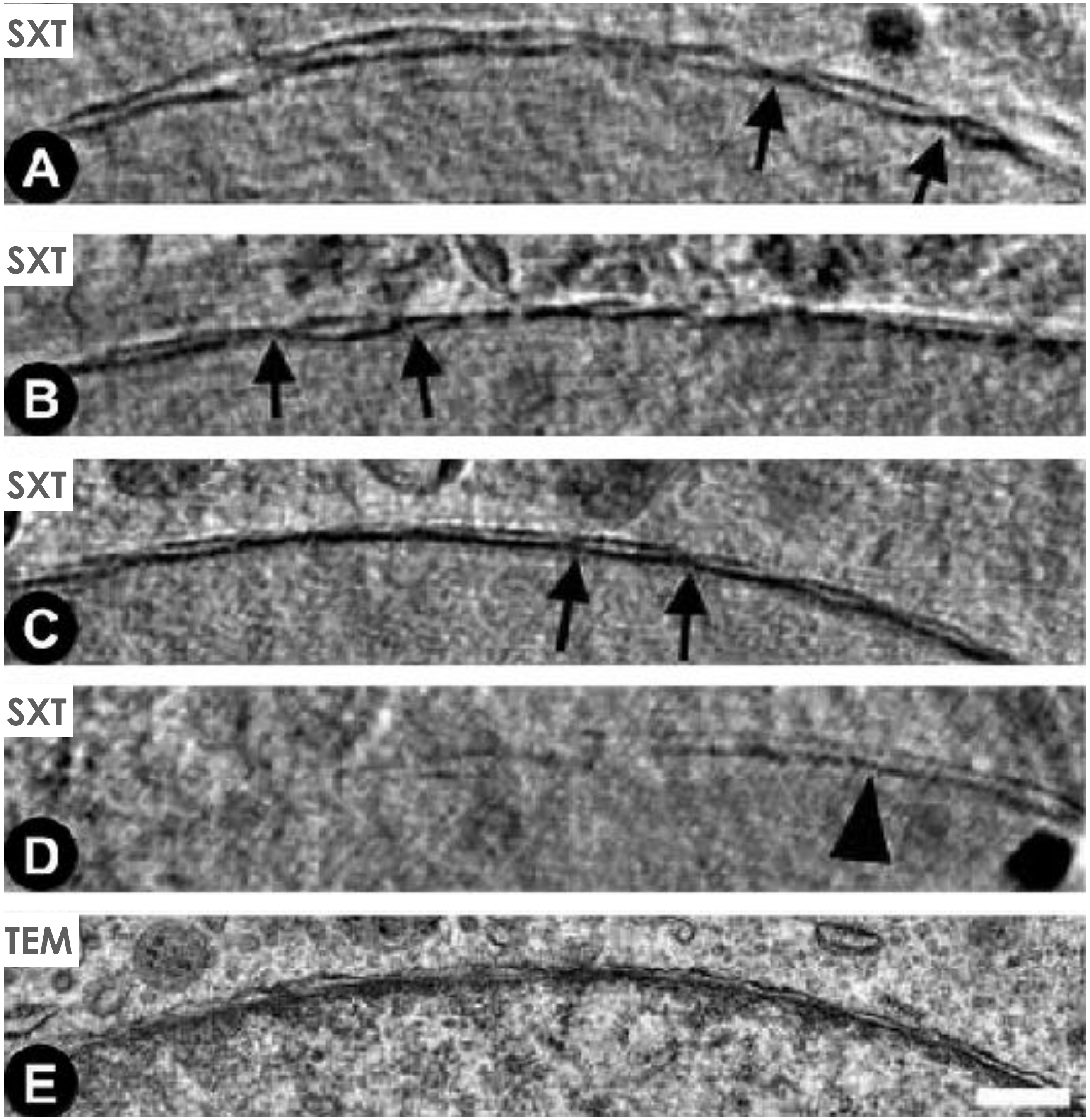

Mitochondria

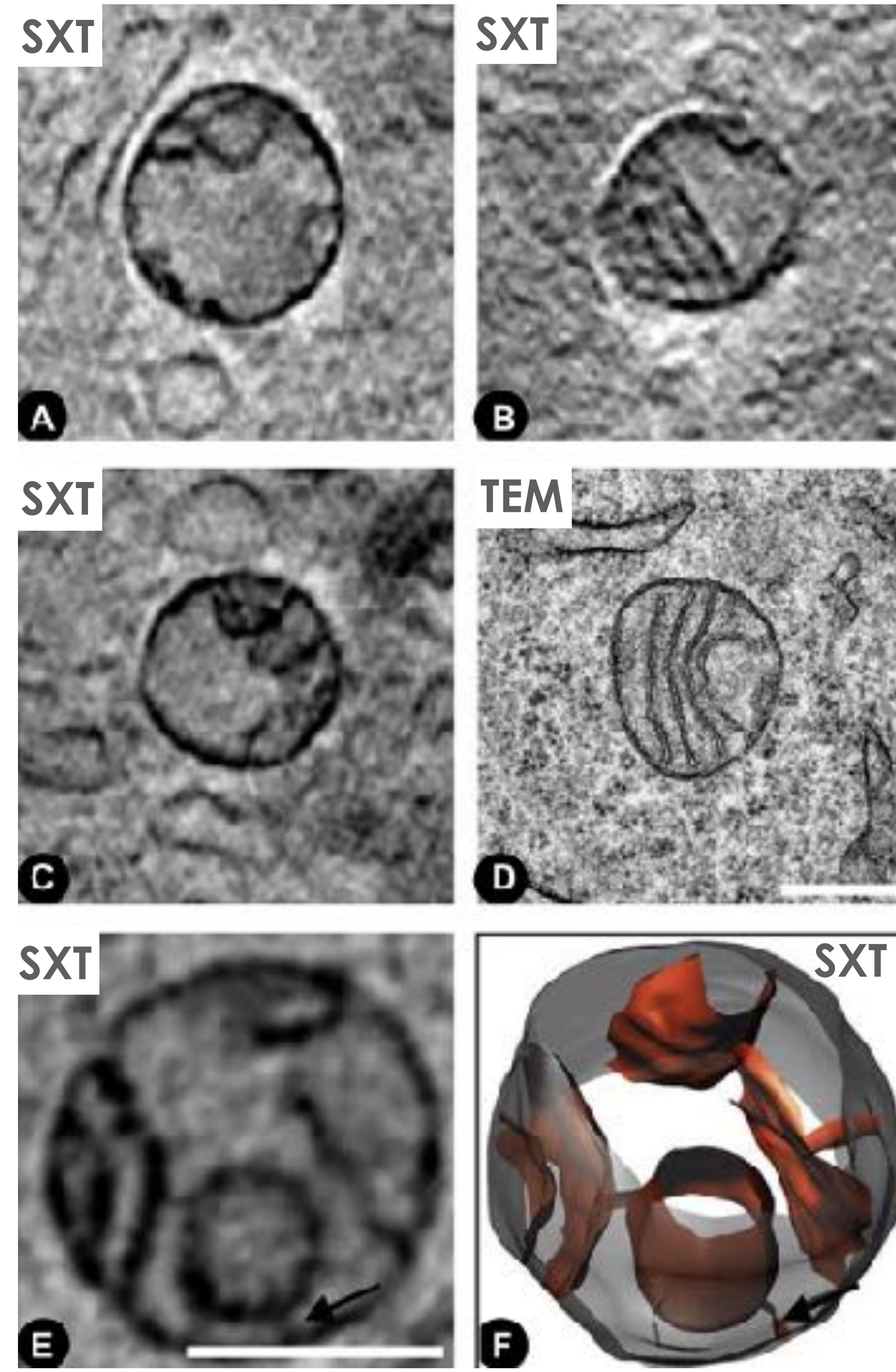

Müller et al. J. Structural Biology. (2012) 177, 179-192

SXT and TEM Comparisons

Nucleus

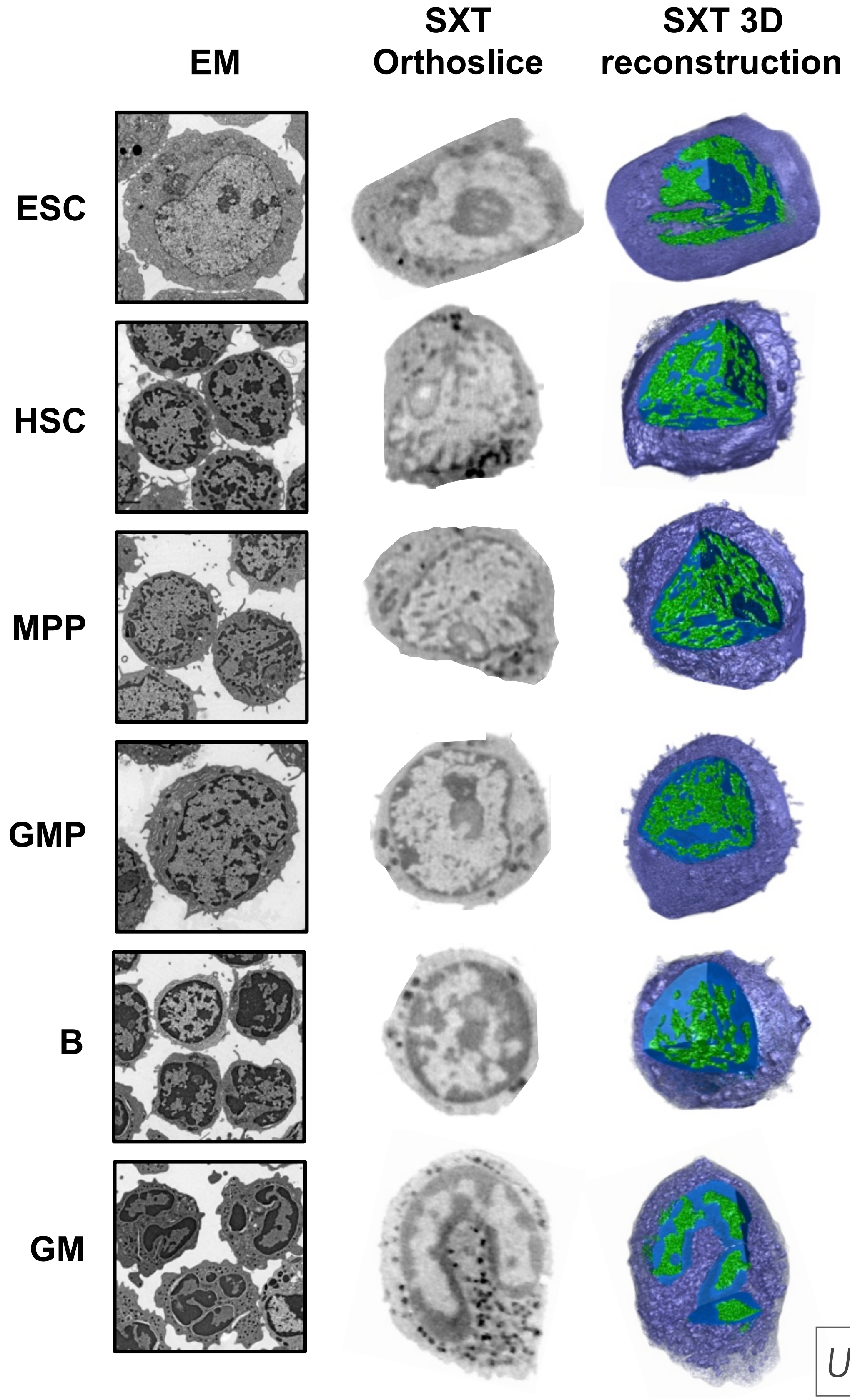

Ugarte et al. Stem Cell Reports. (2015) 5(5), 728-740.

SXT and TEM Comparisons

Nucleus

TEM

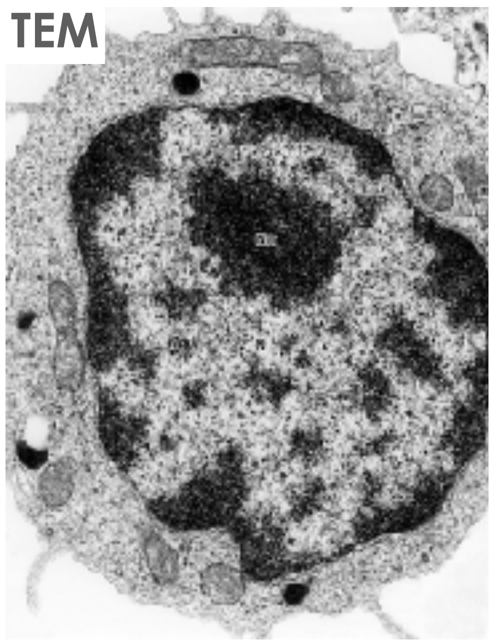

Full-rotation tomography, NCXT

SXT

Olfactory epithelial sensory neuron from mouse tissue

SXT

Mouse lymphoblastoid cell

SXT

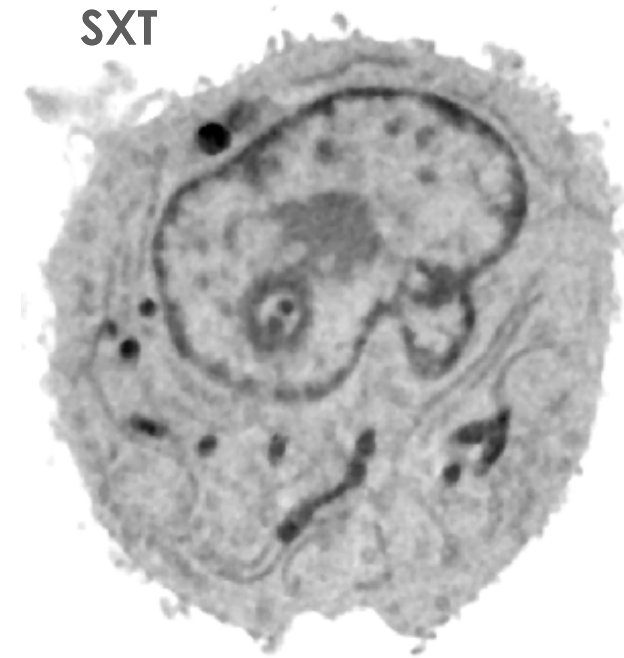

Mouse lymphoblastoid cell

Limited-tilt tomography, X-ray Microscope in Berlin

SXT

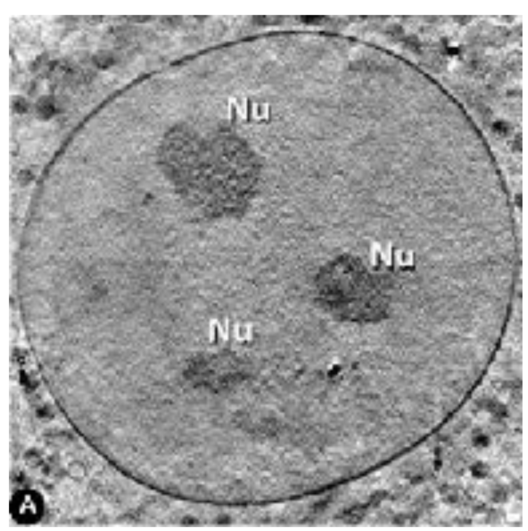

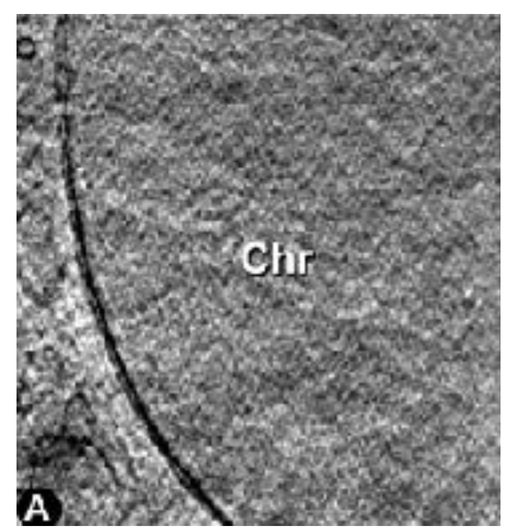

Mouse adenocarcinoma cells cultured on grids

SXT and TEM Comparisons

Nucleoid Organization in *E. coli*

E.Coli hupA38-42 muatnt

SXT

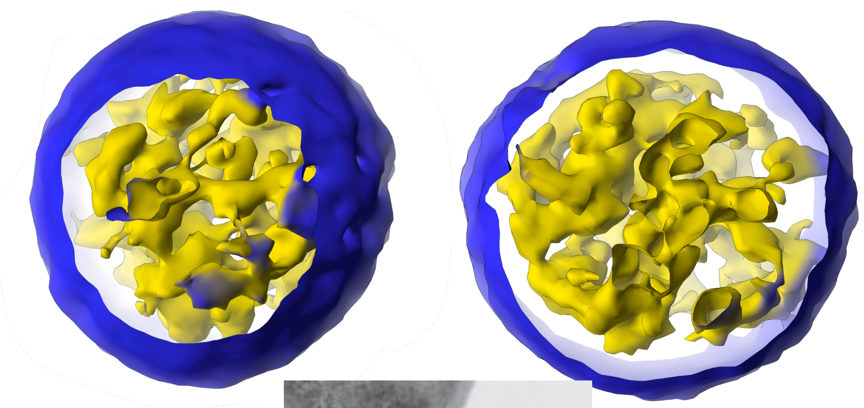

TEM

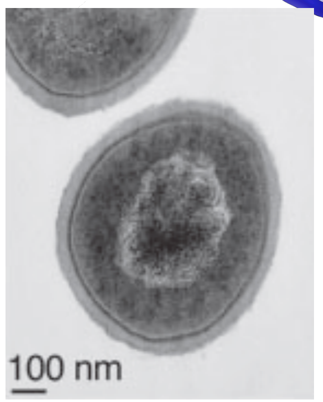

Thin-section transmission electron photomicrographs illustrating the nucleoid ultrastructure in hupA mutant

SXT

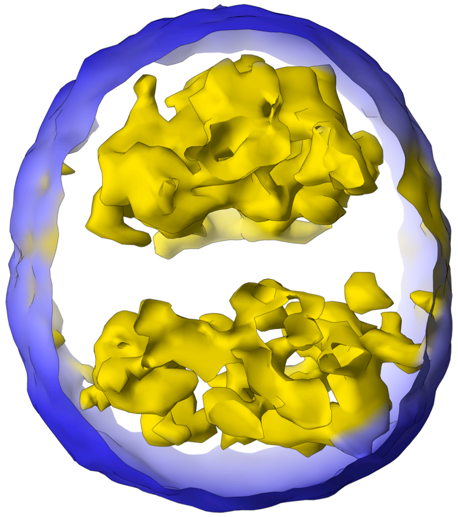

TEM

Michal Hammel, LBNL
John Tainer, MD Anderson Cancer Center & LBNL

SXT and TEM Comparisons

Autophagic vacuole

Cryo x-ray tomography
(A-F)

High pressure freeze, freeze substitute
(G-I)

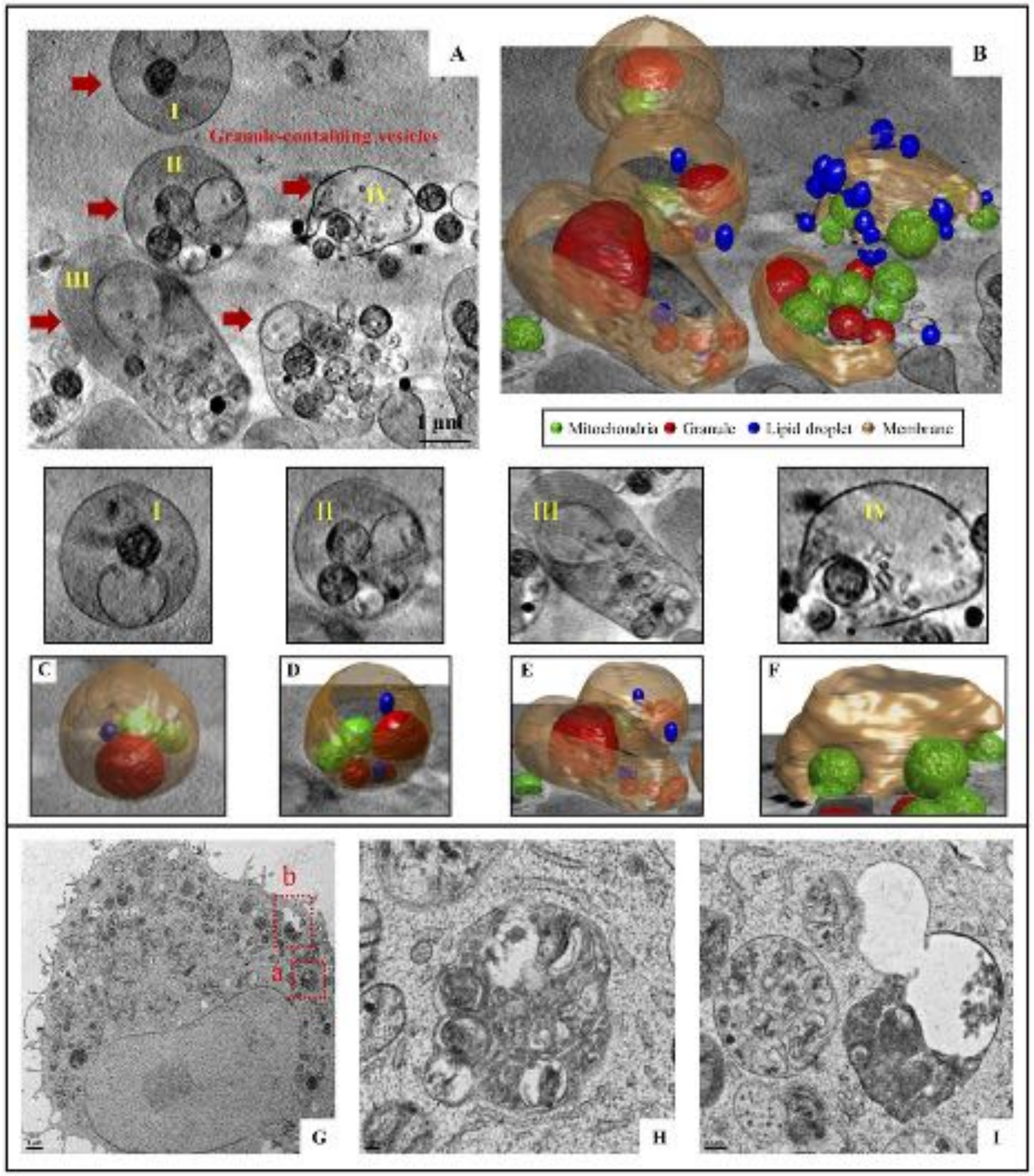

Chen et al. Scientific Reports. (2016) DOI:10.1038/srep34879.

SXT and TEM Comparisons

Plasmodium falciparum

High pressure freeze, freeze substitute

Cryo electron tomography

Cryo x-ray tomography

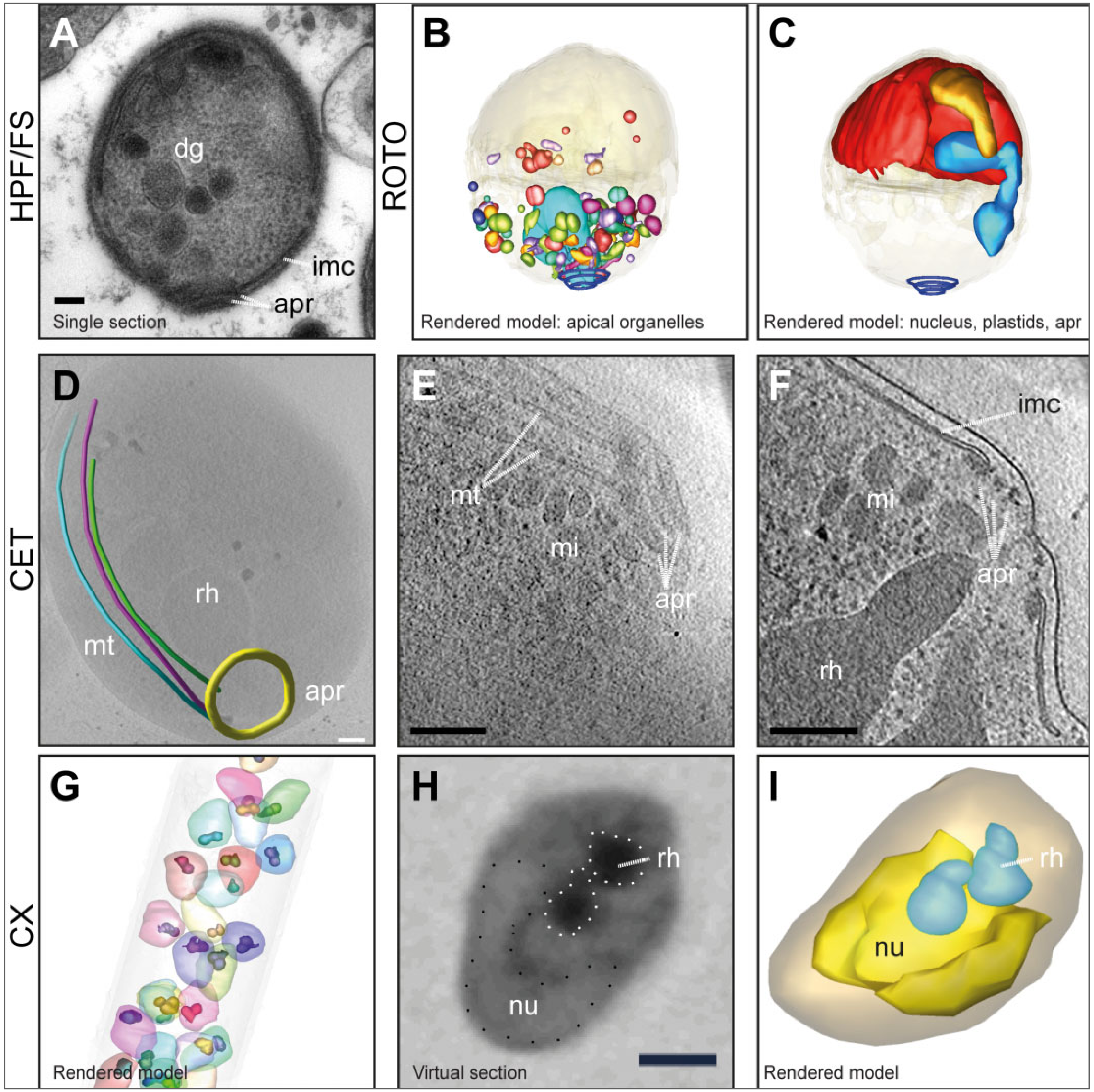

Hanssen et al. Cell. Microbiology. (2013) 15(9), 1457-1472.

SXT & TEM Comparisons of *P. falciparum* Merozoite

Fixation method	Abbreviation	Visualization method	Characteristics	Reference
Glutaraldehyde/reduced osmium tetroxide/ thiocarbohydrazide/ OsO_4	ROTO	TEM and electron tomography of serial sections	Good overall preservation of merozoite shape and organelles. Allows visualization of membranes – membrane contrast far superior to standard osmium treatment, but with loss of contrast for proteinaceous structure and DNA. Unsuitable for post-embedding immunolabelling.	Seligman *et al.* (1966); Willingham and Rutherford (1984)
Glutaraldehyde and osmium tetroxide	GO	TEM and electron tomography of serial sections	Good preservation of membranes. Variable contrast for proteinaceous structures. Generally unsuitable for post-embedding immunolabelling.	Aikawa (1966)
Glutaraldehyde fixation only	GF	TEM and electron tomography of serial sections	Good preservation of cytoplasmic details. Allows easy identification of invasion organelles. No membrane preservation (membranes appear white). Compatible with post-embedding immunolabelling.	Bannister and Kent (1993); Riglar *et al.* (2011)
High-pressure frozen and freeze substituted	HPF/FS	TEM and electron tomography of serial sections	Methodologically more complex and fixation requires more expensive infrastructure. Excellent preservation of merozoite and organelle structure and shape, lacking ruffles sometimes observed in the chemical fixations (ROTO, GO, GF). Dense granules and mitochondria appeared to be smoother, denser and more turgid. Compatible with post-embedding immunolabelling.	Studer *et al.* (2008); Waller *et al.* (2000)
Cryo-preservation by plunge freezing in liquid ethane	CET	Electron tomography of whole cells (individual)	Excellent whole-cell preservation down to potentially molecular detail. Resolves some cytoskeletal elements not discernible in embedded cells. The resolution and contrast degrade with sample thickness, practically limiting the cell thickness to ~ 0.5–1 μm. No need for staining. Not readily suitable for immunolabelling internal structures	Cyrklaff *et al.* (2007); Kudryashev *et al.* (2010)
Cryo-preservation in capillaries for X-ray imaging	CX	X-ray tomography of whole cells (multiple)	Excellent whole-cell preservation – no material lost through sectioning. Contrast not altered by staining. Resolution higher than light microscopy but lower than electron microscopy. Membranes not visible. Fast acquisition image and tomography of multiple cells. Not readily suitable for immunolabelling internal structures	Hanssen *et al.* (2011; 2012)

Hanssen et al. Cell. Microbiology. (2013) 15(9), 1457-1472.

Structures Imaged Using SXT

Mitochondria

Mitochondrial changes in mast cell degranulation

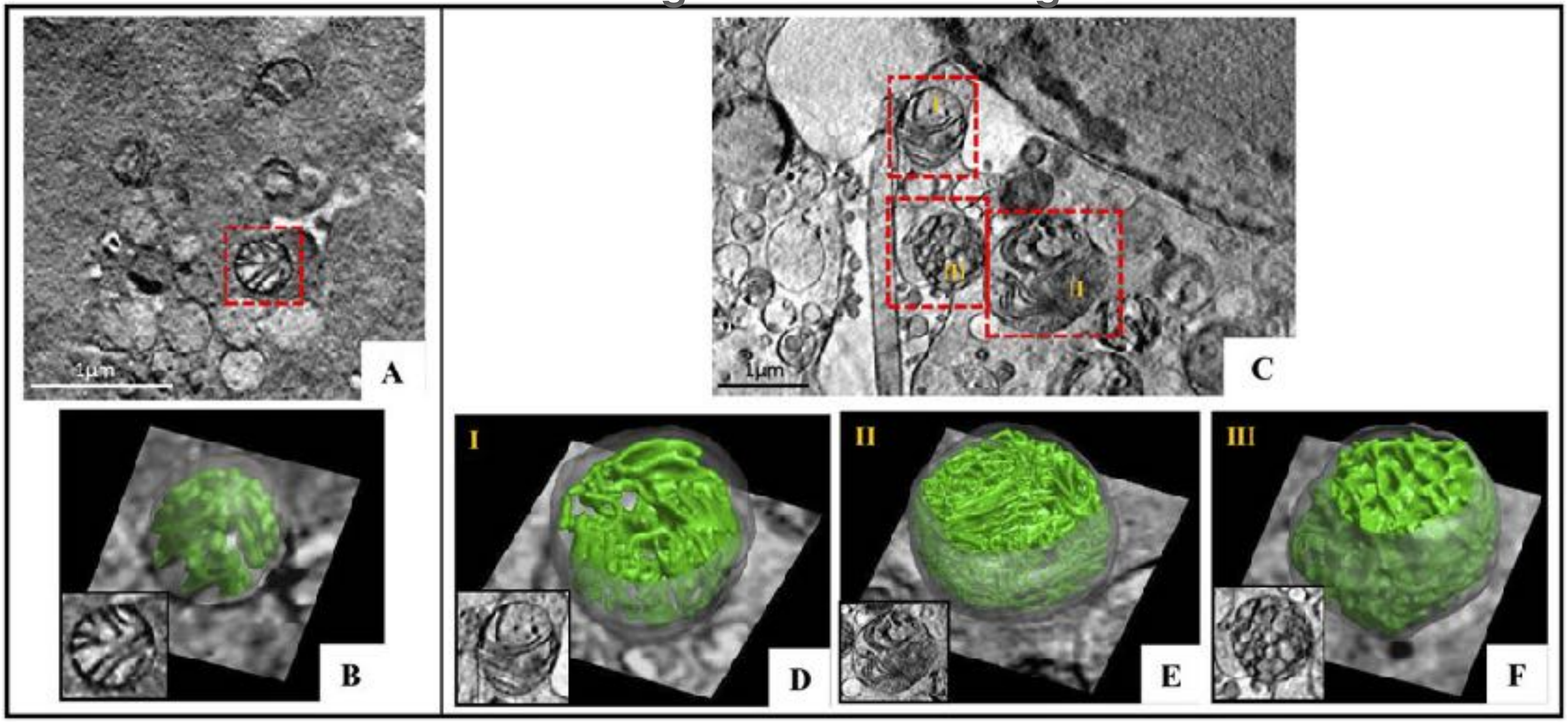

Segmented images of cells from SXT reconstructions before (A) and after (C) 30 min of activation. (B,D–F) 3D reconstructed structures from SXT in the rectangle area of (A) and I, II, III of (C).

Chen et al. Scientific Reports. (2016) DOI:10.1038/srep34879.

Structures Imaged Using SXT

Endosomes

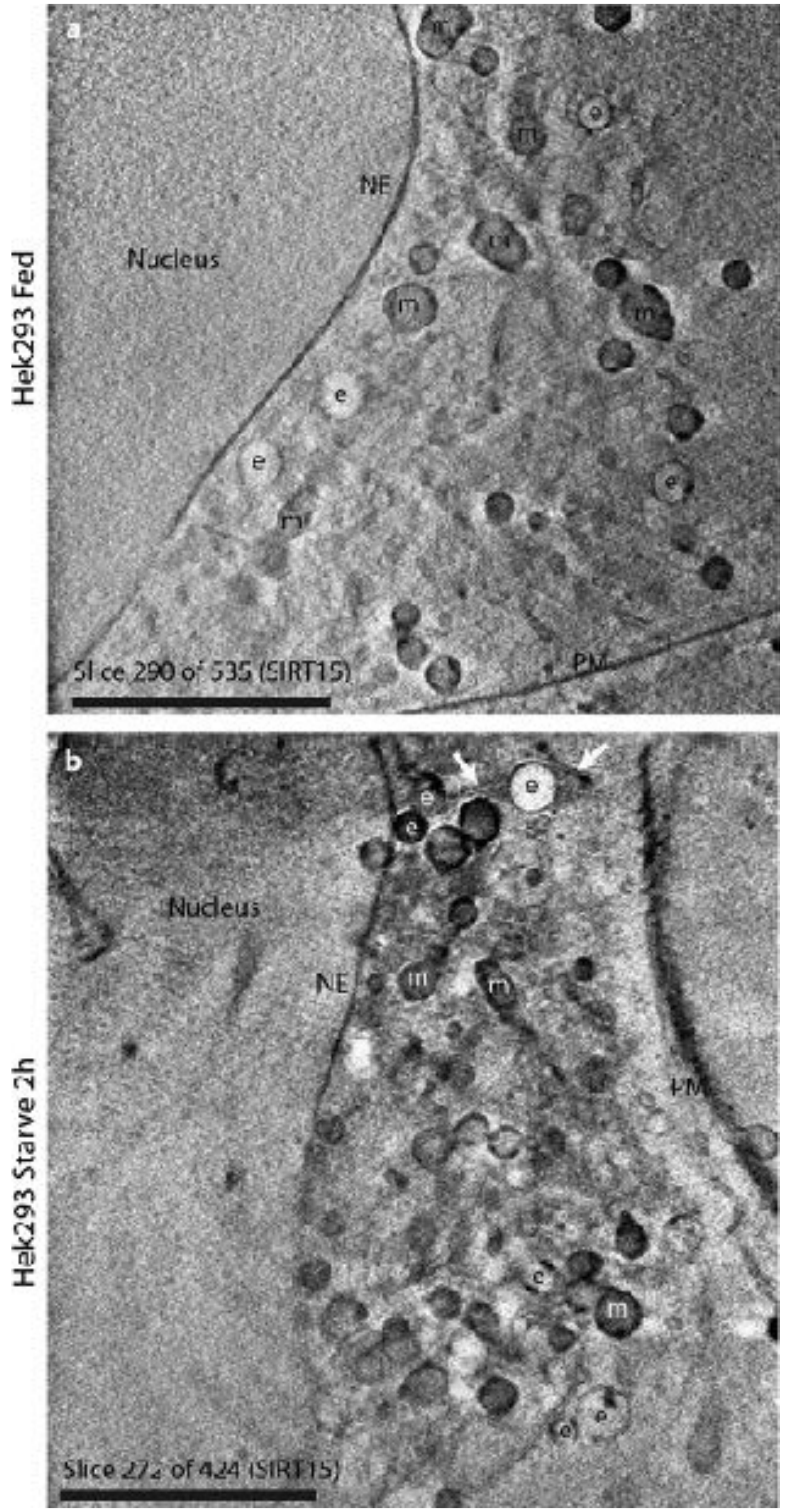

Duke et al. Ultramicroscopy (2014) 143, 77-87

Comparisons between X-ray Tomography

&

Light Microscopy

Mitochondria in the Yeast, *S. cerevisiae*

Wild type **dnm1 knockout** **fzo1 knockout**

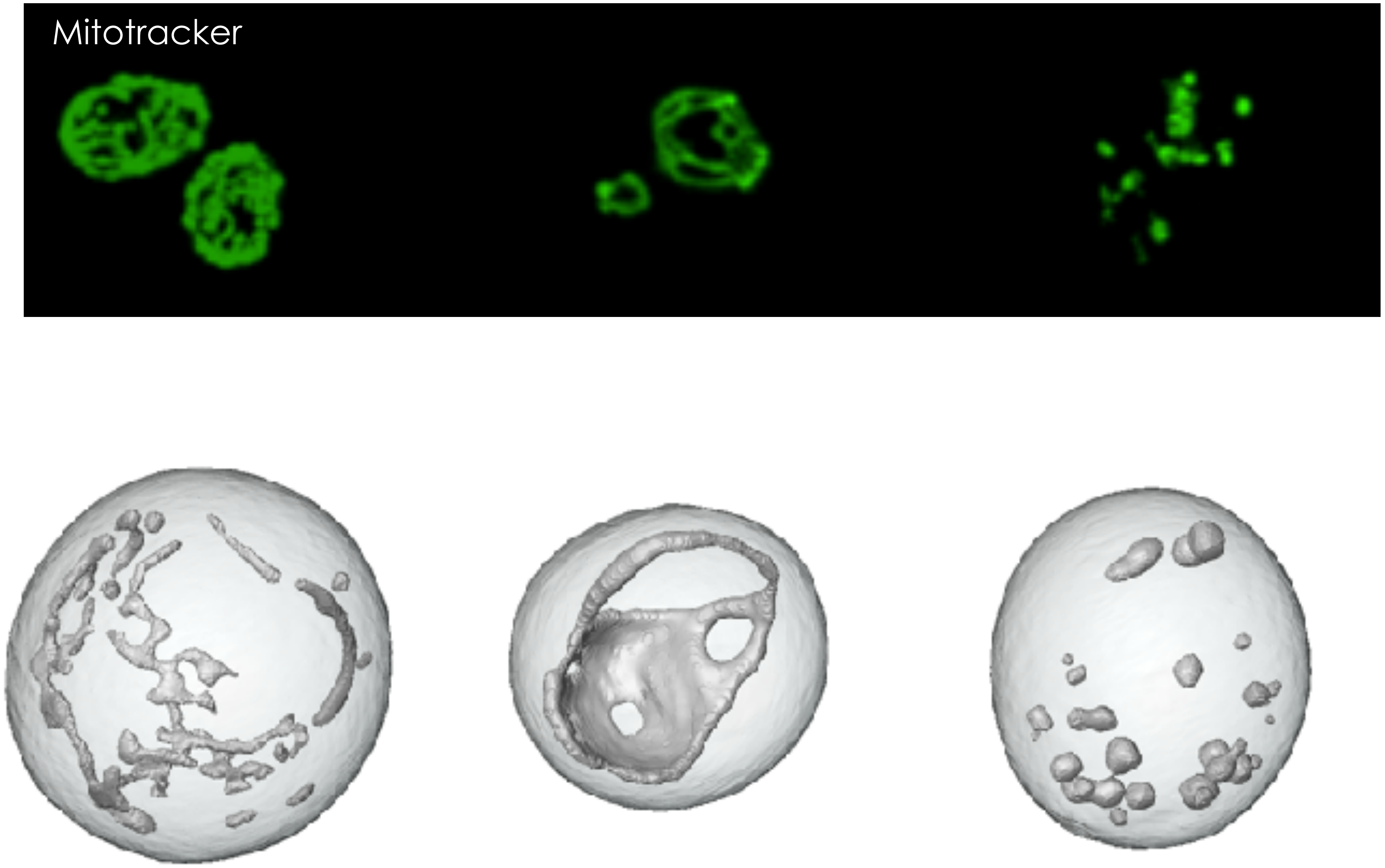

Membrane Invaginations in Yeast, *S. cerevisiae*

FM-64 live-cell stain

Wild type

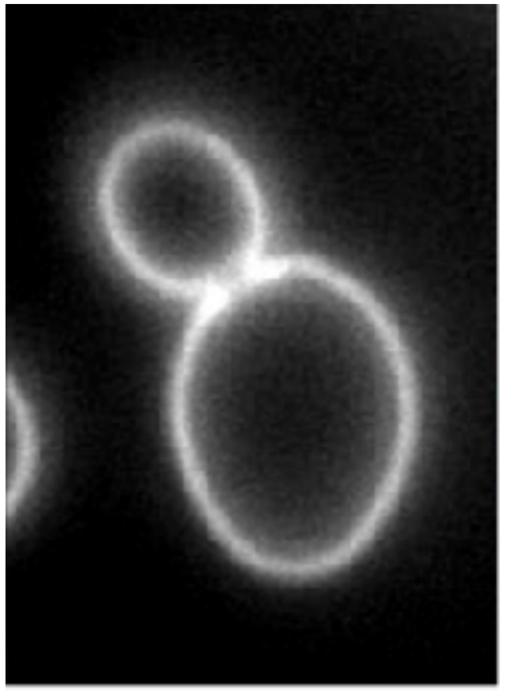

sjl1Δ sjl2Δ mutant

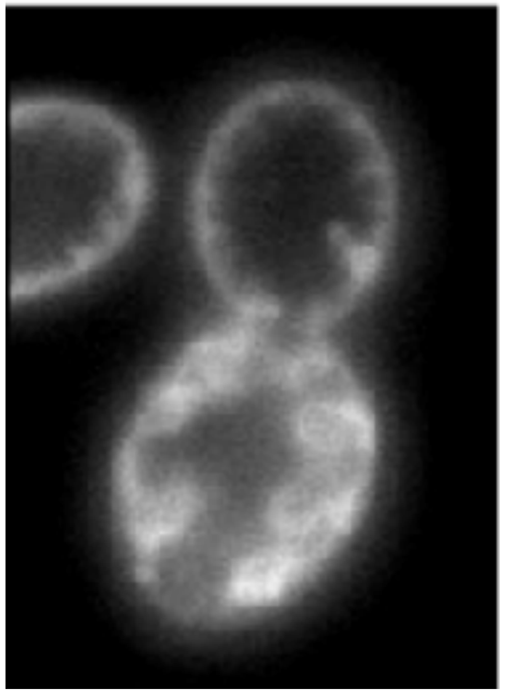

Image from Sun et al. J Cell Biol 177, 355-67 (2007)

SXT of sjl1Δ sjl2Δ synaptojanin mutant

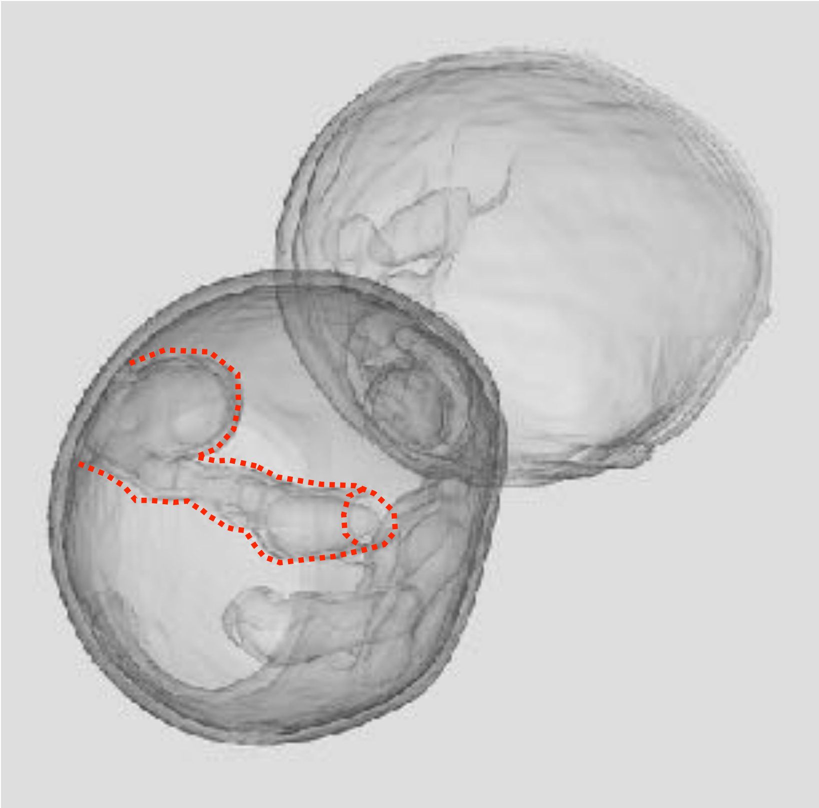

Yidi Sun & David Drubin, UC Berkeley

National Center for X-ray Tomography (NCXT), supported by NIH-NIGMS and DOE-BER

Candida albicans

Yeast-like

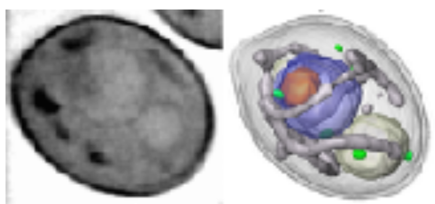

Hyphal

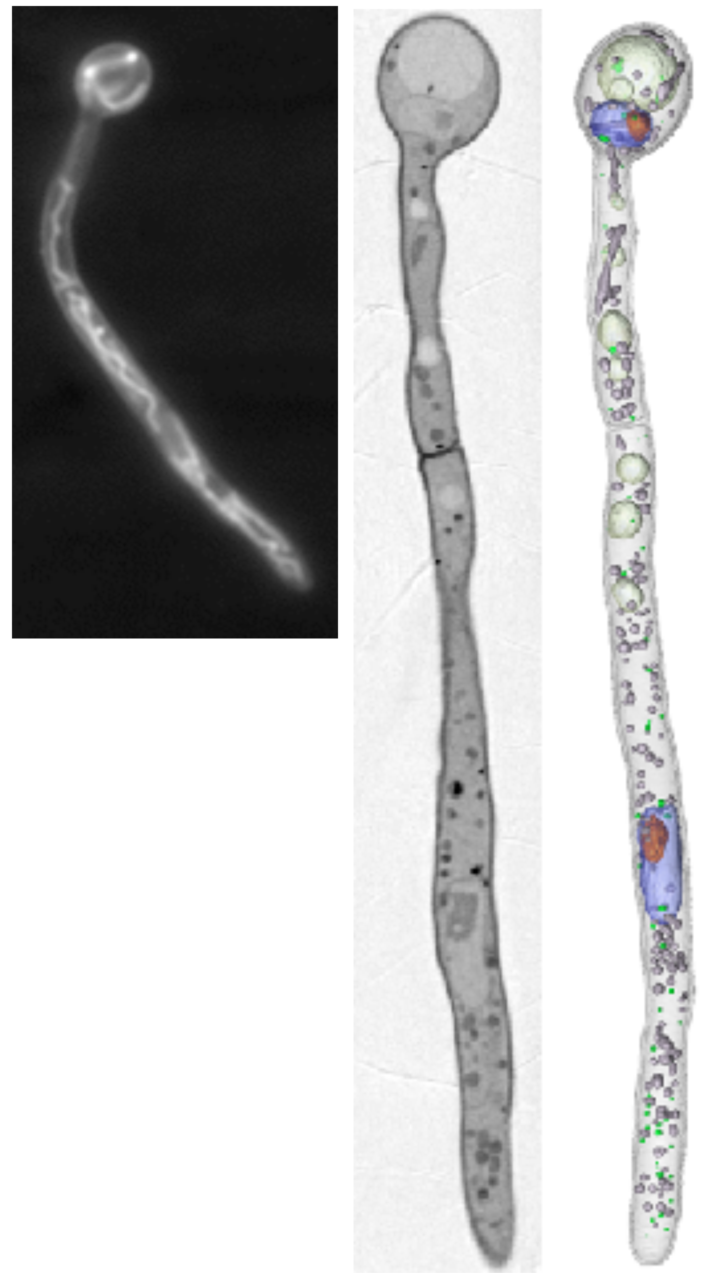

Peptoid 1-treated

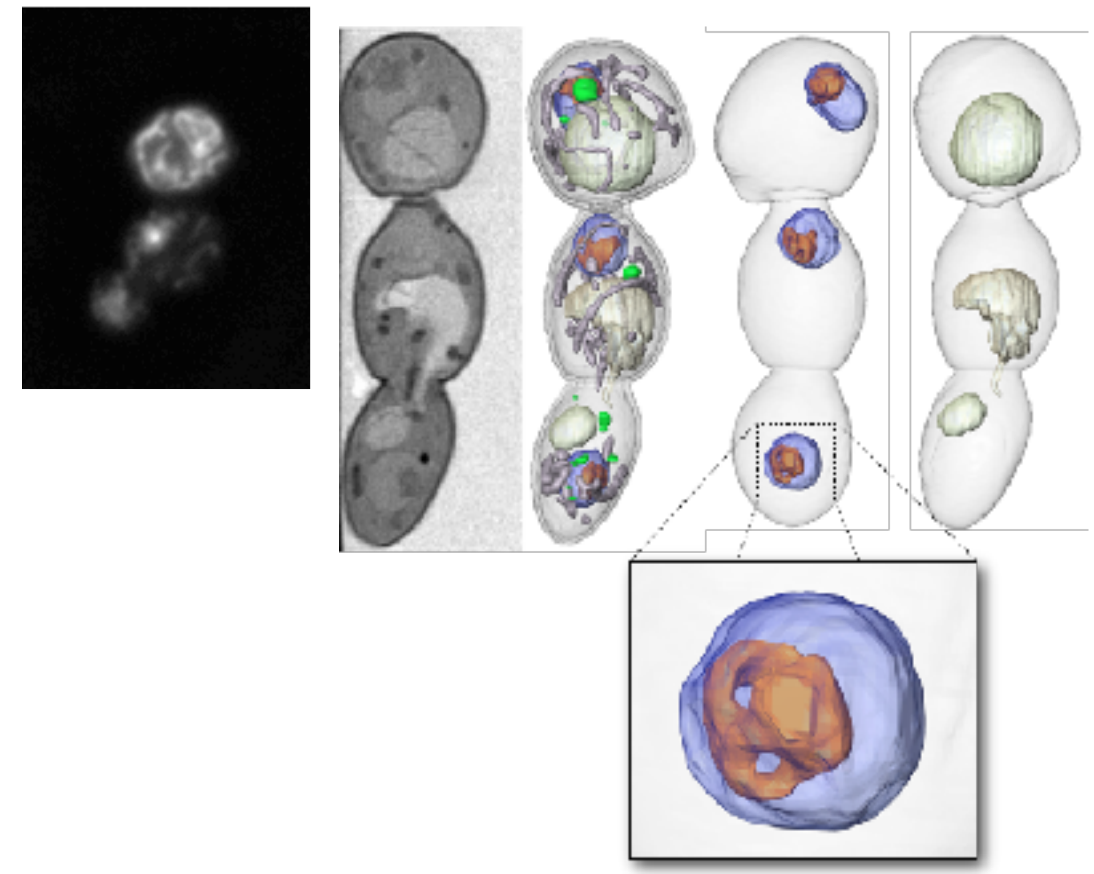

Peptoid 2-treated

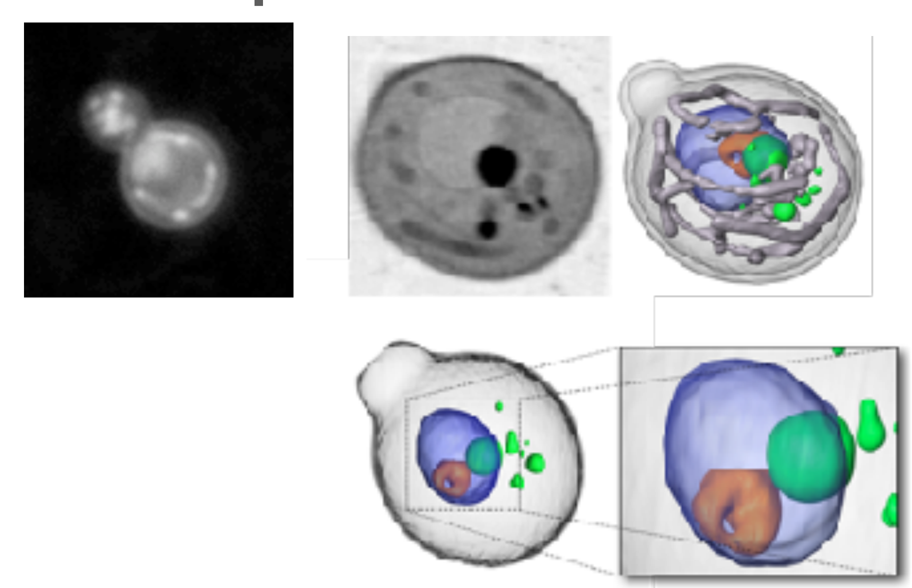

Uchida et al. PNAS. (2009) 206(46), 19375-19380.

Mouse Olfactory Epithelial Cells

Multipotent stem cell

Neuronal progenitor

Mature neuron

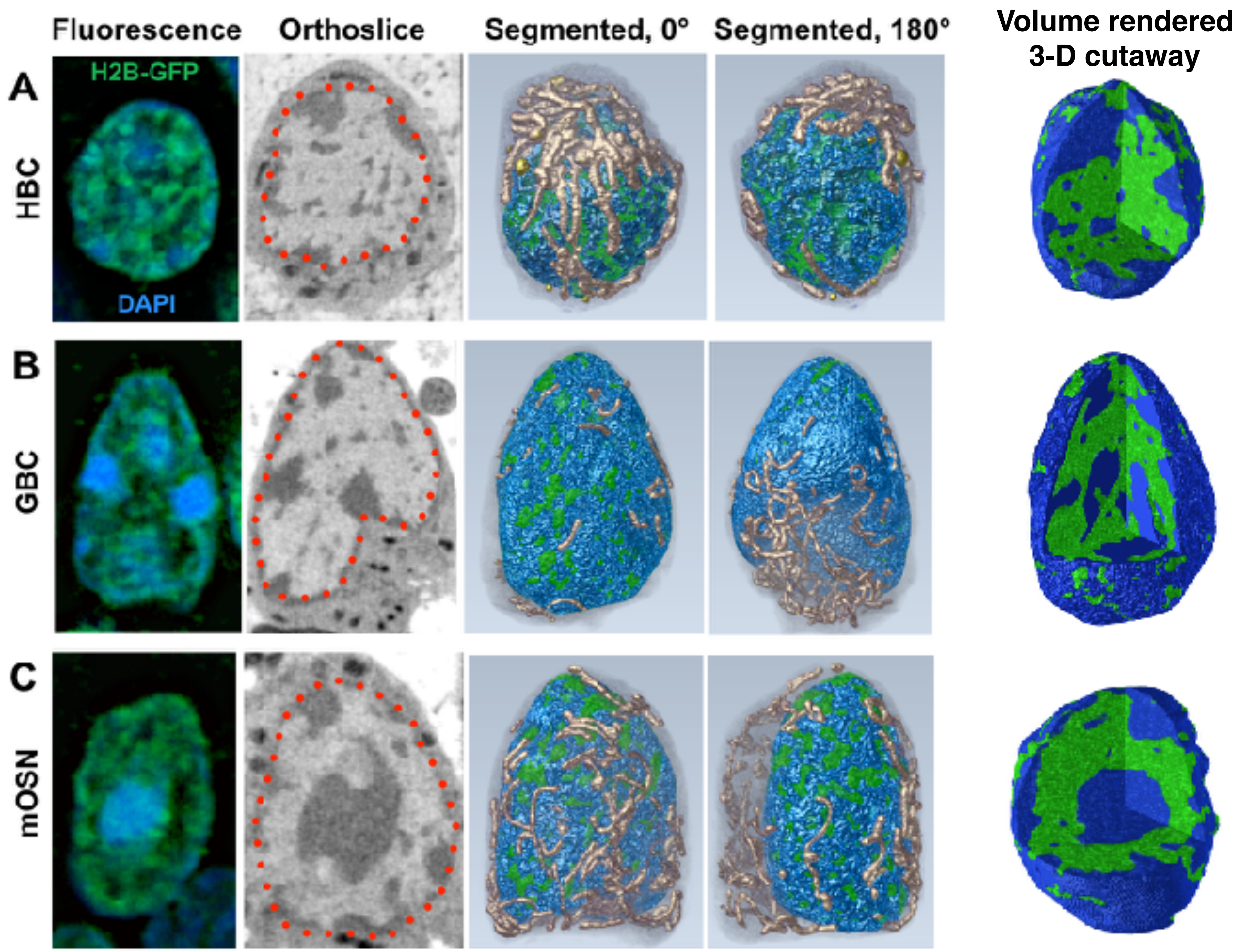

Le Gros et al. Cell Reports. (2016) 17(8), 2125-2136.

Silenced Genes in Olfactory Sensory Neuron

FISH

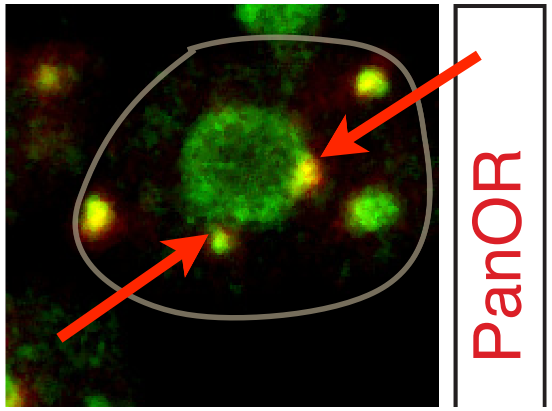

Silenced olfactory receptor (OR) genes

SXT Orthoslice

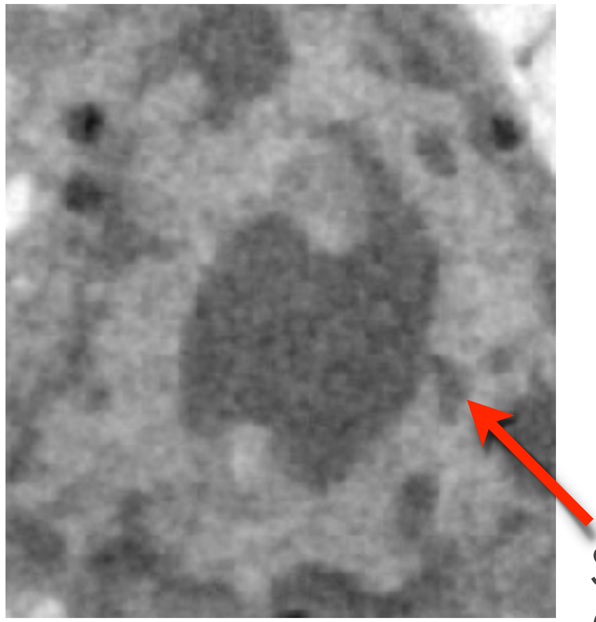

Silenced OR genes

Clowney et al. Cell (2012) 151, 724-737

Nucleoid Organization in *E. coli*

SXT

WT E.Coli

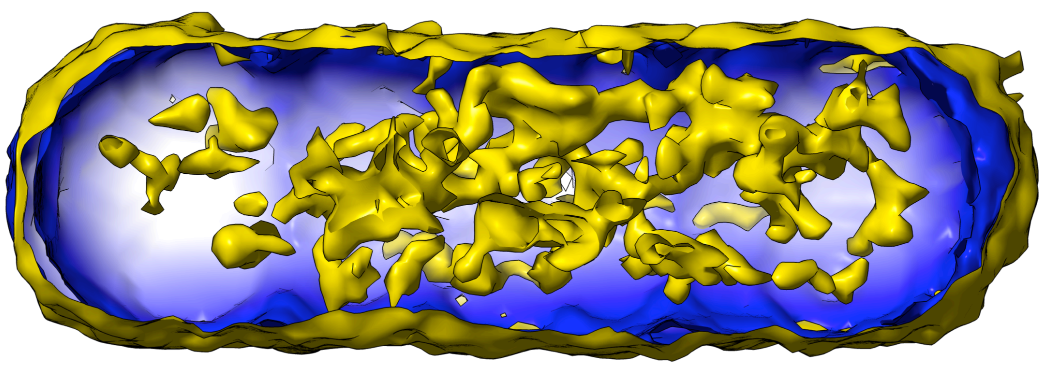

Fluorescence

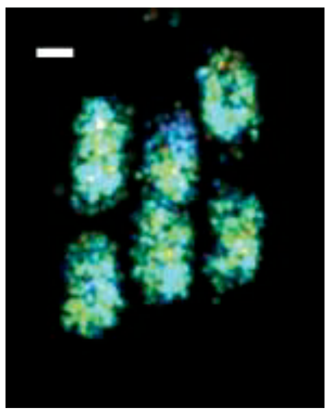

Super-resolution imaging of major nucleoid-associated proteins in living E. coli cells.

Michal Hammel, LBNL
John Tainer, MD Anderson Cancer Center & LBNL

Correlated Fluorescence and X-ray Tomography - Same Cell

Correlated Fluorescence and X-ray Tomography

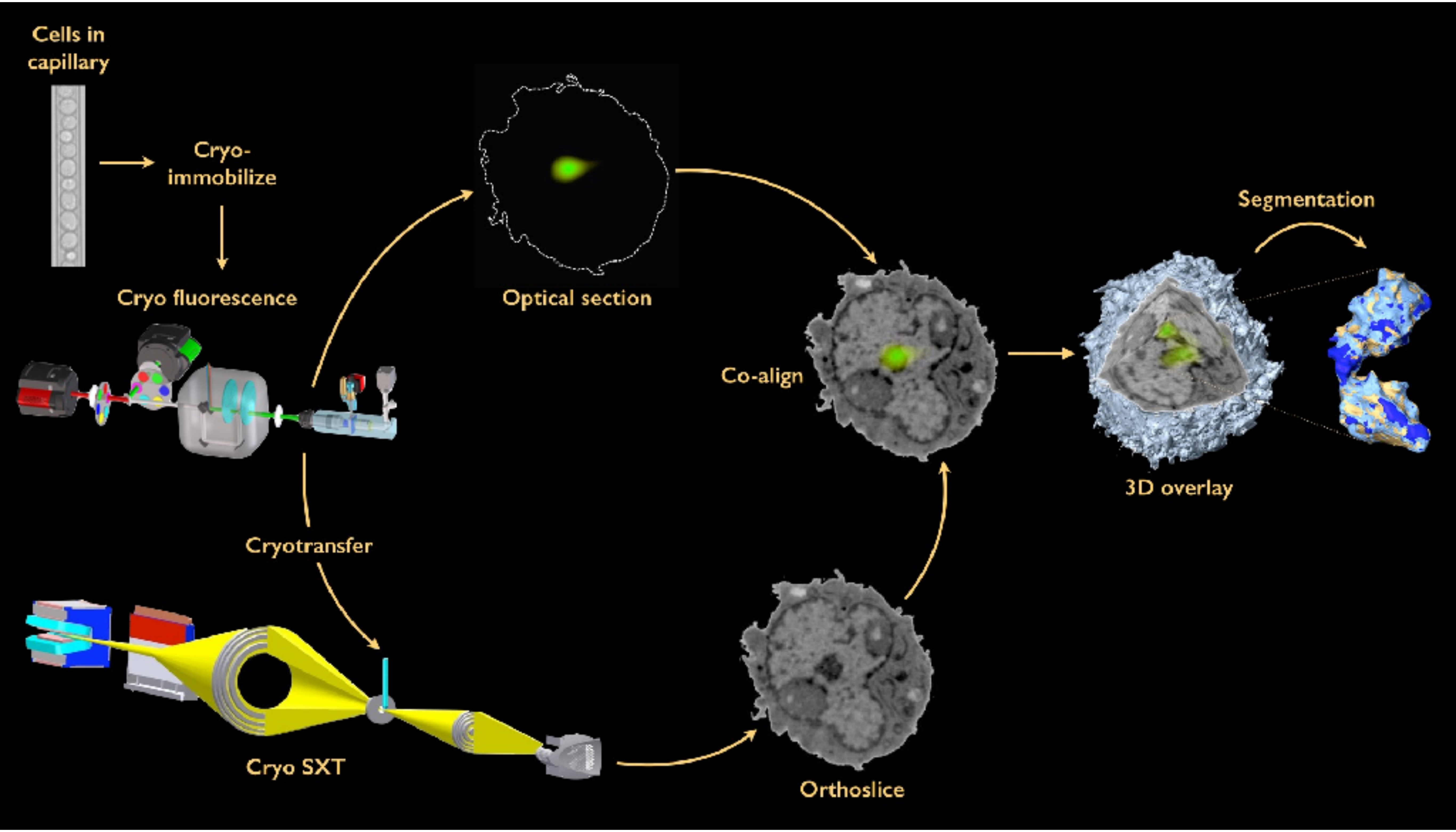

Do M, Isaacson S, McDermott G, McDermott G, Le Gros M, Larabell C. (2015) Arch Biochem & Biophys 581:111-121

Vacuoles in *S. pombe*

Fluorescence **Soft X-ray Tomography**

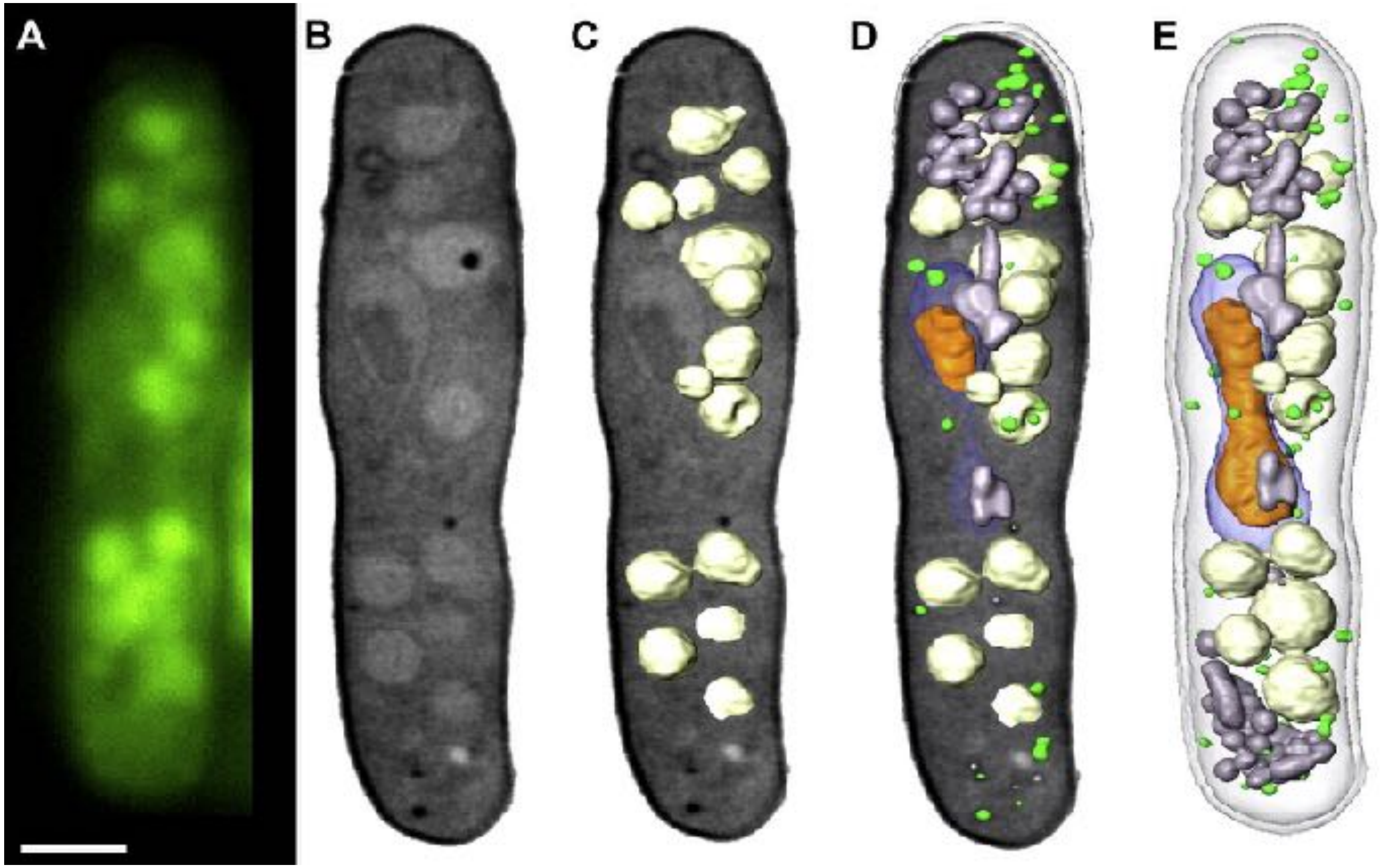

Smith et al., J. Struct. Biol. (2013) 184, 12-20.

Lipid drops labeled with BODIPY

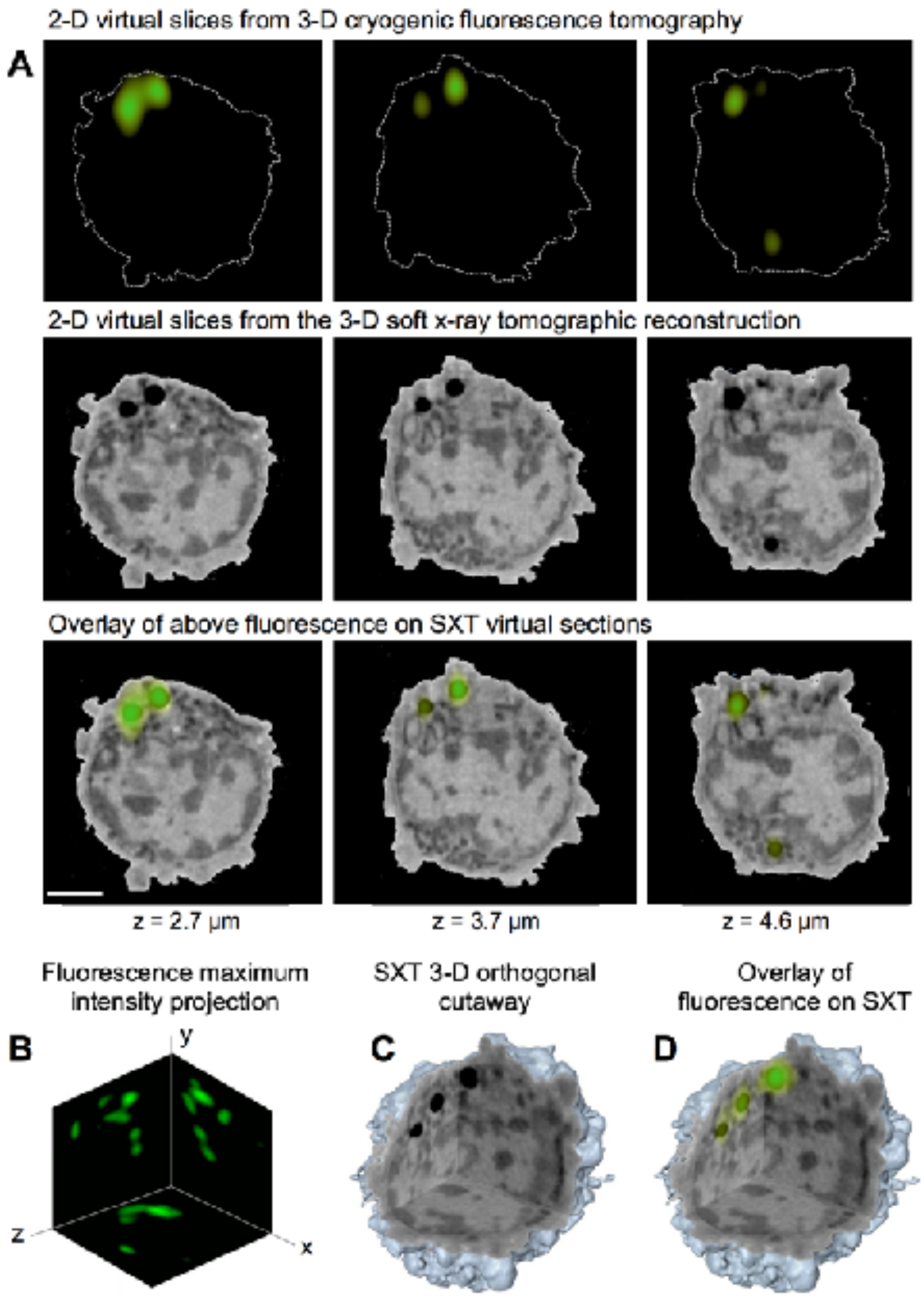

Lipid drops easily identified in SXT because they are very highly absorbing

Smith et al. Biophysical Journal.(2014) 107(8), 1988-96.

Lysosomes Labelled with Lysotracker

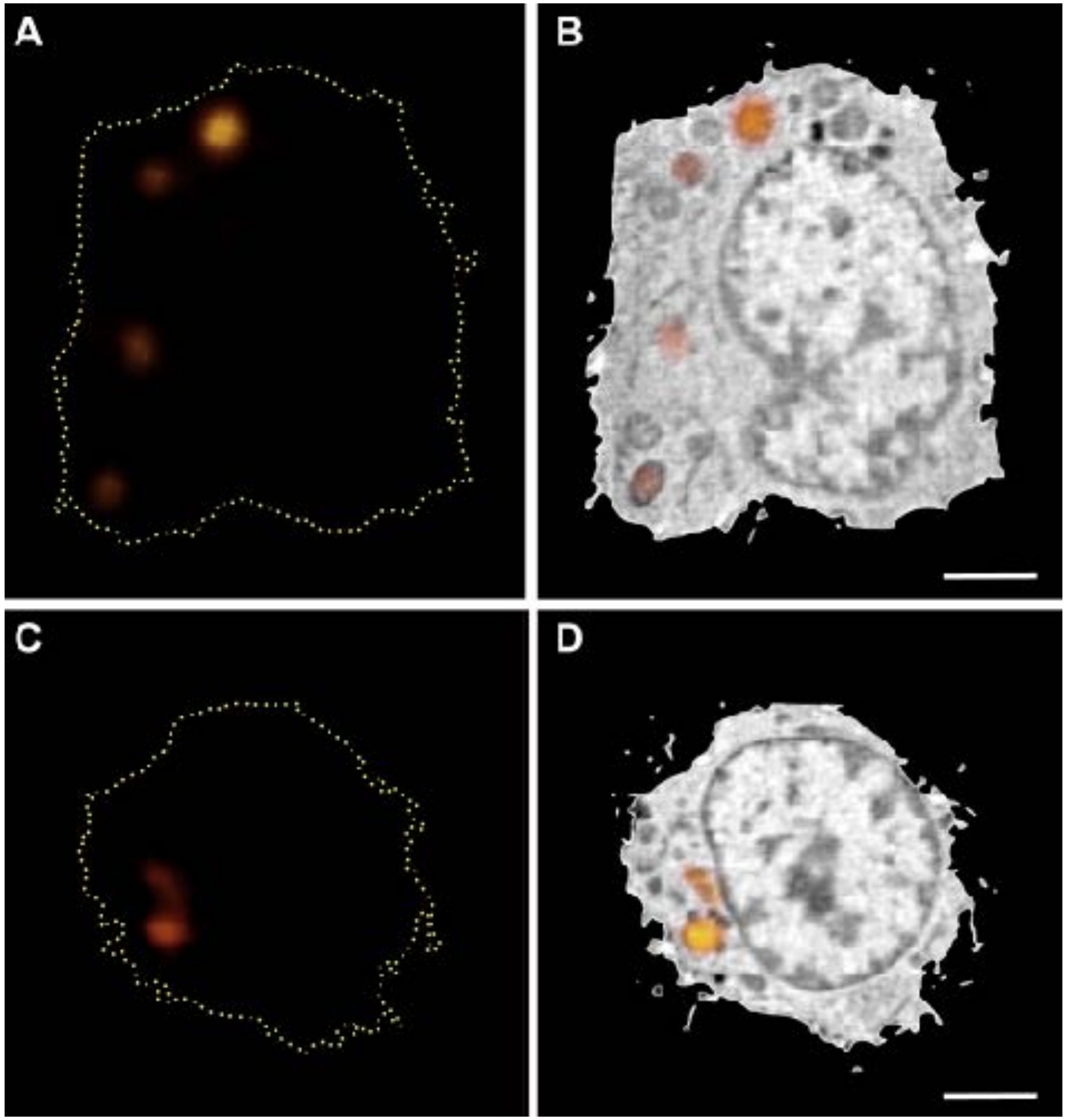

Smith et al. Biophysical Journal.(2014) 107(8), 1988-96.

Nucleus and Nucleolus in Yeast, *S. cerevisiae*

Fluorescence | **SXT Orthoslice** | **Overlay** | **SXT Segmented**

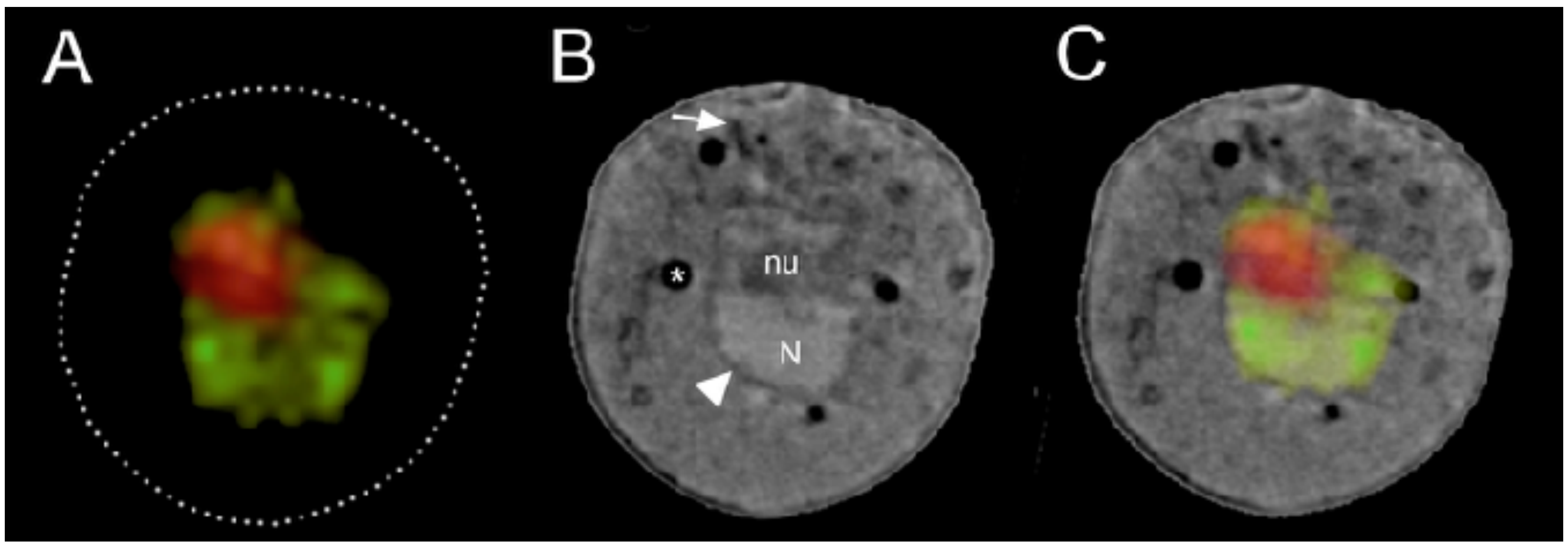

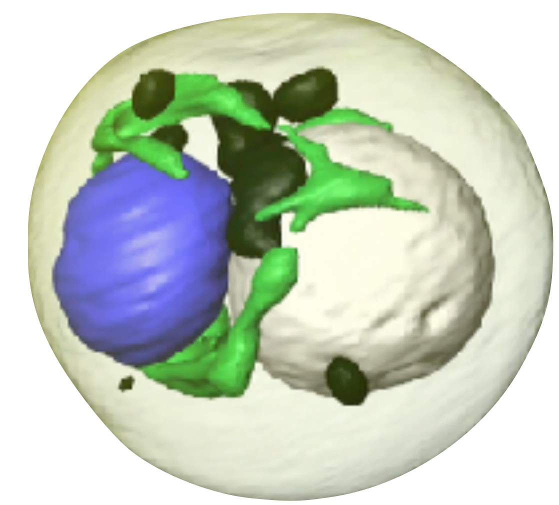

Nucleolus
Nucleus

Walters et al. Current Biology. (2014) 24(23), 2861-2867
Cinquin et al. J. Cellular Biochem. (2014) 115(2), 209-216

Inactive X chromosome

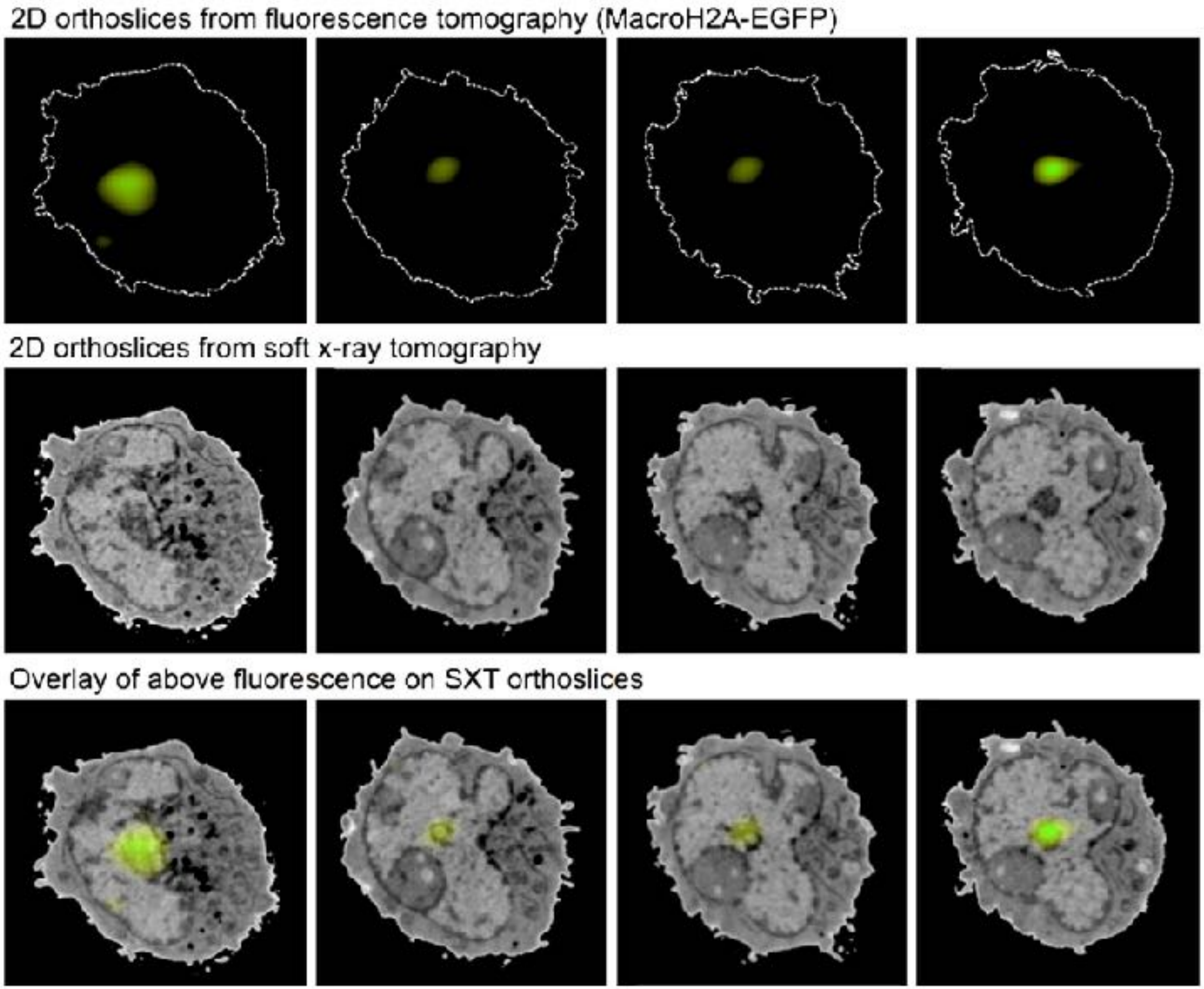

Smith et al. Biophysical Journal.(2014) 107(8), 1988-96.

Inactive X chromosome

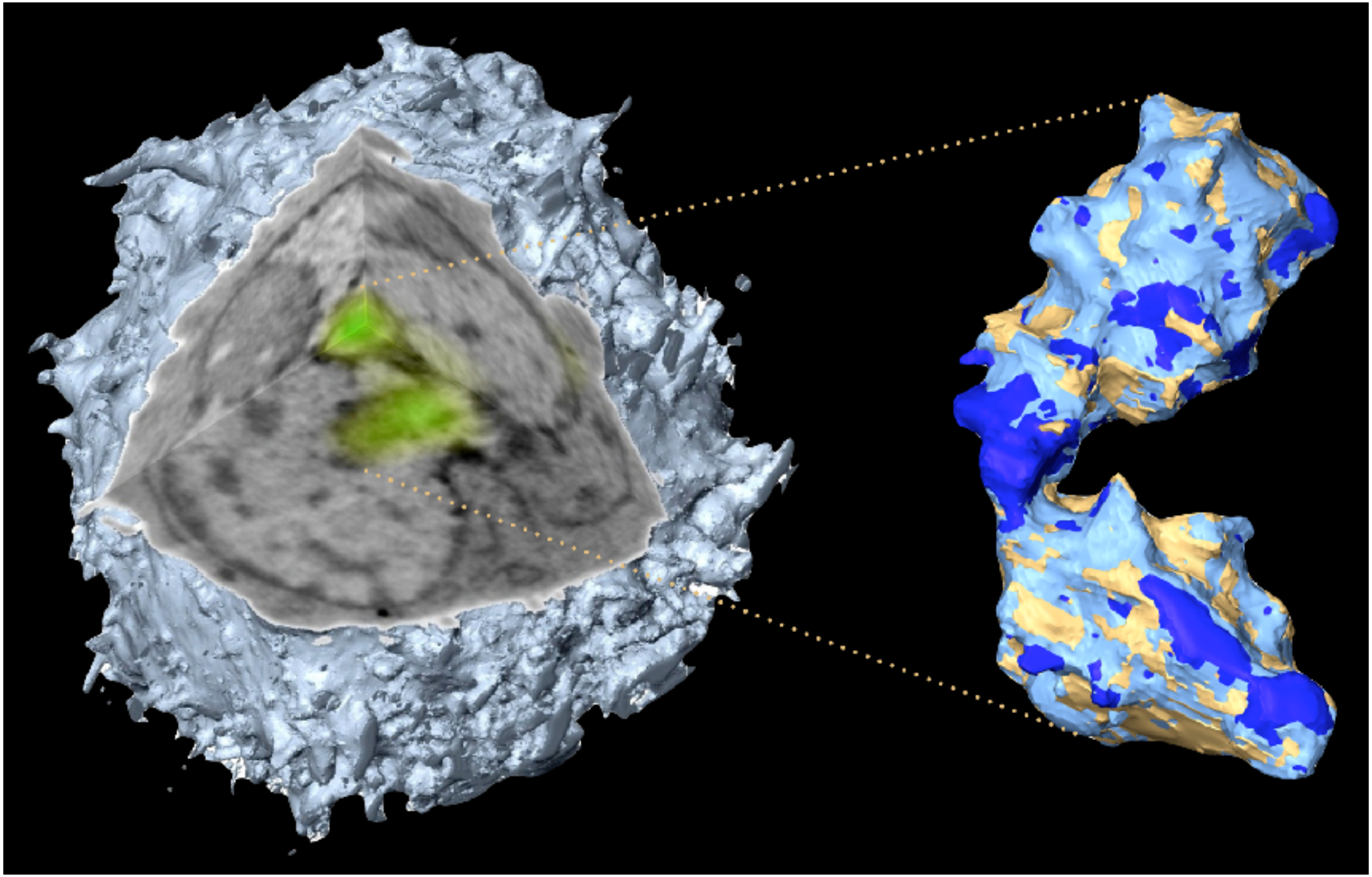

Smith et al. Biophysical Journal.(2014) 107(8), 1988-96.

ER-Mitochondria Contact Sites

Live-cell fluorescence

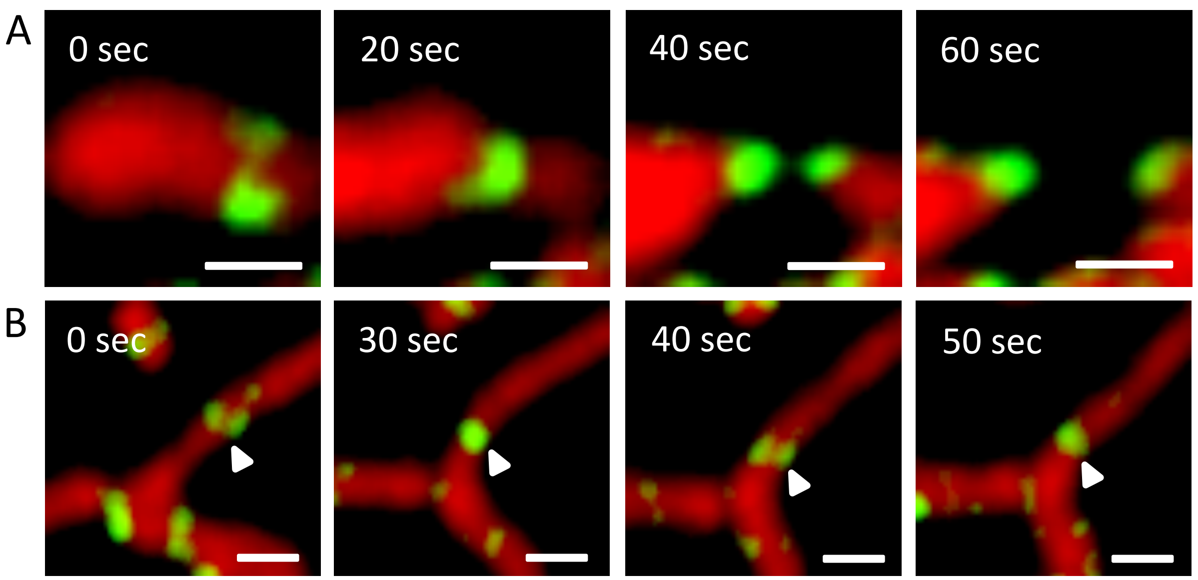

Mitochondria
MiD51-GFP

Fluorescence overlay on SXT | SXT Orthoslice | High mag SXT

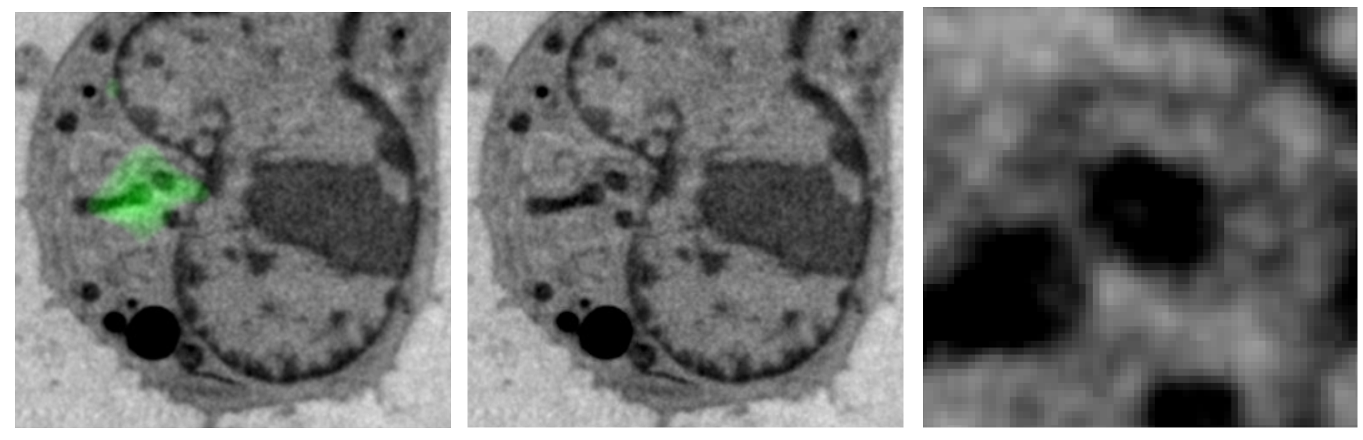

Fluorescence overlay on SXT | SXT | SXT segmentation

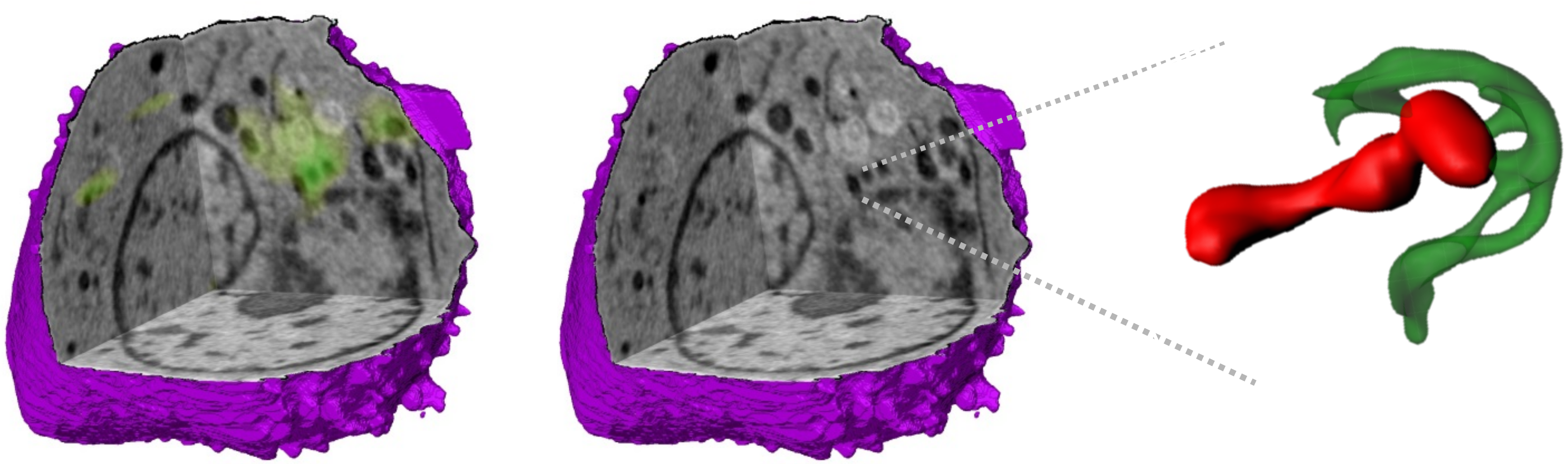

Mitochondria
Endoplasmic reticulum

Elgass et al. J. Cell Science. (2015) 128(15), 2795-804.

ER-Mitochondria Contact Sites

Over expression of MiD51 results in fragmented mitochondria that have a decreased LAC value (are less x-ray absorbing).

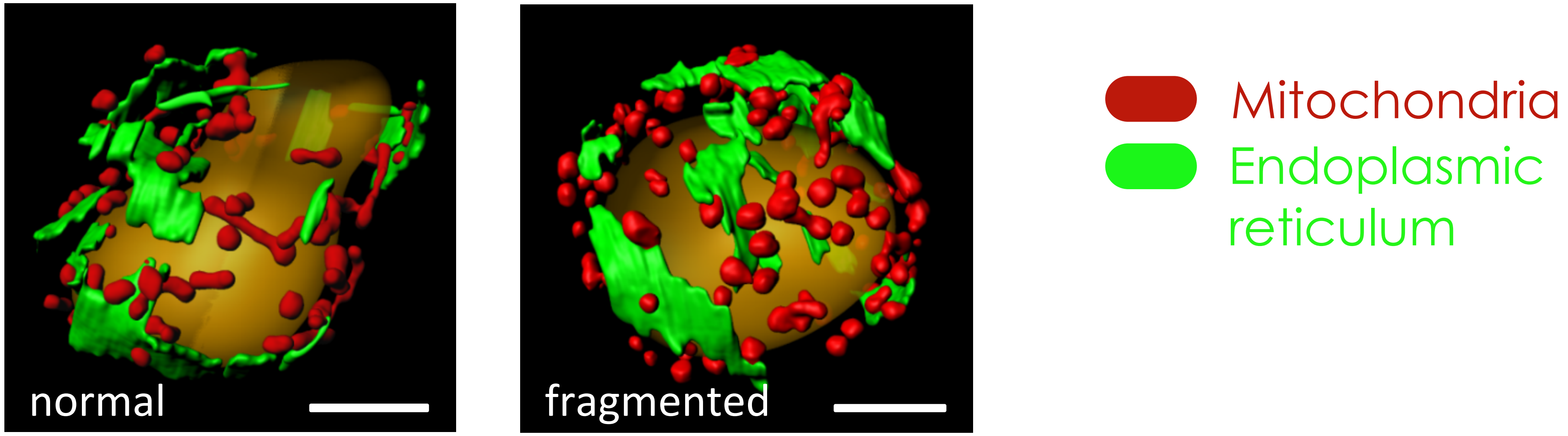

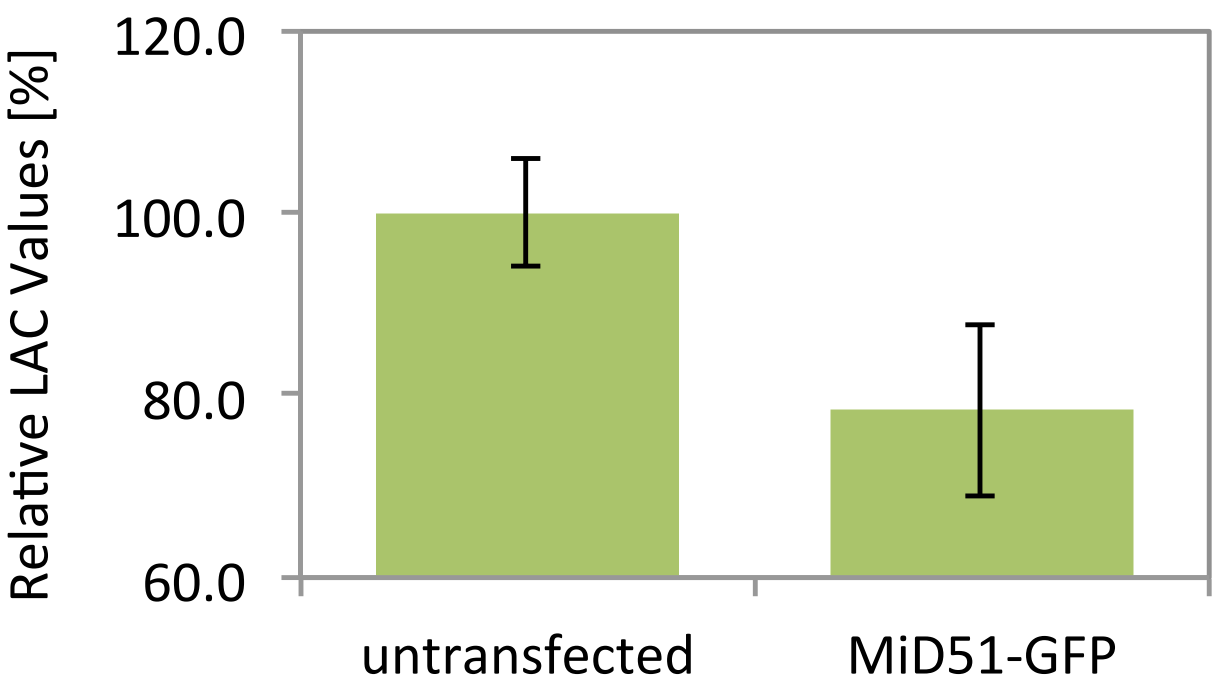

Elgass et al. J. Cell Science. (2015) 128(15), 2795-804.

Nucleolus

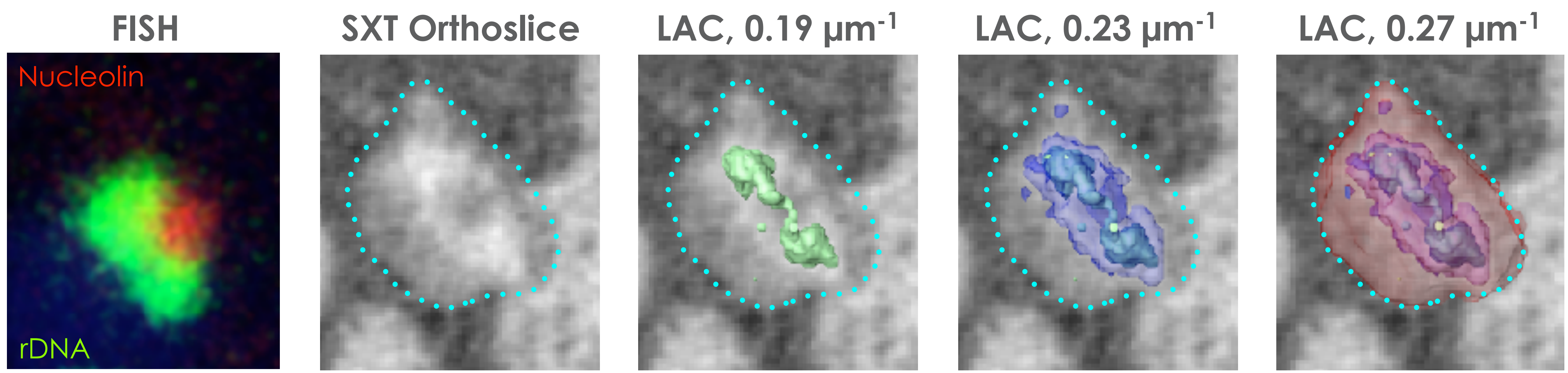
FISH
SXT Orthoslice
LAC, 0.19 μm-1
LAC, 0.23 μm-1
LAC, 0.27 μm-1
Nucleolin
rDNA